CHAPTER 6

SYSTEMS FOR MEASUREMENT OF MODEL POSITION, ATTITUDE, AND VELOCITY

by

C. S. James, R. J. Carros, A. G. Boissevain,
R. I. Sammonds, and M. E. Wilkins

NASA-Ames Research Center

SYSTEMS FOR MEASUREMENT OF MODEL POSITION, ATTITUDE, AND VELOCITY

C. S. James, R. J. Carros, A. G. Boissevain
R. I. Sammonds, and M. E. Wilkins

6.1 INTRODUCTION

The data-gathering process for a great many aeroballistic-range tests consists of recording the position, attitude, and time of arrival of a model at several accurately surveyed points along its flightpath. One of the earliest and simplest approaches to this task utilized the yaw card - a sheet of paper through which the model flies. In the environments of most tests of current interest this approach is inapplicable, although it still finds limited use. Most current data-gathering systems for documenting projectile motion in ballistic ranges are fundamentally photographic in concept. This is a rather obvious choice because it is a convenient form of measurement capable of fast response and high precision, it does not disturb the phenomena being observed, and it can provide visualization of the projectile and its surrounding flow field. In general, such data-gathering systems are laid out in the form of measuring stations set at intervals along the flightpath. The measurements are repetitive and it suffices therefore to discuss the geometric arrangement and operation of the components of a single measuring "station".

The components which typically make up a photographic measuring station are the following:

(a) A point source of high-intensity, short-duration light. This is most often in the visible spectrum, but is sometimes an X-ray source;

(b) A system of optics (i.e., mirrors, lenses, prisms, etc.) for collimating and directing the light across the flightpath and onto a photographic film or projection screen;

(c) A photographic film, or camera, for recording the transient image of the model and flow field;

(d) An optical shutter for limiting the duration of light incident on the photographic film;

(e) A trigger subsystem which is capable of sensing the arrival of the model and initiating the action of the light source and shutter;

(f) Fiducial markers which are photographed simultaneously with the model, and which form a part of the range spatial reference system.

In addition to these components, there is a chronograph system which receives signals from enough stations, at the times of passage of the model, to provide the necessary time increments for the calculation of velocity and deceleration. Many geometric arrangements are possible, and there are alternative choices of components as well. The selection of a particular system, therefore, is dictated by factors such as the types of studies to be emphasized, the velocity range to be covered, the model scale, and cost. Counterflow capability also strongly constrains total range length and the placement of station components. In turn, the constraint on total range length usually results in more severe requirements on precision in the measurement of time increments and model position. (cf. Section 7.11)

In the sections which follow, after a brief description of the use of the yaw card, representative optical arrangements and components of the photographic measuring station are discussed in relation to the environments in which they must function. The final section considers the requirements for extracting the desired numerical data from the exposed photographic film.

6.2 THE YAW CARD - C. S. James

The most economical and least sophisticated of all measuring stations is the yaw card. As the name implies, it consists simply of a sheet of paper hung in a plane normal to the flightpath with its center on the launcher bore sight. As the model flies through the paper, it punches out a hole which registers the frontal silhouette of the model at that instant. Figure 6.1 is a typical puncture from a finned projectile. From the shape and dimensions of the hole and the known geometry of the model the angles of yaw and roll may be inferred. Model position is obtained from the relationship of the hole to the bore line or some other suitable reference. The time of model passage may be determined most simply, perhaps, through the use of an electrically conducting grid painted directly on the yaw card. This grid then becomes a break switch when the model penetrates the paper. The most satisfactory paper for yaw card use is a short-fibered, relatively low-strength and lightweight paper which will punch out easily and cleanly without tearing, and which will minimize the disturbance to the model. The "construction" paper, used by children in school projects, works well.

One or two yaw cards, strategically placed, can be surprisingly useful in diagnosing model and sabot-launching problems, as indicated in Section 3.8, or can indicate whether or not sabot pieces have flown downrange. The yaw card's usefulness in the vicinity of the gun is limited by its vulnerability to muzzle blast, although shredded yaw cards frequently can be reassembled to yield valuable data. In this regard, distinctively patterned and colored cards make the sorting job easier. By the use of multiple cards mutually related through spacial-reference and chronograph systems, all necessary measurements may be obtained for the determination of aerodynamic forces and moments. This technique has been used at the U.S. Naval Ordnance Laboratory (NOL)[6.1] and is used in the Aero-ballistic Range at the Canadian Armament Research and Development Establishment (CARDE)[6.2], which is a large enclosed range having available 80 such stations with capacity for 2.7-m by 3.7-m yaw cards. Figure 6.2 shows a typical station.

The precision of measurement to be expected from a yaw card system depends rather strongly on the configuration flown. In particular, accurate yaw angles are easily obtained with slender shapes, but difficult with bluff shapes. Roll angles are easily measured with finned configurations; while auxiliary means, such as a colored index which leaves a wipe mark on the yaw card may be required for a body of revolution. The potential accuracy anticipated for ideal conditions in the CARDE facility is stated as 0.1 degree for attitude angles, 0.25 degree for roll angle, and 1.6 mm for position. Limitations on the use of yaw cards are the possibility of damage to delicate models from impact with the yaw card, and the effect of the impact on model motion.

6.3 OPTICAL ARRANGEMENTS OF THE PHOTOGRAPHIC MEASURING STATION – C.S. James

Several types of optical system are used in ballistic-range testing – often for specialized purposes other than observing projectile motion (e.g., flow visualization). These which employ light transmitted through the flow field, and which therefore view the model in silhouette, include the shadowgraph, the schlieren, and the interferometer[6.3, 6.4]. Systems which view the model by reflected light or by the luminosity of the event itself include various forms of high-speed framing and streak cameras[6.5, 6.6, 6.7]. A hybrid technique, which in a sense employs both transmitted and reflected light, is that of holography[6.8, 6.9]. Holography is basically a form of interferometry and is a relatively new technique. While it has not yet been exploited to any extent in ballistic ranges, it appears to hold much promise for the future in that it is potentially capable of recording on film a stereoscopic representation of a model and flow field which can be reconstructed after the event and viewed from different vantage points.

Where the emphasis is on position and attitude measurement at multiple stations, the shadowgraph system is invariably chosen over other systems for reasons of dependability, accuracy, and simplicity. While the shadowgraph is not as sensitive to density modulations in the projectile flow field as the schlieren, nor as quantitative in this respect as either the schlieren or the interferometer, stable optical alignment is easily obtained. The shadowgraph can provide high local contrast both in the model silhouette, which is desirable for angle- and position-reading accuracy, and in the features of the flow field, which is helpful in resolving much of the fine structure present. Among the major ballistic ranges of the world, therefore, differences in their primary optical systems are invariably those of configuration, chosen in each case to meet particular requirements, rather than of optical principle.

6.3.1 Shadowgraph Configurations

The simplest form of shadowgraph consists of a point source of light and a photographic film situated on opposite sides of the flightpath. Since, in general, the model axis will not be parallel to the film plane, it is desirable to provide two orthogonal systems in order to record two projections of the model. Such a configuration is illustrated in Figure 6.3. The entire arrangement may be built inside a pressure vessel so that no optics are needed except for a small quartz window in the cannister which contains and isolates each spark-light source from the pressure and humidity variations in the range tank. Aside from its simplicity, the principal advantage of this so-called direct-shadow configuration lies in its ability to resolve much of the detail present in both the inviscid and viscous flow field surrounding the model. The light field is uniformly conical and of uniformly varying intensity since there are no optics to degrade it. A typical shadowgram is shown in Figure 6.4.

The flightpath corridor, shown by cross-hatching in Figure 6.3 can be made reasonably large in relation to the tank dimensions, for this configuration. It is limited principally by film size and the illumination angle obtainable with the light source. The large flight corridor can be an advantage particularly at downrange stations where it is needed to accommodate dispersion in model flightpaths. The magnification depends on the ratio of distances of the film and of the model from the light source, while the sensitivity in recording density changes in the flow field depends on distance of the film from the model. By varying the distance of the film plane from the flightpath, then, some control of both effective sensitivity and magnification can be exercised. A modification of this direct shadowgraph, which substitutes a plane mirror for one of the light sources, is employed in the Aerodynamics Range[6.10, 6.11] of the Ballistic Research Laboratories (BRL), and in the 285-foot Pressurized Ballistic Range[6.12] of the Naval Ordnance Laboratory (NOL). Figure 6.5 is a schematic of the NOL configuration. Where internal space is limited, which is the case with the 0.9 meter-diameter NOL facility, this arrangement can sometimes be an advantage in simplifying the placement of components, or in minimizing the need for windows. The economics of substituting a mirror for a light source could also be advantageous. On the other hand, the resolution of the flow field by the vertical light beam will be somewhat degraded by the mirror. Figure 6.6 shows the two orthogonal views of a model in the NOL range. An advantage of this arrangement is that both pictures are made at the same instant. With two light sources, small differences in their timing are possible, which translate into uncertainties of model position and velocity unless chronographs are used for each.

For aerodynamic testing at subsonic and supersonic speeds up to a Mach number of 10 or 12, the direct shadowgraph is quite satisfactory. Somewhere in the Mach number 10 to 12 range, depending on the bluffness of the model, its material, and on free-stream density, the model shock layer and wake begin to radiate with sufficient intensity to cause fogging of the photographic film. At the same time, the increased model velocity causes the model to move enough during the 0.2-to 0.6-μsec effective duration of the typical spark-light source to produce undesirable blur of the photographic image.

The remedies for these problems are to selectively attenuate the light from the model shock layer, allowing only that from the shadowgraph source to reach the film, and to shorten the effective duration of the exposure to minimize the motion blur. Various methods have been devised to accomplish these improvements.

Wavelength filtering in the visible and ultraviolet spectrum is a means of selective attenuation. To be effective, the output of the light source should be strong in a portion of the spectrum where the radiative output from the projectile is weak, and where the sensitivity of the photographic film is high; and the filter must have a reasonably narrow transmission band. These are difficult requirements to meet with an unfocused system where the entire photographic film must be covered by the filter. Some success in exploiting this technique with focused systems (cf. Section 6.4.2) has been reported, however[6.13, 6.14].

If the shadowgraph system uses an X-ray source, filtering becomes a simple matter, but flow visualization is lost. Pulsed-X-ray sources of sufficiently short duration (less than 10^{-7} sec) are available[6.15] which can cope quite well with the motion blur problem in, say, the 5 to 10 km/sec velocity range. The CARDE Range 5 utilizes a direct X-ray shadowgraph system which is nonorthogonal[6.16]. A sketch of the configuration is shown in Figure 6.7(a). With this arrangement, both views of the model appear on one sheet of film, which is doubly exposed. Figure 6.7(b) is a representative station photograph. X-ray systems can be used in undarkened ranges and near the gun for launch and sabot-separation diagnostics.

Another method of achieving selective attenuation is to image the shadowgraph light source at an aperture placed in front of the film, as illustrated in Figure 6.8. The light from the model, originating at a shorter object distance, will not be in focus at the aperture; hence, it will be largely blocked from striking the film. A shutter in conjunction with the aperture will further block long-duration light from the model wake or from muzzle or impact flash, and can be used to reduce motion blur. The additional components add to the cost, and to the complexity of alignment, operation, and maintenance. Furthermore, the addition of an electro-optical shutter (transmissivity typically less than 0.4; cf. Section 6.5.2) usually requires the substitution of a much brighter light source to produce acceptable pictures.

If the aperture alone is sufficient to attenuate the unwanted light, the motion-blurring may be reduced by shortening the duration of the light pulse. Pulsed light sources of 10^{-8} sec or less duration are currently available (cf. Section 6.4). This approach has been taken with considerable success at the Lincoln Laboratory Re-Entry Simulating Range[6.17]. Figure 6.9 is a shadowgraph taken in that facility, which uses essentially the configuration of Figure 6.8 in conjunction with a magnifying camera to obtain greatly magnified shadowgrams. The 20-nsec exposure reduces motion blurring to the extent that spalled surface fragments from the sphere moving at 5.9 km/sec are clearly discriminated.

The optical arrangement of Figure 6.8 is called a focused shadowgraph. In addition to its usefulness as a means of selective attenuation, another valuable use, for which it was originally exploited, is the control of the effective shadowgraph sensitivity of the system. The position of the object plane imaged on the film may be adjusted by moving the film toward or away from the focusing lens. If the object plane is made to coincide with the model flight path, the shadowgraph sensitivity is minimum (ideally zero). Departure of the object plane from the flightpath increases the sensitivity. This device is frequently of value in reducing the optical distortion of the flow field in regions of strong density gradient, as, for example, the nose region of a bluff body in supersonic flight (see Chapter 8 for a further discussion).

The focused shadowgraph of Figure 6.8 has been illustrated with lens optics. Lenses permit close coupling and axial alignment of components, and are adaptable to direct magnification of the shadow image. Mirrors, on the other hand, are more economical for a large field of view, and avoid possible problems of striae or chromatic aberration. Figure 6.10 is the mirror-optic counterpart of Figure 6.8. The necessary departure from an axisymmetric lightpath introduces additional aberrations, in the usual installation, which can be troublesome if accurate measurements of projectile position are required. (See Reference 6.3 for a discussion). Illustrated in Figure 6.10 is a means of avoiding aberrations due to nonsymmetry of the optical path, which can be economically feasible for a modest field of view. If the light source and its image lie respectively on the parallel axes of the large parabolic collimating and focusing mirrors shown by the dashed lines, each mirror will operate as an axisymmetric component with a vignetted field. For the same focal length, a mirror diameter slightly more than twice that of the smaller full-field mirror (f/number slightly less than half) is required. But since only a small portion of the surface is used, a mirror of this diameter can be cut into sectors, as shown in the insert of Figure 6.10, to provide four (or more) components, thus offsetting in part the higher cost of the larger parabolic mirror. The dashed circles indicate the equivalent working area of the smaller full-field mirrors. The apex of each sector from the large mirror can be used as a reference for alignment by placing it at point A in the figure.

Two alternative noncollimated but focused shadowgraph configurations, which utilize single optical elements to focus the conical light field, are shown in Figures 6.11 and 6.12, together with representative shadowgrams from each. The first of these[6.18] makes use of a Fresnel lens inside the range tank, with the other components located externally; while the second[6.19] uses a spherical-segment mirror and folds the light field to contain it entirely within the range tank. In the second case, the light field is intercepted twice by the model and two images are

registered on the photographic film. Both of these versions retain the advantage of attenuating light from the model flow field by differential focusing, and require one less optical element than the configurations of Figures 6.8 and 6.10. While they are both adapted to a relatively wide field of view, a wide field calls for a large lens or mirror, and the economics of such large components are usually against high optical quality. To overcome this weakness, both versions utilize the large focusing elements not as objectives to produce an image of the projectile on the film, but rather as efficient light-gathering screens. A small objective lens is then placed at the aperture to re-image on the film the shadows of the projectile and its flow field which fall on the screen.

An advantage that all focused shadowgraphs have over the direct shadowgraph is that the film size may be independently specified to strike the best compromise between cost, storage, and handling limitations, on the one hand, and the requirements of film-reading accuracy, on the other.

A simple shadowgraph configuration which has been used for many years in large ballistic ranges is sketched in Figure 6.13. It is an outgrowth of the direct shadowgraph, which, through the use of a camera, allows film size to be independently chosen. Because there are no expensive optics, this configuration is economical for covering a large flight corridor. Light from the source casts a shadow of the model and of the flow field onto a projection screen placed on the opposite side of the flightpath. The screen is usually coated with glass beads which reflect each incident ray approximately back on itself. A camera, placed as close to the light source as practicable, photographs the visible image on the screen. The camera, then, sees both the focused silhouette image from the screen and a displaced defocused image of the directly illuminated model. Figure 6.14(a) is a downrange view of the Ballistic Research Laboratories (BRL) Transonic Range[6.20], which uses this configuration. Figure 6.14(b) is a representative shadowgram.

In its capacity as a reflector, the beaded screen performs a function similar to that of the spherical-segment reflector in Figure 6.12(a), but its light-gathering efficiency is considerably lower and it does not have the selective light-attenuation capability of the focused shadowgraph. It has been found[6.19] that the efficiency of this type of reflector can be improved considerably if a lenticular motion-picture screen is used and mounted on a cylindrical support. Such a screen, when flat, reflects light as would a cylindrical reflector. If the cylindrical support is curved, with the proper radius, in the orthogonal plane, the screen will then act as a spherical reflector. Difficulties with beaded screen in variable-pressure range enclosures due to dust adhesion have been reported[6.21]. The repeated pressure cycling between vacuo and atmospheric tends to work dust particles into the inter-bead voids, reducing the reflection efficiency of the screen.

A novel arrangement of optical components for a focused shadowgraph[6.22], illustrated by Figure 6.15, permits orthogonal viewing in an enclosed range with a single light source, and a single shutter and camera. Some of the more expensive components are thus eliminated, and possible timing uncertainty resulting from operation of two light sources is avoided. Figure 6.15(a) illustrates very simply the principle involved. A projectile flying a path, normal to the page, which falls within the dashed boundary will intercept two bundles of rays, A and B, of a collimated light beam. Bundle A will be intercepted after reflection from the mirror, while bundle B will be intercepted before reflection. Since these bundles are incident on the projectile at right angles to each other, two orthogonal shadows of the projectile (and flow field) will be cast on the film. Figure 6.15(a) is itself a workable system which can be used with either a point source or a collimated beam.

Figure 6.15(b) is the focused version of this arrangement. Light from the source, collimated by lens L1, passes the flightpath in one direction; is routed around the range structure by mirrors M1 and M2; passes the flightpath in a direction normal to the first; and finally is focused at the aperture of the camera by lens L4. Lenses L2 and L3, working together, focus an inverted image of the projectile at a point slightly displaced from the projectile itself. The image is also rotated a quarter of a turn by the mirrors M1 and M2. Lenses L2 and L3 are spaced two focal lengths apart so that the light beam emerges recollimated from L3. The projectile and its inverted rotated image are focused in the film plane by lens L4. Fiducial wires are placed as shown to provide a position and angle reference. The shadowgram, then, consists of two images moving in opposing directions and diametrically displaced from the center.

Photographic stations of this configuration are installed on two small ranges at Ames Research Center. Figure 6.16 is a representative shadowgram from one of these stations. Figure 4.1 shows one of the installations.

6.4 LIGHT SOURCES – R.J.Carros

Since much of the data collected in ballistic ranges is on film, the development of light sources suitable to the task has been an important factor. The light sources are usually required to be of very short duration to effectively "stop" high-speed models in their flight. Because the duration is short, the intensity must be correspondingly high, to bring about photographic exposure. The development of suitable light sources has been evolutionary, over a period of several decades.

We will describe some types which represent the best state of development available in 1968. Undoubtedly, further developments will be made.

For purposes of classification, we will divide the discussion into sections on spark gaps, laser sources, X-ray sources, and other sources. In terms of overall usefulness to date, the first class is by far the most important.

6.4.1 Spark Gaps

To illustrate the requirement for short duration, consider for example a model traveling at a velocity of 3 kilometers per second, It will move 3 millimeters in 10^{-6} seconds. It is clear then that for even such moderate model velocities, a light source of less than one microsecond duration is required to limit blurring. Because of the short duration, the source must also be very bright to expose the photographic film properly. A light source which meets these requirements – and is perhaps the one most widely used in ballistic range facilities – is the capacitance-discharge spark gap, or Libessart spark, which consists of a pair of electrodes connected across a high-voltage capacitor. The spark is discharged on command at the desired instant by a voltage pulse applied to a trigger electrode. A circuit diagram of this system is shown in Figure 6.17. The trigger voltage pulse ionizes the air in the vicinity of the main electrodes making it conductive. The energy stored in the capacitor is then discharged into the gap, vaporizing some electrode material and heating it and the air in the current path to very high temperatures, in the order of tens of thousands of degrees Kelvin. The hot plasma becomes the source of the spark gap light. Values commonly used for the voltage and capacitance are in the order of 7,000 volts and 0.12 microfarads, providing a stored energy of about 3 joules.

A photograph of a spark gap light source of this type is shown in Figure 6.18. The cylindrical cover has been removed to show the array of capacitors around the electrodes and the charging resistors and trigger pulse transformer. The principal electrodes shown disassembled in the lower part of the photograph are made of aluminum because both aluminum atoms and aluminum oxide molecules are efficient radiators at the plasma temperatures. A 1-mm diameter hole is drilled on axis at the apex of the ground electrode to allow the light to leave the gap. The 1-mm diameter is a compromise between the light-quantity and point-source requirements. The trigger electrode, also shown in the figure, is made from stainless steel.

Care must be exercised in the design and construction of the spark gap light source to keep the inductance of the system low so that the natural frequency of the capacitor-discharge loop will be high and the light duration, consequently, short. A good part of this is accomplished by placing the capacitors close to the electrodes thus keeping the path length to the electrodes as short as possible. The importance of low inductance in the circuit has been emphasized in the literature[6.23, 6.24]. The effective duration of the source described above is approximately 0.3 microsecond, which is commonly measured at the half-height of the peak light output. An oscilloscope record of the light output of this type of spark, as a function of time, is shown in Figure 6.19. References 6.23 through 6.27 include some examples of other short duration spark gap light sources.

The radiated spectral power as a function of wavelength for the type spark gap of Figure 6.18 is shown in Figure 6.20. Also shown in Figure 6.20 for comparison are two curves of the spectral radiance of a blackbody radiating at temperatures of $20,000^{\circ}$ K and $23,000^{\circ}$ K. This comparison suggests that the spark gap light source is radiating nearly as a blackbody at a temperature above $20,000^{\circ}$ K. To test this conclusion, the following experiment was performed. Two high-voltage electrodes with a common ground electrode were arranged as shown in the schematic diagram in Figure 6.21. The spacing of each high-voltage electrode from the ground electrode was approximately 2.5 mm, which is the same spacing as that of the principal electrodes in the spark gap light source of Figure 6.18. The high-voltage power supply was used to charge the capacitors and a trigger pulse amplifier was used to supply the trigger voltage to fire the sparks at the desired time. The voltage signal, from the 1P28 photomultiplier tube with S-5 response, is a direct measure of the spark gap light output and was recorded on an oscilloscope.

First, capacitor A only was charged (switch open). Spark A was then fired and the output recorded by the oscilloscope camera. A record obtained is shown in Figure 6.22(a). Then both capacitors were charged to the same voltage as in the first step and both spark gaps were fired simultaneously from the common trigger pulse to record the signal shown in Figure 6.22(b). These measurements were made for charging voltages of 3.5, 4.0, 4.5, 5.0, and 5.5 kilovolts. The data obtained from the oscilloscope records were reduced to the form shown in Figure 6.23. The percentage of light output from spark gap B transmitted through the plasma in spark gap A is over 60% at 3.5 kilovolts, but diminishes rapidly with increasing voltage to a level of 18% at a charging voltage of about 5 kilovolts and greater. One may then conclude that the plasma in gap A has considerable opacity to the radiation from gap B and that the plasma in gap A is behaving as a nearly blackbody at a temperature slightly greater than $20,000^{\circ}$ Kelvin. Therefore, to increase its luminous output, it would be necessary to increase the plasma temperature.

6.4.2 Lasers

As noted earlier, one approach to rejecting from the spark photograph light emitted by the model flow field is to use spectral filtering in the light path. This approach is particularly favored by a laser light source which produces intense light at a single frequency. All other frequencies can thus be blocked by the filter. Lasers can be switched to provide light durations of the order of 10 nanoseconds. A schematic diagram showing a laser as a light source, and the placement of the filter in a filtered focused shadowgraph system is shown in Figure 6.24. The system is otherwise unchanged from those discussed earlier. Since the laser output is a small diameter beam, a diverging lens is used to spread the light to the diameter required to cover the desired field at which point it is again collimated. It is necessary to pulse the flash tube of this type laser typically 500 microseconds prior to photographing the event. During this period of 500 microseconds, the so-called pumping action takes place and light intensity builds up to a peak. Therefore, a timing arrangement to start the laser must be provided. Timing of the photograph, however, is determined by operation of the Kerr cell, which is switched open when the model arrives at the photographic station. The usual timing signal would therefore be applied to the Kerr cell. Ballistic-range facilities which have used laser light sources include US Naval Ordnance Laboratory, MIT Lincoln Laboratory, General Motors Corporation, and Laboratoire de Recherches Balistiques

et Aérodynamiques (cf. References 6.17, 6.28, 6.29). A shadowgram made with a laser system in use at the US Naval Ordnance Laboratory is shown in Figure 6.25. The double image is a result of the geometry of the photographic system, as indicated in Figure 6.12(a). Lasers are not presently used widely in ballistic range photographic systems, however, because the "state of the art" is such as to present some problems including maintenance, non-uniform or mottled background in the photograph, and starting the operation of the flash tube 500 microseconds before use. Maintenance involves replacement of some components within the laser such as the flash tube, Kerr cell, mirrors, windows, and ruby rod which may become damaged after only a few hundred pulses due to the high energy levels in the laser. Some of the literature refers to the requirement that optics in the laser photographic system, such as range windows and mirrors, be maintained very clean to prevent scattering of the light which would result in a mottled background in the photograph. A mottled background may also be caused by non-uniform light emission from the laser rod. However, laser rods can be chosen selectively to minimize this problem. The relatively high initial cost of the laser may also limit its use to only a few selected stations to examine such details as model integrity, ablation, and shock shape on radiating models. All things considered, the laser has very attractive potentialities and, as research and development continues, the laser will most likely see increasing use in ballistic range facilities.

6.4.3 X-ray Sources

Still another source of electromagnetic radiation used to produce an image on photographic film is the X-ray source. Since radiation from the X-ray will pass through film covers opaque to visible light, radiation from the model shock layer can be blocked in an X-ray picture. Short duration or "flash" X-ray systems are commercially available. They consist of a high-voltage supply, a pulser, an X-ray tube, and a trigger system. A block diagram of a typical system is shown in Figure 6.26. The pulser is charged to the desired voltage from the high-voltage supply. Upon receiving a signal from the trigger system the pulser discharges to the X-ray tube which in turn emits radiation to photograph the event.

In addition to the use of this system to photograph self-luminous models, a second, perhaps more important, use of these systems has been to photograph the model and sabot in the vicinity of the launching gun muzzle, where radiating gun gases make conventional photographic techniques unusable. The photographs in Figure 6.27 illustrate this use. They show a sequence of X-ray photographs of a model and sabot emerging from the launch gun muzzle and follow the process of early sabot separation. Photographs of this type are extremely valuable when launching problems are being experienced.

The laser light source with appropriate filters to prevent gun gas radiation from exposing the film is also potentially useful to obtain photographs near the gun.

It is a disadvantage of X-ray systems, used to obtain photographs of a model downrange, that they do not make any of the flow field characteristics visible. Hence, the penalty for this approach to photographing models in luminous flow fields is the loss of flow visualization.

6.4.4 Other Light Sources

Although the spark, X-ray, and laser are most often used in ballistic range photographic systems, other light sources have been used and have application in some special circumstances. These light sources include flash lamps, flood lamps, carbon-arc search lights, self-luminosity of models or surrounding flow fields, and explosive light sources. Flash lamps have been used singly or in groups of two or more and pulsed sequentially to either back light or front light an event to be recorded by either a single exposure or a motion picture camera. The flood lamp and carbon-arc search light (as used in Reference 6.30) may also be used for front or back lighting an event. The luminosity from a radiating model is also used as a light source in some photographs made for radiation studies; see for example Figure 9.1. All of these light sources are of long duration and therefore a shutter must be used to limit the exposure time and to stop motion of the event. These sources are then, with the exception of self-luminosity, limited to test circumstances where the event motion is relatively low speed so that the shutter may remain open long enough to sufficiently expose the film but yet not long enough to record event motion (blur) on the photograph. As described in the following section, image-intensifier-type cameras are often used to photograph a self-luminous event. Explosive light sources have short duration and therefore are suitable for photographing high-speed events. The explosive light source described in Reference 6.31 has a duration of 3×10^{-8} seconds and contains a few tenths of a gram of lead azide and PETN, which when detonated have sufficient energy to produce luminosity by shock compression of the air. For additional information on light sources, the reader is referred to such publications as Proceedings of International Congresses on High-Speed Photography and the Journal of the Society of Motion Picture and Television Engineers.

6.5 SHUTTERING – A.G.Boissevain

The "shuttering" provided by the short duration of the spark gap light source (about 0.3 microsecond for a capacitance discharge spark) effectively stops the motion of low velocity models and the necessary image sharpness for measurement is obtained. At increasingly high velocities, shuttering to achieve shorter exposures becomes necessary to limit motion blurring and thus retain image quality. Furthermore, as has been noted, when light from the model shock layer and wake must be rejected to preserve useful images, active shutters may also be required. These factors have led to a requirement for electro-optical or electromechanical shutters in modern, high performance ballistic range optical systems.

Other reasons for shuttering may also arise. Fog exposure of the film may occur due to a variety of causes, including room light, muzzle flash from the gun, flow field emission from sabot parts, light flashes from model

and sabot impacts, light from adjacent shadowgraph stations and from station-triggering light screens, and luminosity carried in the flow of counter-flow facilities. These problems can in some cases be overcome by simple solutions, such as limiting the time the film is uncovered or creating a spectral mismatch between the unwanted light source and the film response. As an example of the latter, the use of red photobeams and red-insensitive film is mentioned. The use of shutters, however, can largely overcome all of the above problems.

Shuttering systems can be grouped broadly as electromechanical and electro-optical. In the following paragraphs, several types within each class will be discussed briefly and their usual applications indicated.

6.5.1 Electromechanical Shutters

6.5.1.1 Moving-Film and Rotating-Mirror Cameras

High velocity events such as ballistic range models in flight can frequently be photographed without blur by means of a moving film or rotating mirror camera system. The principle is simply one of holding the model image stationary on the film for a long enough time to bring about exposure. The two sketches in Figure 6.28 show typical operation. For maximum effectiveness the film velocity or equivalent mirror rotational speed must be carefully matched to that of the model image to avoid blur in the direction of movement. While cameras employing this principle are commercially available, they may, for particular applications, have to be designed to meet test requirements and built to order or modified (cf. References 6.5, 6.6).

6.5.1.2 Spectrograph Shutters

For radiation studies in a ballistic range, a series of luminous events occur which may require shuttering to isolate the event of interest. An unshuttered spectrograph may superpose some response to all the events from the gun-muzzle flash to the impact of the model. Photomultiplier tubes and other radiometers that produce signals in the form of voltages are not of concern in this respect since such signals can be time-resolved by oscilloscope presentation.

In order to protect a spectrographic film from sources of light, other than the ones of interest, total blockage of the light is desirable. The spectrographic entrance slit is usually a convenient place for a shutter since the slit width is small. A shutter that takes advantage of this fact is sketched in Figure 6.29. A single current-carrying wire acting as the shutter is placed over the slit. Placed adjacent to this flexibly mounted wire is a fixed wire connected in series with the first such that the current flow is in the same direction in both wires. Discharging a capacitor through this circuit causes the wires to repel one another and the one which is free is rapidly displaced. A similar effect can be achieved by placing the shutter wire in a strong magnetic field parallel to the direction of light. This same concept can be used to close a slit that is initially open by providing a mechanical stop to the displaced conductor. Closing times on the order of 5×10^{-6} seconds can be obtained[6.32]. A modification of the design which permits the shutter to open and then close is to use the moving wire to displace a slide with a second slit cut into it. As this slide is pushed past the fixed slit, the shutter effectively opens and closes[6.33, 6.34].

A similar shutter, but on a larger scale, is one in which a light, stiff blade with appropriate openings is placed in tracks across an aperture. An explosive charge then drives the blade across the aperture[6.35, 6.36]. The dimensions of the openings in the blade can be matched to the translational rate of the blade to give a specified opening rate, open dwell time, and closing time. Figure 6.30 shows the salient features. A shutter of this type has closed a 3 mm hole in 1×10^{-4} seconds.

Another technique for shuttering spectographic openings is shown in Figure 6.31. In this arrangement an explosive squib is oriented so that the gases generated blow against a bi-stable shutter. Its usual mode of operation is to close the aperture after the event of interest. A closing time of about 3 milliseconds from receipt of signal for a 40 mm-diameter hole has been achieved.

There are several other types of shutter that depend on blocking out the incoming radiation by an irreversible action. One of these consists of a tube through which the light passes. On receipt of a signal an explosive charge, wrapped around the tube, causes it to collapse. (This technique may also be applied to locking gas flow into a container). A light foil cylinder can be made to collapse in a similar manner by placing it within a short coil. Discharging a capacitance through the coil causes the foil to collapse. Another approach uses shock loading from an explosive to destroy the transmissivity of a normally clear sheet of glass or plastic placed in the optical train[6.37]. The use of an exploding wire to activate a shutter is discussed in Chapter 9, and shown schematically in Figure 9.6.

6.5.2 Electro-Optical Shutters

Electro-optical shutters include Kerr cells and image-converter tubes.

6.5.2.1 Kerr-Cell Shutters

The method of operation of Kerr cells has been well discussed in the literature[6.38]. Briefly, they have the capability of rotating plane-polarized light on application of a high voltage across a pair of plates along two sides of the cell. The cell is placed in the light path between crossed polarizers, which normally block the light. When voltage is applied to the cell, rotation of the polarization of the light by the cell permits it to pass through the second polarizer. Hence, the shutter is opened when the voltage is applied.

The rotation of the plane of polarization by the cell is a function of the type of Kerr-effect fluid it contains, the magnitude of the voltage gradient impressed at right angles to the light path, and the length of the plates. These factors are adjusted to bring about 90^{o} rotation of the plane of polarization.

Kerr cell shutters may be placed at the image of the light source in focused shadowgraph systems, where the aperture required is small. The duration of the light pulse which they pass depends on the duration of the applied high voltage pulse, which can be as short as one or two nanoseconds. These shutters have the disadvantage, however, of heavily absorbing light, especially at short wave-lengths. Since they pass only plane polarized light, a loss of 50% of the incident intensity is inherent. Further losses occur by absorption in the fluid and by reflection and absorption at the polarizers. The transmission through the fluid drops rapidly with wavelength below about 3500 Å. The polarizer transmission also falls off in the ultraviolet. Figure 6.32 shows the measured transmission of a representative shutter at the present state of the art as a function of wavelength. The sharp reduction at 3200 Å is probably due to absorption of the Kerr effect fluid. Unfortunately, much of the energy of a typical spark unit is at wavelengths shorter than 3000 Å (0.30μ), as shown in Figure 6.20

It should be noted that the Kerr cell and polarizers act as a refractive optical unit and can introduce aberrations and distortion into the optical system.

If the polarizers are made of crystal, their acceptance angle is small (on the order of 10 degrees), which limits the f/number of the optical system with which it is to be used. The size of the polarizer largely determines the cost of the whole unit because its cost varies as the cube of the dimension. Cost of the cell itself is not so critically dependant on size.

The improvement in picture quality made possible by the use of Kerr-cell shutters is shown in Figure 6.33. The two photographs are of the same burning aluminum model in flight. The optical system used is a parallel light focused shadowgraph of the type shown schematically in Figure 6.10. In obtaining the first picture, a 3 mm aperture was placed around the image of the source. In the second, the aperture was replaced by a 20-nanosecond-exposure Kerr cell.

6.5.2.2 *Image-Converter Cameras*

In an image-converter tube, the photons of an image focused on its receiving screen cause the proportional emission of electrons. Application of a voltage pulse directs these electrons, and effectively amplifies them in the process, to the emitting screen of the tube where they activate the phosphors of the screen, which emit photons, forming a duplicate of the image existing on the receiving screen at the time of the voltage pulse. Voltage pulses as short as a few nanoseconds in duration have been used successfully. Shuttering is achieved by operating on the electrons rather than on the photons[6,7].

One form of image converter tube uses deflection plates to translate the beams of electrons to one side, allowing consecutive pictures of the same event to be recorded on the emitting screen without overlap. Figure 6.34 shows three sequential photographs of a model taken with such an image converter camera. The exposure of each image was 0.2 microsecond and the time delay between exposures was 5 microseconds.

6.6 SPATIAL REFERENCE SYSTEMS - R. I. Sammonds

Since one of the most basic uses of ballistic ranges is to record motion histories of models flown through them, both out of interest in the motion itself and for determination of the aerodynamic forces and moments acting on the models, it is important to provide the means for accurate position and attitude measurement in the spark photographs. The means for doing this are the spatial reference systems.

The accuracies demanded of these systems are, in some cases, the greatest that the ingenuity of the system designer can provide. The reason is simple: Accuracy in the measuring system is essential to accuracy of the aerodynamic data obtained. The more accurate the measuring system, the more marginal the cases that can be treated. Accurate systems are especially necessary in very short ranges, such as counterflow facilities, where the combination of maximum measurement precision and lightweight model design may be required to make possible the collection of accurate results. On the other hand, short ranges make it easier to maintain high accuracy. Accuracies achieved in these systems have been better than 0.1 mm (100 microns) in the three linear coordinates, and better than 0.1^{o} in attitude angles.

Spatial reference systems are generally based on the following properties and principles:

(a) The straightness of wires drawn taut (e.g. grid wires), and the straightness and verticality of plumb lines;

(b) The accurately known form of catenaries;

(c) The dimensional stability of statically determinate steel structures;

(d) The principle of self-recording of random small changes in optical alignment and shifting of the reference system itself.

Where reduced accuracy is acceptable, the reference system may be established and aligned using surveyors' instruments and thereafter presumed stable so that subsequent distortions are not recorded. In such cases,

distance fiducial marks can be placed in the photographic or yaw card stations, using a steel measuring tape, and the range centerline can be established by identifying the extension of the gun axis (boresite) at each station without any instruments other than the practiced eye of a technician.

On the other hand, ranges required to produce the best possible translational and rotational histories must be equipped with stable and accurate fiducial systems. Although most systems depend on similar concepts, their actual configurations are largely dictated by the type and size of test section, the type of shadowgraph system, and the accuracies required. Because of the adaptation of fiducial systems to conform to other range requirements, the descriptions to follow will be of particular systems which have proven reliable. The systems have been adapted to both direct-projection and focused shadowgraphs and to parallel and conical light beams. We will first examine a collimated (parallel) light system, which may be either direct-projection or focused.

6.6.1 Fiducial System for Collimated Light Field

In collimated light systems, the downrange distance, x, between adjacent stations is conveniently determined from images in the shadowgraph pictures of plumb lines hanging at carefully gaged locations along a continuous steel rod. The lateral and vertical displacements, y and z, may be measured relative to taut wires above and beside the flight path running roughly parallel to the range axis. The plumb lines provide a reference direction for the pitch angle, θ, in the side photographs, and the taut wire above the flight path provides a reference for the yaw angle, ψ. Such a system, in which the photographic station components lie outside the range enclosure, or test section, is illustrated in Figure 6.35 where the complete arrangement of bars, plumb bobs and wires for two stations is shown schematically. The other station components are deleted for clarity.

All plumb-line pairs are at identical spacing, S, as shown in Figure 6.35. This spacing is determined by the grooves machined in the sleeves on the rod. The spacing, S', between corresponding plumb lines in adjacent stations, determined by the spacing of the sleeves along the rod, is also constant. The rods from which the plumb lines are suspended are offset longitudinally (i.e., in the flight direction) a small amount so that the line images will not be superimposed in the shadowgraph picture. The two catenary wires, on the opposite sides of the flightpath, are adjusted for proper position and tension so that they have the same sag and are parallel. Again the wires are offset slightly (vertically) so that the two images are displaced in the shadowgraph. The taut wires above and below the flightpath are arranged in pairs, two above the flightpath and two below. These wires are installed so that the two pairs are parallel and have the same spacing, t. The pairs are offset laterally so that their images are not superimposed. Typical shadowgrams with this arrangement are shown in Figure 6.36 where wires, A, C, and F are the plumb lines and catenary, respectively, on the side of the test section nearest the film and B, D, and E are the plumb lines and catenary on the other side. Similarly, H and J are the taut wires above and G and I the taut wires below.

The principle underlying this particular fiducial system stems from the necessity of accurately locating the model in space when the light beams are neither exactly collimated nor perpendicular to the range centerline. Although it is entirely possible to have the optical system perfectly collimated and aligned, it is more practical to install a fiducial system that can be used to correct the model position for small angular variations due to misalignment and lack of collimation. This, in fact, is the reason for the multiple wire system described here. With this system of reference wires, the calibrated spacing between the plumb lines and the taut wires on the sides of the range nearest to the film plane can be related to the spacing of these wires in the shadowgraph picture to determine the magnification of the optical system. Further, relating the spacing of the plumb lines and taut wires on either side of the range, in the shadowgram, (corrected for magnification) will indicate the accuracy of collimation of the light beams. Relating the amounts of offset of the plumb lines, catenaries and taut wires, as measured from the shadowgram, to the calibrated offset distances will determine the alignment of the optics. The working equations for these corrections are developed in detail below.

Referring to Figure 6.37, it can be seen that the mathematical expressions necessary to determine the model orientation in space, Δx, y, z, corrected for light angularity and lack of collimation ($\epsilon_1 \neq \epsilon_2$) are as follows:

$$\Delta x = AM - (y + \Delta y_1)\,\epsilon_x \tag{6.1}$$

$$z = FM + (y + \Delta y_2)\,\epsilon_z \tag{6.2}$$

$$y = GM - (z + \Delta z)\,\epsilon_y , \tag{6.3}$$

where ϵ_x, ϵ_y, ϵ_z are small-angle approximations for $\tan \epsilon$. Since each equation has two unknowns in it, we can determine y by substituting Equation (6.2) into Equation (6.3), which gives

$$y = \frac{GM - \epsilon_y\,(FM + \Delta z + \Delta y_2 \epsilon_z)}{1 + \epsilon_y \epsilon_z} . \tag{6.4}$$

Similarly, substituting Equation (6.3) into Equation (6.2) and rearranging we get

$$z = \frac{FM + \epsilon_z\,(GM + \Delta y_2 - \Delta z \epsilon_y)}{1 + \epsilon_y \epsilon_z} . \tag{6.5}$$

and substituting Equation (6.4) into Equation (6.1) gives

$$\Delta x = AM - \epsilon_x \left[\frac{GM + \Delta y_1 - \epsilon_y (FM + \Delta z - \Delta y_1 \epsilon_z + \Delta y_2 \epsilon_z)}{1 + \epsilon_y \epsilon_z} \right], \tag{6.6}$$

where

$$\epsilon_x = \epsilon_1 + K_1 (AM - AB) = \frac{AB - AB_c}{W_1} + K_1 (AM - AB)$$

$$\epsilon_y = \epsilon_4 + K_2 (GM - GH) = \frac{GH - GH_c}{W_3} + K_2 (GM - GH)$$

$$\epsilon_z = \epsilon_3 - K_1 (FM + EF) = \frac{EF - EF_c}{W_2} - K_1 (FM + EF)$$

and

$$K_1 = \frac{\epsilon_2 - \epsilon_1}{BD} = \frac{BD - BD_c}{W_1 (BD)}$$

$$K_2 = \frac{\epsilon_5 - \epsilon_4}{HJ} = \frac{HJ - HJ_c}{W_3 (HJ)} .$$

The definitions and the use of K_1 and K_2 assume linear variation in the angularity of the light beams.

For this analysis, the length increments AM, AB, and BD are measured in the plane formed by the plumb lines A and C; increments EF and FM are measured in the vertical plane containing the catenary wire, F; and increments GH, HJ and GM are measured in the horizontal "plane" containing the taut wires G and I. In reducing a set of test data, however, these lengths, or distances, are measured on the photographic film (e.g., Figure 6.36) so that the apparent distances between plumb lines, catenary wires, etc., must be corrected for the magnification of the image-forming optical system in order to determine the true distances used in the foregoing equations. This can be accomplished (Fig.6.37) by taking ratios of the known calibrated spacings of the plumb lines in the horizontal view, AC_c, and the taut wires in the vertical view, GI_c, to the apparent distances, AC_a and GI_a, read from the photographic film. The true distances are then obtained from

$$\left.\begin{aligned} AM &= AM_a \left(\frac{AC_c}{AC_a}\right); \quad AB = AB_a \left(\frac{AC_c}{AC_a}\right); \\ BD &= BD_a \left(\frac{AC_c}{AC_a}\right); \quad EF = EF_a \left(\frac{AC_c}{AC_a}\right); \\ FM &= FM_a \left(\frac{AC_c}{AC_a}\right); \quad GM = GM_a \left(\frac{GI_c}{GI_a}\right); \\ GH &= GH_a \left(\frac{GI_c}{GI_a}\right); \quad HJ = HJ_a \left(\frac{GI_c}{GI_a}\right). \end{aligned}\right\} \tag{6.7}$$

where $\frac{AC_c}{AC_a}$ is the magnification factor for the side film (horizontal view) and $\frac{GI_c}{GI_a}$ is the magnification factor for the bottom film (vertical view).

Since both Δx and z are determined from the side film, the assumption has been made that the magnification at this film plane is the same in both the horizontal (Δx) and vertical (z) directions. However, for certain optical systems where spherical aberration and coma effect due to off-axis mirrors are a problem the above assumption may lead to significant errors in the determination of EF and FM. A discussion of this problem is given at the end of Section 6.6.1.1.

6.6.1.1 Optical Distortion of Fiducial System

If the optical system includes windows through which light must pass, and if the windows are not perpendicular to the light path, or if the surfaces of the windows are not parallel (prism effect), or if distortions are present due to imperfections in the glass, error can arise in Δx, y, and z. The nonperpendicularity of the light path with respect to the window can come about from either systematic or random causes. If the range walls containing the windows are flared, as they are in a counterflow facility to allow for boundary layer growth, the windows are systematically inclined. If during construction of the tunnel the window walls are not aligned perfectly, there will be random variations in the window inclination. Although these errors are generally quite small the equations for Δx, y, and z (Equations (6.4) through (6.6)) will now be modified to account for

the refraction of the light through the windows. Consider the pair of windows included in the shadowgraph station schematic of Figure 6.38. We can see that

$$\Delta x = AN - (y + \Delta y_1) \tan \epsilon_x .$$

where $AN = AM + MN$

and MN is obtained as follows:

Since the angles ϵ_x and ϵ_t are small, the following relations apply:

$$i = \epsilon_x - \epsilon_t \quad ; \quad \mu = \frac{i}{r} \text{ (Snell's law of refraction)}$$

$$y' \approx t .$$

Thus, from the law of sines,

$$\frac{x'}{\sin (i-r)} = \frac{x'}{i - \frac{i}{\mu}} = \frac{y'}{\sin (90^o - i - \epsilon_t)} = \frac{y'}{1} = t$$

or

$$MN = x' = t\left(i - \frac{i}{\mu}\right) = t(\epsilon_x - \epsilon_t)\left(1 - \frac{1}{\mu}\right) ;$$

thus

$$\Delta x = AM + t(\epsilon_x - \epsilon_t)\left(1 - \frac{1}{\mu}\right) - \epsilon_x (y + \Delta y_1) . \tag{6.8}$$

Substituting for y (Eq. (6.4)) we get

$$\Delta x = AM + t(\epsilon_x - \epsilon_t)\left(1 - \frac{1}{\mu}\right) - \epsilon_x \Delta y_1 - \epsilon_x \left[\frac{GM - \epsilon_y (FM + \Delta z + \Delta y_2 \epsilon_z)}{1 + \epsilon_y \epsilon_z}\right] . \tag{6.9}$$

This now corrects Δx for the longitudinal taper of the test section and angularity of the light rays. If the convergence angle of the range walls remains constant and the windows are of uniform thickness, the correction due to ϵ_t will be the same for all stations and thus would not affect the relative model position.

If the windows have a component of inclination in a plane normal to the range axis, then corrections similar to that for Δx may be required also for y and z. Figure 6.39 has been drawn to represent the case where the window pairs are inclined by angles of ϵ_y and ϵ_z with respect to the vertical and horizontal light beams (which might occur, for example, if the range enclosure became warped or twisted about its axis). The situation is analogous to a perturbation of the light rays of Figure 6.37 due to the presence of windows. Thus,

$$y = GM + t\epsilon_y \left(1 - \frac{1}{\mu}\right) - \epsilon_y (z + \Delta z) ,$$

$$z = FM - t\epsilon_z \left(1 - \frac{1}{\mu}\right) + \epsilon_z (y + \Delta y_2) .$$

Substituting each of these equations into the other gives

$$y = \frac{GM - \epsilon_y \left[FM + \Delta z + \epsilon_z \Delta y_2 - t\left(1 - \frac{1}{\mu}\right)(1 + \epsilon_z)\right]}{1 + \epsilon_y \epsilon_z}$$

$$z = \frac{FM + \epsilon_z \left[GM + \Delta y_2 - \epsilon_y \Delta z + t\left(1 - \frac{1}{\mu}\right)(\epsilon_y - 1)\right]}{1 + \epsilon_y \epsilon_z} .$$

Substituting this value of y into the basic equation for Δx (Eq. (6.8)) gives,

$$\Delta x = AM + t(\epsilon_x - \epsilon_t)\left(1 - \frac{1}{\mu}\right) - \epsilon_x \Delta y_1 - \epsilon_x \left\{\frac{GM - \epsilon_y \left[FM + \Delta z + \epsilon_z \Delta y_2 - t\left(1 - \frac{1}{\mu}\right)(1 + \epsilon_z)\right]}{1 + \epsilon_y \epsilon_z}\right\} . \tag{6.10}$$

This set of equations corrects y and z for light angularity and Δx for both wall convergence and light angularity. As previously stated, however, these corrections may be so small in actual practice that they can be ignored.

Minor irregularities in the windows and mirrors, as well as spherical aberration due to the use of spherical mirrors, and the coma effect due to an off-axis optical system cause distortions in the shadowgraphs that can lead to significant errors. These distortions can be compensated for by mapping the field of view of each station using a calibrated grid or perforated plate placed on the axis of the range (flightpath). The grid is photographed with the shadowgraph system. Measurements made on the photograph are then compared with the known dimensions of the grid.

6.6.2 Fiducial System for Conical Light Field

Conical projection shadowgraphs, like those described in Section 6.3.1, are often used. For a conical light field several types of reference system are feasible. For instance, where reflecting surfaces (CARDE Aeroballistic Range[6.2] and NOL 1000 ft Hyperballistics Range[6.12]) or fresnel lenses (VKF 1000 ft Hypervelocity Range[6.18]) are used, marks or grids can be fastened to them which, when related to the surveyed position of the light source provide by themselves a good earth-fixed reference. A notched fiducial bar located at the intersection of the side and bottom film planes (BRL Aerodynamics Range[6.11], and NOL Pressurized Ballistics Range[6.12]) can also be used to establish the origin and orthogonality of the local station coordinate system. Each self-contained station of this type is aligned to the optical axis (centerline) of the range through reference to the two faces of the fiducial bar[6.11]. Systems of this nature rely on the stability of the mounting system and no account is taken of short-term shifts of the station components relative to the range axis. Where accuracy demands improved inter-station relationship, an auxiliary reference system consisting of plumb lines accurately spaced at each station, and a catenary wire, similar to that previously described for the collimated light system, can be added.

If the conical light field is produced by a point light source and there are no distorting optical elements between the light source and the fiducial references, the position and attitude of the model in the station coordinate system, as they appear in the shadowgram, need only be corrected for magnification due to the conical projection in order that they be determined accurately. However, since the magnification of a model image may differ from point to point on the film (significant for long bodies at high angle of attack) the projected angle shown in the shadowgraph picture may be distorted. This distortion must be taken into consideration when determining the corrected angle.

Once the position and attitude of the model have been established within each station coordinate system, they must then be related to determine the overall model motion and trajectory. In a rigid system, this would be accomplished directly by having aligned the stations in the range shell. However, when a secondary reference system (range coordinates) is used to improve the interstation relationship, the model position and attitude previously determined with respect to the station coordinate system must be translated and rotated into the secondary reference system.

The working equations for these operations are developed in detail below in two parts. Section 6.6.2.1 covers the equations necessary to accurately locate the position and attitude of the model in the station coordinate system, and Section 6.6.2.2 derives the equations necessary to relate the model position and attitude in each station to the range coordinate system in order to determine the overall model motion and trajectory. If a rigid system is under consideration then only the first part is needed.

6.6.2.1 Station-Coordinate System

The particular system under consideration is a simple direct shadowgraph which uses grid wires adjacent to the orthogonal film planes to establish the station reference system. The station axes ($\Delta x'$, y', and z'), shown in Figure 6.40, are defined as follows:

The y' axis is the line passing through the side spark perpendicular to the side film and is positive to the right when looking downrange. The z' axis is the line passing through the top spark perpendicular to the bottom film and is positive upwards. The y' axis and the z' axis intersect at $0'$, the origin of the station coordinate system, thus forming the y'-x' plane. The $\Delta x'$ axis is the line passing through $0'$ perpendicular to the y'-z' plane and is positive downrange. Grid wires just above the side and bottom film planes mark the intersections of the $\Delta x'$-y' plane, the $\Delta x'$-z' plane and the y'-z' plane with the side and bottom films. The plane containing the bottom grid wires is parallel to the $\Delta x'$-y' plane and the plane containing the side grid wires is parallel to the $\Delta x'$-z' plane. Thus, the grid wires form a precisely orthogonal set of reference lines.

The apparent model position and orientation (Δx_a, y_a, z_a, θ_a, ψ_a), as measured from the shadowgram, are corrected for the conical light projection (magnification) within the station coordinate system in the following manner:

In the notation of Figure 6.41, the relationship for the magnification of the coordinates of a single point, m, is

$$\frac{y'}{y_a} = \frac{C_B - z'}{F_B}, \qquad \frac{z'}{z_a} = \frac{C_S - y'}{F_S} = \frac{\Delta x'}{\Delta x_a}, \tag{6.11}$$

where the subscript, a, stands for the apparent values read from the film. At this point, it should be noted that the film platens must be very flat in order that the apparent values of Δx, y, and z may be accurate. Any waviness in the film will show up as a waviness in the image of the grid wire in the shadowgram.

Solving Equations (6.11) simultaneously gives expressions for the location of the model in the station coordinate system.

$$\Delta x' = \Delta x_a\left(\frac{z'}{z_a}\right) = \Delta x_a\left(\frac{C_S F_B - y_a C_B}{F_S F_B - y_a z_a}\right),$$

$$y' = y_a\left(\frac{C_B F_S - z_a C_S}{F_S F_B - y_a z_a}\right),$$

$$z' = z_a\left(\frac{C_S F_B - y_a C_B}{F_S F_B - y_a z_a}\right), \tag{6.12}$$

where C_S, F_S, C_B, and F_B are calibrated values. The magnification of the coordinates of two points on a model will be different if they are at different distances from the film plane. It would also appear from this analysis that it would be impossible to determine unequivocally the magnification of a model if there were no specific points through which the light rays from both sparks would pass; for instance, a large diameter sphere. However, by suitable mathematical manipulation, it is possible to arrive at an expression that can be used to determine the sphere diameter

$$d = 2r = 2\left[\frac{\sin \phi_3}{\cos \phi_4}\left(\frac{C_B - C_S \tan \alpha_4}{1 - \tan \alpha_4 \tan \phi_4}\right)\right], \tag{6.13}$$

where, with reference to Figure 6.42,

$$\phi_3 = \frac{1}{2}\left[\tan^{-1}\left(\frac{OC}{F_B}\right) - \tan^{-1}\left(\frac{OA}{F_B}\right)\right],$$

$$\phi_4 = \frac{1}{2}\left[\tan^{-1}\left(\frac{OC}{F_B}\right) + \tan^{-1}\left(\frac{OA}{F_B}\right)\right],$$

$$\alpha_4 = \frac{1}{2}\left[\tan^{-1}\left(\frac{OD}{F_S}\right) + \tan^{-1}\left(\frac{OF}{F_S}\right)\right],$$

where OA, OC, OD, and OF are measured from the film and F_S, F_B, C_S, and C_B are calibrated values.

Concomitantly, when the magnification at the nose of a body differs from that at the base, the result is a distortion of the angular position of the model projected onto the film. This angle distortion can be quite large for long bodies at high angles of attack; it also changes with Δx, y, and z. The equations relating the apparent angles of pitch, θ_a, and yaw, ψ_a, and the true angles of pitch, θ', and yaw, ψ', and the projected pitch angle, θ'_p (in the station coordinate system) are as follows:

$$\psi' = \tan^{-1}\left[\frac{(C_S - y')(C_B - z')\tan\psi_a + (C_S - y')(\Delta x' \tan\psi_a - y')\tan\theta_a}{(C_S - y')(C_B - z') - (\Delta x' \tan\theta_a - z')(\Delta x' \tan\psi_a - y')}\right]$$

$$\theta'_p = \tan^{-1}\left[\frac{(C_S - y')(C_B - z')\tan\theta_a + (C_B - z')(\Delta x' \tan\theta_a - z')\tan\psi_a}{(C_S - y')(C_B - z') - (\Delta x' \tan\theta_a - z')(\Delta x' \tan\psi_a - y')}\right]$$

$$\theta' = \tan^{-1}\left[\tan\theta'_p \cos\psi'\right] = \tan^{-1}\left[\frac{\tan\theta'_p}{\sqrt{(1 + \tan^2\psi')}}\right]$$

$$\alpha'_r = \tan^{-1}\sqrt{(\tan^2\psi' + \tan^2\theta'_p)}, \tag{6.14}$$

where the angle convention is shown in Figure 6.43. Since the angles of yaw and pitch are dependent on each other, it is necessary to decide on some angle sequence in order to derive the above equations. For this particular analysis, the model was assumed to have first yawed through some angle, ψ', and then pitched through some angle, θ'. In this manner, the apparent angle of yaw, ψ_a, seen in the bottom film, is a direct projection of the true angle of yaw, ψ', whereas the apparent pitch angle, θ_a, in the side film, is the projection of the angle, θ'_p.

6.6.2.2 *Range-Coordinate System*

The relationship of the photographic stations to one another may be accomplished by a second reference system, somewhat like that described in Section 6.6.1, supported from the range structure. A system consisting of plumb lines, suspended from a calibrated steel rod, and a single catenary wire, is shown in Figure 6.44. One plumb line is photographed in the side view of each station, while the catenary is photographed in both views. The model position and attitude, determined with respect to each station coordinate system, may then be translated (x_0, y_0, z_0) and rotated $(\epsilon_1, \epsilon_2, \epsilon_3)$ into the common range coordinate system in the following manner.

The local range axes, Δx, y, and z (Fig. 6.44) are determined by the catenary wire, stretched the length of the range under a known tension, and the plumb lines. The vertical plane containing the catenary and parallel to the plumb line is the Δx-z plane. The y-z plane is the plane perpendicular to the Δx-z plane which contains the plumb line. The origin, O, of the local range coordinate system is defined to be the point at which the catenary wire intersects the y-z plane. The sign convention for the range axes is the same as that for the station axes. (Correction must be made for the sag of the catenary wire when determining z values for the entire range).

The equations to accomplish the translation and rotation of the model center-of-gravity coordinates from station axes to range axes are:

$$\left.\begin{aligned} \Delta x_{CG} &= \Delta x'_{CG} + x_0 + y'_{CG}\epsilon_1 + z'_{CG}\epsilon_2 \\ y_{CG} &= y'_{CG} + y_0 - \Delta x'_{CG}\epsilon_1 - z'_{CG}\epsilon_3 \\ z_{CG} &= z'_{CG} + z_0 - \Delta x'_{CG}\epsilon_2 + y'_{CG}\epsilon_3 \,. \end{aligned}\right\} \tag{6.15}$$

where

$$\left.\begin{aligned} \Delta x'_{CG} &= \Delta x' + l\cos\psi'\cos\theta' \\ y'_{CG} &= y' + l\sin\psi'\cos\theta' \\ z'_{CG} &= z' + l\sin\theta' \,, \end{aligned}\right\} \tag{6.16}$$

and l is the distance from a measurement-reference point on the model axis ($\Delta x'$, y', z') to the center of gravity of the model ($\Delta x'_{CG}$, y'_{CG}, z'_{CG}). The coordinates x_0, y_0, and z_0 are the range-system coordinates of the station-system origin, O'. The angles, ϵ_1, ϵ_2, and ϵ_3, are, respectively, the angles of yaw, pitch, and roll of the station system with respect to the range system.

In order to solve these equations for Δx_{CG}, y_{CG}, and z_{CG} it is necessary first to determine x_0, y_0, and z_0 and ϵ_1, ϵ_2, and ϵ_3. If we notice that these equations for Δx_{CG}, y_{CG}, and z_{CG} hold not only for the center-of-gravity location at the model but for any point in space, we need only find a point, or points, one or more of whose range coordinates are known and all of whose station coordinates are known in order to solve for x_0, y_0, and z_0. To accomplish this, we define two points, Q and W, illustrated in Figure 6.45.

Define Q to be the point of intersection of the plumb line with the $\Delta x'$-y' plane and define W to be the point of intersection of the catenary wire with the y'-z' plane. Further, let H_Q be the distance from Q to the side film. Since Q is on the plumb line, all of whose points are by definition in the y-z plane, it follows that $\Delta x_Q = 0$. The station coordinates of Q (see also Figure 6.41) are:

$$\left.\begin{aligned} \Delta x'_Q &= \Delta x_{Qa}\,\frac{F_S - H_Q}{F_S} \\ y'_Q &= -F_S + C_S + H_Q \\ z'_Q &= 0 \,. \end{aligned}\right\} \tag{6.17}$$

Similarly, since W is on the catenary wire, we have $y_W = z_W = 0$ and the station coordinates of W are given by:

$$\left.\begin{aligned} \Delta x'_W &= 0 \\ y'_W &= y_{W_a}\left(\frac{C_B F_S - z_{W_a} C_S}{F_S F_B - y_{W_a} z_{W_a}}\right) \\ z'_W &= z_{W_a}\left(\frac{C_S F_B - y_{W_a} C_B}{F_S F_B - y_{W_a} z_{W_a}}\right) . \end{aligned}\right\} \tag{6.18}$$

We may now use equations (6.15) to solve for x_0, y_0 and z_0 as follows:

$$\left.\begin{aligned} x_0 &= \Delta x_Q - \Delta x'_Q - y'_Q\epsilon_1 - z'_Q\epsilon_2 = -\Delta x'_Q - y'_Q\epsilon_1 \\ y_0 &= y_W - y'_W + \Delta x'_W\epsilon_1 + z'_W\epsilon_3 = -y'_W + z'_W\epsilon_3 \\ z_0 &= z_W - z'_W + \Delta x'_W\epsilon_2 - y'_W\epsilon_3 = -z'_W - y'_W\epsilon_3 \,. \end{aligned}\right\} \tag{6.19}$$

Substituting these values of x_0, y_0 and z_0 into Equations (6.15) and adding Δz (the correction for catenary sag) to z_{CG} gives:

$$\left.\begin{aligned} \Delta x_{CG} &= \Delta x'_{CG} - \Delta x'_Q + z'_{CG}\epsilon_2 + (y'_{CG} - y'_Q)\,\epsilon_1 \\ y_{CG} &= y'_{CG} - y'_W - \Delta x'_{CG}\epsilon_1 - (z'_{CG} - z'_W)\,\epsilon_3 \\ z_{CG} &= z'_{CG} - z'_W - \Delta x'_{CG}\epsilon_2 + (y'_{CG} - y'_W)\,\epsilon_3 + \Delta z\ . \end{aligned}\right\} \qquad (6.20)$$

Note that there is a slight error in z_{CG} due to the fact that Δz is calculated at the plumb line instead of at W. However, this error is sufficiently small (0.25 mm) regardless of station size or configuration, as long as the plumb line is within a few centimeters of the y'-z' plane, that it may be neglected.

We are now ready to compute ϵ_1, ϵ_2, and ϵ_3, where again ϵ_1 is the angle of yaw of the station coordinate system with respect to the range coordinate system, ϵ_2 is the angle of pitch, and ϵ_3 is the angle of roll. The sign conventions for these angles are as follows:

ϵ_1 is positive when the Δx axis, viewed from above, is rotated clockwise from the $\Delta x'$ axis.

ϵ_2 is positive when the z axis, viewed from the side spark, is rotated counter clockwise from the z' axis.

ϵ_3 is positive when the z axis, viewed looking along the direction of the positive x axis, is rotated clockwise from the z' axis.

Notice, first, that these angles are small, and thus we can reasonably make the assumption that they are independent of each other; and second, that ϵ_3 and H_Q cannot be measured from either the side or bottom film. Therefore, ϵ_3 must be calculated from independent mechanical measurements made in the range, from which we also obtain H_Q, the distance between the plumb line and the side film platen. The assumption is made that although the range may bend about the y and z axes, or change length due to expansion or contraction, it is not as likely to twist about the Δx axis importantly. Additional reference wires could be included to eliminate this assumption, but actual measurements have shown that twisting is negligible in the only case studied by the authors.

From Figures 6.46 and 6.47 we can see that the apparent values of ϵ_1 and ϵ_2 are given by:

$$\left.\begin{aligned} \tan \epsilon_{1_a} &= \frac{Y_L - Y_R}{X_{GRID}} \\ \tan \epsilon_{2_a} &= \frac{Z_L - Z_R}{X_{GRID}}\ , \end{aligned}\right\} \qquad (6.21)$$

and z_{W_a} and y_{W_a} are given by

$$\left.\begin{aligned} y_{W_a} &= C_1 Y_L + C_2 Y_R - Y_{GRID} \\ z_{W_a} &= C_1 Z_L + C_2 Z_R\ , \end{aligned}\right\} \qquad (6.22)$$

where C_1 and C_2 are constants depending on the grid wire spacing. Using the Equations (6.14) and the assumption that ϵ_1 and ϵ_2 are small angles we may now solve for ϵ_1 and ϵ_2 as follows:

$$\left.\begin{aligned} \epsilon_1 &= \frac{(C_S - y'_W)(C_B - z'_W)\tan\epsilon_{1_a} + (C_S - y'_W)(\Delta x'_W \tan\epsilon_{1_a} - y'_W)\tan\epsilon_{2_a}}{(C_S - y'_W)(C_B - z'_W) - (\Delta x'_W \tan\epsilon_{1_a} - y'_W)(\Delta x'_W \tan\epsilon_{2_a} - z'_W)} \\ \epsilon_2 &= \frac{(C_S - y'_W)(C_B - z'_W)\tan\epsilon_{2_a} + (C_B - z'_W)(\Delta x'_W \tan\epsilon_{2_a} - z'_W)\tan\epsilon_{1_a}}{(C_S - y'_W)(C_B - z'_W) - (\Delta x'_W \tan\epsilon_{1_a} - y'_W)(\Delta x'_W \tan\epsilon_{2_a} - z'_W)} - \frac{dz}{dx}\ . \end{aligned}\right\} \qquad (6.23)$$

where dz/dx represents the slope of the catenary at the plumb line.

Since Equations (6.14) determined the model attitude angles in the station coordinate system (ψ', θ'_p, θ', α'_r), these angles must be corrected for the rotation of the station. Thus

$$\begin{aligned} \psi &= \psi' - \epsilon_1 \\ \theta_p &= \theta'_p - \epsilon_2 \\ \theta &= \tan^{-1}(\tan\theta_p \cos\psi) \end{aligned}$$

and

$$\alpha_r = \tan^{-1}\sqrt{(\tan^2\psi + \tan^2\theta_p)}\ . \qquad (6.24)$$

6.6.2.3 Non-Orthogonal Projection

Although most ballistic ranges have orthogonal-viewing shadowgraph stations it is sometimes desirable, or necessary, to use other viewing geometries. One facility in particular, the 122-meter CARDE Range 5 uses a non-orthogonal arrangement such that two light sources produce two images of the model on one piece of film[6.16] (see Figure 6.7) The proper location of the light sources, film plane and the fiducial system, consisting of two plumb lines and two catenary wires, result in geometrical relationships through which the spatial location and attitude of the projectile can be determined. This "stereo" system is explained in detail in Reference 6.16. There are, however, no real differences in principle between this system and that discussed in Section 6.6.2.1.

6.6.3 Error Sources and Determination of Accuracy

Systematic errors in recording on photographic film the position and attitude of a model in space are incurred to the degree that the recording system does not conform to the geometric relationships assumed for it. Such errors are introduced by optical refraction of light rays and by misalignment of the photographic and fiducial elements of the system. These errors must be accounted for by calibration, either through calculation, or by direct comparison of quantities measured in space with those deduced from measurements on the film. The calibration itself is, of course, subject to small residual systematic errors.

Significant random errors also may accrue from various sources. If a vibration environment exists, care must be exercised to prevent transient distortions of the reference system. Such problems may arise, for instance, in counter-flow facilities, and in transonic or subsonic tests where shock waves and pressure fields about the model may disturb an exposed reference system.

Apart from the effects of dimensional changes in the photographic film during processing, errors can arise if the film is allowed to curl or is not held precisely in the image plane during exposure. This is particularly true of a conical projection system. Complete or partial compensation for film misalignment can sometimes be effected by appropriate design and placement of the reference grid, as, for example, in a focused shadowgraph.

The accuracy of the system, once installed and calibrated, may be assessed by the consistency of the data which it produces or by artificial tests. The accuracy of the y and z measurements, for instance, can be checked by photographing catenary wires stretched through the range. A heavy projectile having low drag can be used to check the distance measurement, Δx, as well as the y and z measurements. This technique is particularly effective if the range can be evacuated.

If accurate account is kept of the apparent residual errors in the motion fit to the measured coordinates in all the stations for all the tests, systematic errors at a given station can be identified (cf. Section 7.11.5). Once the bias inserted into the results by a given station error is well documented, an arbitrary correction can be applied to the measurements made at this station. The running account of residual errors also permits early detection of changes in optical alignment and other shifts in the system which might degrade overall performance.

It should be noted that the two fiducial systems described in detail, herein, are designed to get the maximum accuracy available from the facility. The degree of attention to be given to accurate measurement systems depends entirely on the uses intended for the facility under consideration.

6.7 TIME- AND VELOCITY-MEASURING DEVICES – C.S.James

The most rudimentary ballistic-range test requires the simple determination of a velocity, while a more elaborate test usually calls for a complete time history of the projectile flight, through which various photographic and photometric measurements may be mutually related and used to study the projectile behavior. Time intervals of interest vary from several seconds for a large outdoor range to a fraction of a microsecond for a short enclosed range. In some tests, time resolution to the nearest 10^{-9} sec or less is desirable.

The one feature common to all modern ballistic time-measuring devices is an electrical or electronic time base. This time base can be simply the frequency of the power source, or it can be an oscillator controlled by a tuning fork or crystal, depending on the precision required. Beyond this common point considerable variety is found in the manner with which current systems meet their particular requirements. Some of these are purely electronic[6.1, 6.39, 6.40, 6.41]; others are fundamentally optical[6.42, 6.43, 6.44, 6.45]. They may be single-channel units capable of measuring one time interval, or multichannel units capable of measuring 50 or more time intervals[6.18]. Some units measure the time interval required to move a given distance[6.40, 6.42, 6.43]; others measure the distance covered in a given time interval[6.46].

While electronic counting or optical recording techniques are employed in the large majority of systems, two additional methods may be identified. Oscilloscopes, as opposed to counters, have been used both in interior ballistics, in conjunction with microwave interferometry[6.41, 6.47], and, to a limited extent, in the aerodynamic range[6.45, 6.48] to record and display time increments. Doppler Radar techniques, which have long been useful in large outdoor ranges over great distances, have found increasing application in the laboratory[6.39, 6.49, 6.50]. Applicability of this method in enclosed ranges is enhanced as the techniques for producing and transmitting microwave beams of shorter wavelength and narrower beam width improve.

Representative systems which utilize each of these techniques are described briefly in the following sections.

6.7.1 Electronic-Counter Chronograph

The electronic-counter chronograph, because of its flexibility, reliability, and simplicity of operation is the most widely used time-measuring device in ballistic-range work. Commercial units are available which are capable of recording, in digital form, time increments as long as 1 sec to as many as seven significant figures, on the one hand, or of resolving a time increment to the nearest 10 or 20 nsec, on the other. A typical hookup for a single-channel counter is shown in Figure 6.48 where the optical arrangement represents half of a typical orthogonal-viewing photographic station. The counter, together with those at all other stations, is started by a signal from a point in the launcher cycle, or from a sequencer or other reliable source. The counter is stopped upon the arrival of the projectile at the photographic station by a signal either from the shutter, if one is used, or from the light source. The element which controls the precise time of film exposure is selected as the signal generating element to minimize error in the time-position-attitude relationship. The interstation time increment is obtained by subtraction of adjacent counts. There are other ways of connecting and starting the counters, but the one described is believed the most reliable, in terms of both minimizing data loss due to individual station malfunction, and of accuracy in time measurement by minimizing the uncertainty due to tallied or untallied fractional counts.

While there is great flexibility in the single-channel counter, manual reading is a potential source of error when many photographic stations and counters are employed. A solution to this problem is the multiple-event digital chronograph developed for the VKF 1000-foot hypervelocity range[6.18, 6.51], which receives annunciation of projectile arrival at any of 59 measurement stations and presents the corresponding times in tabular form immediately after the shot. This system incorporates a principal 10-MHz counter which is gated by the event signals to record successive time intervals, and a secondary counter which continues the time-base count while each recorded interval in the principal counter is being unloaded to a core storage. Events must be separated by at least the cycle time for this operation, which is 50×10^{-6} sec. Time-interval resolution is 2×10^{-7} sec.

6.7.2 Optical Chronographs

Chronographs have been designed which combine optical recording with an electronic time base. One design uses a rotating prism as the time-position link. Another employs a reel-type streak camera for this purpose.

6.7.2.1 Rotating-Prism Chronograph

A rotating prism chronograph[6.45] was employed in the first Ames Supersonic Free-Flight Wind Tunnel and served four photographic stations. Figure 6.49 is a schematic of this system, showing one of the photographic stations. The time base in this system was an electronic oscillator which controlled the pulsing of a mercury-arc lamp (Mazda BH-6) usually at 50 kHz. Light from the pulsed lamp and from each spark source was directed along a common vertical path to a rotating prism and brought to focus on a strip of 35-mm film held against the inner 4.5-meter circumference of a stationary cylindrical drum. Through the combined pulsing of the lamp and rotation of the prism a train of exposed spots, or pips, was spread along the film. The spacing of adjacent pips represented one period of the oscillator, 20 μsec. The firing of each station spark put an additional pip on the film. A segment of such a 35-mm film record is reproduced in Figure 6.50. Flight time of the projectile between stations was determined by counting the full and interpolating the fractional time-base intervals between station pips.

To realize the maximum precision of the system and yet not risk loss of data by overlapping of the record, it was necessary to spread the record of station pips over the full circumference of the drum, but no more. To do this required a reasonably good prediction of the velocity of the projectile, so that the proper rotational speed of the prism could be established. Overlap of the record was prevented by opening a magneto-mechanical shutter just prior to the arrival of the projectile at the first station, and then quenching the pulsing lamp after the prism has subsequently made one complete turn. With a good film record this system was capable of time resolution to the nearest 10^{-7} sec over a total period of 4 msec with the prism turning at 15,000 rpm.

6.7.2.2 Streak-Camera Chronograph

The streak-camera chronograph was developed at the US Naval Research Laboratory (NRL) and evolved from a drum-camera "streak-spot" technique[6.52]. As presently constituted, it is in use both at NRL[6.42, 6.43] and at the Air Force Materials Laboratory[6.44]. In essence, the chronograph functions as follows: As a projectile moves past each successive recording station, its shadow image is projected onto a moving strip of film, together with a time-base reference. The separation of shadow images on the film is interpreted as projectile transit time between recording stations.

A schematic of the arrangement, with one recording station, is shown in Figure 6.51. The system consists of a Fastax streak camera, a pulsed-light source, an illuminated slit at each recording station, and a system of mirrors which, together with the camera lens, project the images of the pulsed source and slits onto the moving film. The time base is a 10 kHz signal generator, which in the one system controls the pulsing of a flash lamp, and in the other controls a shutter which chops the steady output of a tungsten-iodine lamp. The pulsed light is brought to focus on the moving film by the camera lens and produces a train of timing pips. The vertical slit at each recording station is normal to the projectile trajectory and is illuminated from across the flight-path by a steady light source. The image of the slit is rotated into a horizontal direction by a three-mirror system so as to be normal to the direction of film motion when the camera is operated in its normal erect orientation. Lightpath extenders are placed where needed to make all optical path lengths equal. This permits all

images to be focused in the film plane by the single camera lens and ensures equal magnifications. It also ensures that the transmission times from slits to film are equal. The Xenon winker lamps are discussed in a subsequent paragraph.

As the film moves, the slit image from each station sweeps out an exposed band along the film strip. When the projectile, or any other object on the trajectory, passes the recording station, its shadow moves across the illuminated slit producing a shadowgram on the film. Under ideal conditions, prior knowledge of the projectile velocity, together with the optical magnification of the system, allows matching the speed of the film and that of the projectile image, so that there is no spatial distortion of the shadowgram. In practice, mismatches occur which produce moderate fore-shortening or lengthening of the image. This does not significantly affect the time-measuring function of the system.

Figure 6.52 is a portion of a film record, obtained in the NRL facility, for a spherical projectile and several sabot pieces. The film and image motion are from right to left. The spaces between the timing marks in the middle of the film strip each represent 100 μsec. The lower band is from a slit at the first station, while the upper bands are from slits at succeeding stations. At this portion of the film record the model and sabot cluster have passed the first two stations, and their images appear in the first two bands. The horizontal displacement of the projectile images in these bands, measured to the scale of the timing marks, represents the elapsed time of flight between recording stations. With a 1.5-m interval between recording stations, velocity is measured to 0.25 percent accuracy using this system. The number of bands which can be put on one 35-mm film strip depends on the slit length and on the magnification. At NRL as many as six bands are put on one film; and by using three cameras with a common time base and placing the shadowgraph from a common slit on two camera films simultaneously, 16 recording stations have been instrumented.

An advantage which this system has, of particular significance to terminal ballistic studies, is that all objects passing the slits while the camera is recording are photographed. Thus, the space and time separation of sabot fragments, or other debris, from the projectile can be ascertained. Another advantage is that synchronization of the cameras with the projectile flight is required only to the extent that the flight occur while the film is moving near peak speed. The projectile is effectively "self-detected" at each recording station, so that no independent sensor-trigger system is needed.

A limitation of the system is the demagnification required to match the speed of the projectile image with that of the film. The maximum translational speed of the film is about 70 meters/sec. To match this with the image speed of a projectile moving at 7 km/sec requires a magnification of 0.01, so that a projectile of, say, 5-mm diameter would produce an image of 0.05-mm diameter on the film. Smaller images than that become difficult to resolve.

It is of interest to note that, with this magnification, an allowance of 3 mm for the length of the slit image on the film would permit monitoring a trajectory 300 mm in width.

A versatile auxiliary device, used in conjunction with the streak camera, to record the times of occurrence of supplementary events is called a "Winker System"[6.43, 6.44]. An auxiliary slit is imaged on the film in the same alignment as the velocity measurement slits. Behind this slit is placed a row of eight small Xenon flash lamps each of which can be caused to discharge, through a thyratron circuit, by an event supplemental to the projectile flight, such as a flow visualization photograph or a radiometric measurement. The lamp discharge places a mark on the film, relating the time of that event to the projectile flight. The lateral position of the mark on the film is directly related to the position of the Xenon lamp in the row, thus identifying the event. The arrangement of this winker system appears in Figure 6.51.

6.7.3 Oscilloscopes as Chronographs

Oscilloscopes have been used to advantage in ballistics where it is desirable to record a large number of time intervals or to obtain a continuous time record of a characteristic such as velocity. Current application appears to be limited almost exclusively to interior ballistic studies[6.41, 6.47, 6.53], but the principle is equally applicable to range work.

6.7.3.1 Raster-Display Recording

The feature which gives the oscilloscope the necessary flexibility in meeting the usually conflicting requirements of precision on the one hand and total recording time on the other is the use of a raster display[6.47]. This may be accomplished without any electronics external to the oscilloscope in the following manner. A dual-trace scope is used (Tektronix 545 with type CA plug-in unit) with the horizontal sweep controlled by the delaying-sweep time base. The saw-tooth signal of the main time base is used as a triggered ramp generator and connected to one of the dual-trace input channels. The signal to be recorded is connected to the other input channel, and the plug-in unit set to add the inputs algebraically. A sketch of this hookup is shown in Figure 6.53. The record may then appear as shown in Figure 6.54, where the horizontal time scale is effectively folded back on itself many times. By knowing the sweep rate, a continuous velocity history – or a number of discrete velocities – is obtained. The vertical modulation of the trace may contain information as well. The number of sweep lines which can be resolved, hence the recording time, depends primarily on the amplitude characteristics of the recorded signal. If one line per millimeter can be resolved, then a total recording test time of 40 milliseconds would be possible with a 4- by 10-cm display and the sweep rate of Figure 6.54. If the record could be read to the nearest 0.2 mm, say, then corresponding time resolution would be 2 μsec. With increased sweep rate, the resolution could be improved by perhaps 2 orders of magnitude but with a corresponding reduction of total recording time.

For the arrangement described, the flyback time is likely to be a significant fraction of the sweep time and therefore must be accounted for. In addition, the nonwriting interval may cause loss of data. To avoid this problem, raster generators have been developed[6.41, 6.53, 6.54] which are substituted for the internal time bases and produce sweep patterns, such as those in Figure 6.55 which permit continuous writing. A block diagram of the generator[6.41] used to produce the sweep pattern of Figure 6.55(a) is shown in Figure 6.56. The staircase voltage signal is applied to one vertical channel of the dual-trace plug-in and added to the data signal, as before. The synchronous triangular voltage signal is applied to the horizontal channel. In addition, the accuracy of the system is improved by placing timing marks along the raster. This is done by applying short negative pulses from a time-mark generator to the cathode of the display tube. Figure 6.57 is an example of the record from such a system. In many circumstances the timing marks could be applied, alternatively, to one of the vertical channels. Reference 6.54 describes a similar raster generator which produces the sweep pattern of Figure 6.55(b).

6.7.3.2 Circular-Sweep Interval Interpolation

Another use has been made of the oscilloscope purely for the measurement of time intervals; namely, for interpolating within the least count of an electronic-counter chronograph[6.48]. The oscilloscope was made to have a five-radius circular sweep display to operate in conjunction with four spark-shadowgraph stations and a set of 1.6 MHz counter chronographs[6.45]. The sweep function is driven by a 400 kHz oscillator to give one revolution for each four counts, or 2.5 μsec. The start-and-stop pulses, defining the interval to be measured, are fed simultaneously to the z-axis grid of the oscilloscope and to the counter. A sweep frequency less than the counter frequency was purposely chosen to eliminate the ambiguity, which would arise with a synchronous frequency, as to whether or not a count was recorded if a start or stop pulse occurred very close to an instant of counter triggering. A radius-control circuit decreases the radius of the oscilloscope circle after receipt of each pulse. This serves to differentiate between start and stop pulses and identifies the spark station originating the pulse. The angular separation of successive bright spots on the oscilloscope trace represents a fraction of 2.5 μsec. The whole number of 2.5 μsec intervals is deduced from the counter reading. To locate the center of the circles and facilitate the angle measurements a sixth innermost circle is fully exposed. Figure 6.58 is a typical oscilloscope record giving three time intervals. Figure 6.59 is a block diagram of the system as it would be used to record four successive time intervals.

Comparison of this system with the rotating prism chronograph described earlier has established an accuracy for this system equal to or better than $\pm 10^{-7}$ sec. Uniformity of the sweep rate was such that angular positions could be read to an accuracy equivalent to $\pm 2.5 \times 10^{-8}$sec. Use of higher-frequency counters would permit a higher rotation rate of the circular sweep and correspondingly greater potential accuracy.

The radius control circuit of the oscilloscope could be made to produce a spiral raster in which case the oscilloscope would be used in a manner analogous to that described in the first example. This would obviate the need for counters, but would greatly shorten the total recording time for a given accuracy. Using the 400 kHz sweep rate as an example, if one-millimeter spacing to a maximum radius of 50 mm were achieved, a 125 μsec recording period would be available.

6.7.4 Doppler-Radar Measurement of Velocity

The Doppler-Fizeau principle has been applied in the ballistic range using CW microwave radar to measure velocity directly from determination of the Doppler frequency, in a head-on orientation of the incident beam and the projectile. The use of this technique and its application to drag determination is treated in Chapter 10. It is sufficient to mention here that such systems have been developed[6.39, 6.55] which are capable of measuring velocities of small projectiles in relatively small range enclosures (e.g., 2-m dia) over distances measured in tens of meters to an accuracy approaching 0.1%.

Doppler radar may also be applied in an interferometer mode, as is now done in the study of interior ballistics (cf. Chapter 10). A unique application of this mode to range measurements, which allows the determination of a time-distance history and at the same time provides sequential triggering of range photographic stations has been employed at the Deutsch-Französisches Forschungsinstitut, Saint-Louis[6.50]. The system is capable, in principle, of measuring both velocity and distance. Used as an unbalanced interferometer to measure distance increments, it is coupled with counter chronographs to obtain a time-distance history. With this combination, accurate measurements of drag are more readily obtained than by the direct measurement of velocity because it does not require an accurate measurement of the time-varying Doppler frequency.

A schematic and block diagram of the arrangement is shown in Figure 6.60. The microwave antenna is placed near the butt end of the range, and its transmitted signal is directed uprange by a metal reflector which is apertured to allow passage of the projectile. The reflected signal from the moving projectile follows the reverse path back to the antenna. The wavelength, λ, of the transmitted signal is 3.16 cm (frequency of 9.5 GHz) in the installation. The photographic stations are spaced along the flightpath at multiples of the half-wavelength, $n_D\lambda/2$. Ahead of the first station is a photoscreen separated from it by a distance $n_0\lambda/2$. The reflected signal received by the antenna is mixed with a portion of the output signal. The resulting signal which oscillates at the Doppler frequency, f_D, is amplified and fed through a gate to a step counter which has stored in it the numbers n_0 and n_D. When the projectile passes the photoscreen, the gate opens allowing the Doppler signal to reach the step counter which sends a signal to a pulse distributor at the end of n_0 half-cycles of the Doppler signal and every n_D half-cycles thereafter. The pulse distributor, in turn, triggers the photographic light sources and counter chronographs in order. At the end of the flight, the projectile penetrates a trigger screen which closes the gate. The design of the microwave unit permits the use of a low-power klystron

of about 20 mW output to track accurately a 3-cm-diameter projectile from a distance of 15 m. Smaller projectiles with sharp tips require higher transmission energies. A velocity-distance relationship having scatter as low as 0.01 to 0.02% has been obtained with this system, so that accurate drag measurements are possible.

6.7.5 Precision Requirements

The precision requirement of a time-measuring system depends in part on the accuracy demanded in the derived quantities of interest, in part on the accuracy of related measurements, and in part on the magnitude of the time interval to be measured. While a comprehensive treatment of error analysis, as it relates to data reduction, is given in Chapter 7, it is useful here to illustrate precision requirements which may be placed on the time-measurement system by considering, in a simplified manner, two example situations - one in which only velocity is to be determined, and one in which drag is to be determined.

Suppose that one is interested in measuring the velocity of a projectile, over a distance interval of 5 meters, to an accuracy of 1 part in 10^3, or 0.1%; and suppose further that the anticipated distance measurement error is, say, 5 parts in 10^4. It can be shown that to good approximation the uncertainty in velocity is

$$\left.\frac{\epsilon(V)}{V}\right|_{max} = \frac{\epsilon(t)}{t} + \frac{\epsilon(x)}{x} , \tag{6.25}$$

where $\epsilon(t)/t$ is the uncertainty in the measured time increment and $\epsilon(x)/x$ is the uncertainty in the measured distance increment. It follows, therefore, that the tolerable error in time, $\epsilon(t)/t$, is 5 parts in 10^4, or equal in this example to the anticipated distance error. For a velocity of 1 km/sec, time must be measured to the nearest 2.5 microsecond; for a velocity of 10 km/sec, time must be measured to the nearest quarter of a microsecond.

As a second example, suppose now that one must determine the drag coefficient of a 1-cm-diameter aluminum sphere flying at a velocity, V, of 5 km/sec in an atmosphere whose density, ρ, is 0.1 atmosphere. The determination is to be made by measuring the time increments, t_1, and t_2, required to cover two successive distance intervals, x, of 5 meters each. Suppose, further, that the drag coefficient, C_D, must be determined within an accuracy of 1%. The governing equation may be written

$$\frac{1}{V^2}\frac{\Delta V}{t} = C_D \frac{\rho A}{2m} , \tag{6.26}$$

where, because $\Delta V \ll V$,

- V may be taken as the average velocity over the combined intervals,
- ΔV is the difference between the two measured velocities: $(x/t_1) - (x/t_2)$,
- t is the time interval over which the velocity changes by ΔV,
- A is the projected frontal area of the sphere,
- m is the mass of the sphere.

The value of C_D is taken as 0.9 for this example. The computation may be greatly simplified if it is assumed that

1. All of the measurement error resides in t; that is, all measured quantities not involving t are exactly known;
2. The quantities involving t may be decoupled and the error limitation in each treated separately. (Care must be taken in making this assumption. For the present example, it is justifiable).

It can then be stated that

$$\frac{\epsilon(t)}{t} = \frac{\epsilon(V^2)}{V^2} = \frac{\epsilon(\Delta V)}{\Delta V} \leq 0.01 . \tag{6.27}$$

At a velocity of 5 km/sec the time required to fly 5 meters is 10^{-3} sec, so that

$$\epsilon(t)_t \leq 0.01 \times 10^{-3} = 10^{-5} \text{ sec} .$$

Similarly, by neglecting second-order terms in $\epsilon(t)$, it can be shown that

$$\epsilon(t)_{V^2} \leq 0.01 \times \frac{t}{2} = 5 \times 10^{-6} \text{ sec}$$

and that

$$\epsilon(t)_{\Delta V} \leq 0.01 \frac{t_2 - t_1}{2} = 7.6 \times 10^{-8} \text{ sec} .$$

It is clear that the error limitation on ΔV determines the permissible error in t.

If the configuration in this example were a slender cone ($C_D = 0.01$) the permissible error in t, $\epsilon(t)_{\Delta V}$, would be only 0.6×10^{-9} sec; and if finite errors in other measured quantities were to be compensated for, this number would be still smaller. Present-day technology would be hard put to meet such a requirement. As a practical matter, however, the accuracy limitations of related measurements must be considered in arriving at a realistic requirement for the precision of time measurement. For example, it is clear from Equation (6.25) that there is little to be gained by requiring a higher order of precision in the time measurement than is attainable in the distance measurement.

In practice, it is found that error limits such as these just calculated can be greatly relaxed if redundant measurements are obtained (e.g., several successive measurements of V or ΔV) and treated simultaneously by a least-squares[6.56] technique. This permits the derived quantity to be determined with an accuracy greater than that of the individual measurements, provided that the measurement errors are random. This subject is treated in detail in Chapter 7.

6.7.6 Sources of Systematic Error

The primary sources of systematic error in time measurements related to ballistics are the accuracy of the time base, differences in transmission time of time-mark signals to the recording device, and the relationship of the time-mark signal to the related distance measurement. Differences in transmission times of electronic signals can usually be reduced to the order of 10^{-8} sec by use of components having the same characteristics, and transmission lines of the same characteristics and length. If the transmission is optical or electrical, a difference in path length of 3 meters introduces a time difference of 10^{-8} seconds or more, which should be accounted for if that order of precision is required. The relationship of the time-mark signal to the distance mark is likely to introduce the greatest uncertainty if not given careful attention, particularly if the projectile is not photographed. Differences in the rise characteristics of light sources, the circuit constants of electronic shutters or sensors, or the sensitivity and directionality of sensors, can introduce time biases as great as 10^{-6} or 10^{-5} sec. Such biases can be minimized if the wave forms and strengths of the signal outputs are matched to each other and to the needs of the electronic counters so that all will operate with similar characteristics.

6.8 SENSORS AND SEQUENCERS FOR INSTRUMENT AND TEST-FUNCTION CONTROL – C.S. James

The extremely short duration of the typical ballistic-range tests, which may last one second for a low-speed flight in a long range, or 10^{-3} sec for a high-speed flight in a short range, is a dominant factor in the design of the equipment used in the conduct of the test. This is particularly true of a short-duration counterflow facility where proper timing of the counterflow generation, launcher cycle, and data gathering is critical. A problem inherent in ballistic-range testing, therefore, is that of coordinating these functions.

Two types of controller have evolved for this purpose: sequencers, which provide a programmed series of command signals to prescribed functions; and sensors, which provide a command signal upon detection of some characteristic of the event. The sequencer tends to be simpler, and more reliable when the time of the event or the rate at which it takes place can be controlled or accurately predicted. When this is not the case, sensors are more reliable. More often than not both types are found in a given facility, with the sequencer coordinating the operational components of the range, and initiating the event, and with sensors controlling the instrumentation. Frequently the two modes of control are directly coupled. For example, a sensor may be used to initiate one or several time-delay circuits, which in turn control subsequent functions.

6.8.1 Sequencers

The sequencers used in ballistic ranges are almost all either electromechanical or electronic in operation. Motor-driven cams operating mechanical switches have some application. Electronic time-delay circuits are most often used where time increments must be short and precise. Multichannel electronic counter circuits and capacitor charge circuits have been built[6.57, 6.58] which can provide considerable flexibility in controlling complex instrumentation over periods ranging from a few microseconds to several minutes. In addition to its control function, the sequencer may also contain the time base[6.57]

Sequencers which are not based upon the time-delay principle, and which might be classified as hybrids, have found some application. One such device[6.59] is used to synchronize a reel-type cine camera with the event. An induction probe is placed near the teeth of the drive sprocket and used to count a preselected number of frames during film acceleration before initiating the event. Another example is the microwave Doppler system described in Section 6.7.4, in which preselected numbers of half-waves of the microwave signal are counted to determine the proper moment for initiating each of the photographic light sources. This system effectively slaves the "sequencer" to the progress of the event.

6.8.2 Sensors

A great amount of ingenuity has been applied in the development of sensing devices. In principle, anything that is capable of responding to some phenomenon associated with the event is a potential sensor. In ballistic ranges the most important sensing function is to trigger the photographic and other data-gathering stations which must operate at the precise moment the projectile passes. Several sensors developed for this purpose are discussed here to illustrate a variety of operating principles. Some of these have found widespread application, while others have found only limited application.

6.8.2.1 Early Systems

Among the early sensors were single-or multiple-strand breakwires, printed circuits, and foil switches. These circuits were interrupted by the projectile - or momentarily connected by it in the case of the foil switch. The projectile must make physical high speed contact with these sensors, with attendant possibility of damage to the projectile. Figure 6.61 is a micro-flash photograph of a projectile, triggered by a multi-strand breakwire, and damage due to the impact is evident on the projectile nose. For situations where projectile damage is of minor consequence, these sensors find application because of their simplicity (e.g., printed circuits painted directly on yaw cards).

Microphones, or pressure switches, have been used as sensors, which respond to the projectile bow shock wave. Their action thus depends on distance away from the flightpath and projectile Mach number. For Mach numbers much above 2, projectile dispersion can cause significant timing uncertainty.

6.8.2.2 Light-Decrease Systems

The term "light decrease" can be used to classify a group of sensor-trigger systems which respond to the interruption or attenuation of a beam or screen of light by the projectile. In this context the word "light" refers to virtually the entire portion of the electromagnetic spectrum from microwave to X-ray. The first systems made use of visible light as do most systems now in use. A steady light source and a photo-sensor are placed on opposite sides of the flightpath. Light from the source is collimated by a two-dimensional lens, or a three-dimensional lens apertured with a slit, to form a screen across the flightpath. The light is then focused onto the sensor by another lens. Figure 6.62 is a sketch of this arrangement. A projectile passing through this screen interrupts part of the light, causing the sensor to respond with an electrical pulse which is amplified and used as a trigger signal. Mirrors are often used in place of the lenses to produce folded optical paths or to make wide screens.

The width of the screen and the size of the projectile determine the strength of the output signal in relation to electrical and optical noise. It is desirable, therefore, to use a screen no wider than is necessary to ensure its penetration by the projectile. For some applications, particularly near the gun, a narrow beam will suffice, in which case the entire beam may be interrupted. To retain the advantage of a narrow beam and still get effectively a wide screen, a folded multipass optical path can be used. Two such arrangements are shown in Figure 6.63. Optical alignment and optical noise due to vibration become more critical with these arrangements, however, and shielding from stray light may be more difficult. The strength of the output signal depends also on the thickness of the light screen in relation to the length and shape of the projectile. For maximum signal strength the thickness of the screen should be no more than the length of the projectile, and for some shapes (e.g., slender cones), considerably less.

Measures to reduce the noise level of the system are sometimes required. These may include the use of a filtered D.C. power supply for the light source, to eliminate any ripple present; use of a photodiode sensor and transistorized trigger circuitry to eliminate microphonic noise in the electronics; shock mounting of optical components to isolate them from vibration; and shielding of the sensor from stray light. Optical noise due to vibration may be minimized by taking care to overfill each optical component, including the sensor, with the incident light by an amount slightly greater than the vibration amplitude of the beam to prevent momentary vignetting, chopping, or extinction of the peripheral rays.

A problem with the visible light system which can arise, particularly when it is used with a direct shadowgraph installation, (Section 6.3.1) is the protection of the shadowgraph film from fogging by the light source in the sensor-trigger system. Shielding is often ineffective. The usual solution, noted earlier, is to use a red filter in front of the light source, a sufficiently red-sensitive sensor, and orthochromatic film in the shadowgraph. There is a case here, however, for shifting the operating region of the sensor-trigger to the infrared. Photodiodes are available which have their peak sensitivity in the near infrared, and have microsecond response time. (An operating infrared system is described in a subsequent paragraph).

When a sensor is used to control a photographic station, there is an advantage to orienting it in such a way that it triggers at the moment the projectile is at the desired point in the field of view, so that no time delay is needed. This obviates the necessity of predicting projectile velocity and pre-setting time delays, and improves the reliability of the system. One way to accomplish this without interfering with the photographic function is to direct the light screen diagonally across the field of view of the photographic station as is shown in Figure 6.64. (The light-increase feature is discussed in Section 6.8.2.4). A configuration which works well with the direct shadowgraph and which can be integrated into the photographic station to give accurate positioning of the projectile in the photographs is that of Figure 6.65. The light source is housed in a canister between the film platens and about half way from their midpoint to their downrange edge. It is covered with a red filter and shielded with a rectangular slit such that it produces a fan-shaped light screen whose width just matches the effective photographic corridor (see Figure 6.3). A series of spherical-segment strip mirrors distributed along an arc between the photographic light sources focuses this light onto two or more photo-sensors. Each sensor is paired with two mirror segments. With the fan-shaped light screen, however, the signal strength varies in proportion to the distance of the projectile from the light source. A very similar arrangement, used in the NOL Hyperballistic Range, makes use of the large photographic station reflector to focus the fan-shaped photoscreen back across the flightpath onto the sensor, as shown schematically in Figure 6.66 (see also Figure 6.12(a)). The photoscreen light source and sensor are placed on opposite sides of the photographic light source.

An extremely simple wide-view light screen has been used for many years on open ranges at CARDE[6.2]. It consists of an apertured photocell placed directly below the flightpath to view the sky. A cylindrical lens is used to image the aperture slit at a height of approximately 2.5 meters above the photocell, the image dimensions being about 2.5 cm by 3 m. Indoors, the illumination has been provided by a back-lighted frosted diffuser and, more recently, by a linear infrared source of about 7 mm width. The infrared operation avoids fogging of photographic film. The sensor used is a 61SV lead sulphide photoconductive cell having a sensitive surface approximately 7 mm square, so that the effective screen thickness is about 7 mm at all points. In the range three cells are used to increase the width of coverage of the flight corridor. Figure 6.67 shows the relation of this light screen to other components in the Aeroballistic Range (cf.Figure 6.2).

When other sources of light can reach the sensor, for example, from the projectile flow field, gun-muzzle flash, or projectile impacts, light-decrease systems fail or become unreliable. Various approaches to the use of light-decrease systems under such conditions have been tried. Where the radiation is from the projectile flow field, a focused system analogous to the focused shadowgraph of Figure 6.8 may provide sufficient attenuation of the flow-field radiation to operate satisfactorily. Near the gun muzzle, where projectile dispersion is small, a visible-light system utilizing a narrow laser beam has been successful[6.60]. By utilizing three means of attenuating the muzzle flash - collimation, polarization, and wavelength filtering - and by interrupting the entire laser beam, a sufficiently high signal-to-noise ratio has been obtained.

Other regions of the spectrum, which permit use of a detector not sensitive to visible light, have also been employed. Some effort was put on the development of a CW X-ray beam attenuation device at the Ames Research Center with poor results. The use of X-ray scattering rather than attenuation might have proved more successful. The microwave region of the spectrum has, on the other hand, been used in "light-decrease" systems with good success[6.29, 6.61, 6.62, 6.63]. Two modes of operation have been developed. In one, the projectile interrupts one leg of a balanced interferometer circuit, upsetting the balance and producing a positive signal. In the other, the projectile simply attenuates the microwave beam. The interferometer circuit tends to be the more sensitive, but also the more complex both in construction and in use because it must be balanced before each firing. The interferometer mode does not function on a true "light-decrease" principle, strictly speaking.

An interferometer system has been developed to trigger the 38 photographic stations in the Hyperballistic Tunnel at the Laboratoire de Recherches Ballistiques et Aérodynamiques[6.61, 6.62]. This system is sketched in Figure 6.68(a). The microwave signal is generated by a klystron and separated into two branches. Ninety percent of the energy is directed into the antenna branch consisting of waveguides G1, cigar antennae E1 and E2, and waveguide G2. The other ten percent of the energy is directed into a regulation branch containing an attenuator and a dephaser. The two branches are rejoined by a T terminal and fed to a crystal detector. Since much of the energy directed to the antenna branch is dissipated in the transmission between the antennae, it is necessary to attenuate the energy passing through the regulation branch to match the amplitudes of the two signals. Before each firing the amplitude and phase of the signal in the regulation branch are adjusted to nullify the signal in the antenna branch. The crystal detector thus senses no signal. The passage of a projectile between the antennae disturbs this equilibrium both in amplitude and phase. The resulting signal (Fig.6.68(b)) is sensed by the detector, amplified, and used to trigger the photographic station. The system is operated at a frequency of 10 GHz (3-cm wavelength), and a microwave power of 50 mW. The antennae are approximately 70 cm apart. With this arrangement the system will detect a metal cylinder 3 cm in diameter and 3 cm long within an ellipsoid joining the antennae and having a maximum diameter of about 10 cm. If the cylinder is a transparent plastic (Plexiglass), the region of sensitivity is about doubled, that is, the ellipsoid has a maximum diameter of 20 cm.

An example of a microwave attenuation system is one developed at the Royal Armament Research and Development Establishment[6.63]. At present it is a two-station system operating at 9.5 GHz (3.16-cm wavelength), and is used to obtain X-ray photographs and to measure velocity. The antenna horns are mounted inside a 2.5-meter-diameter range tank on a swinging support to absorb blast loads (Fig.6.69). The transmitting horns are rectangular in section with the short dimension equal to the short dimension of the waveguide. The long side is oriented in a plane normal to the flightpath and flared to a width of 5 cm. This produces a narrow beam which opens to about 10 cm 0.3 meter away. The receiving horns have a 10-cm square opening and are separated from the transmitting horns by about 0.3 meter. Figure 6.70 is a block diagram of the microwave circuit. In normal operation a simple unmodulated wave is transmitted which results in a steady output from the crystal detector until the beam is interrupted by the projectile. For alignment purposes, the wave is modulated with a 3 kHz square wave which is monitored with an oscilloscope. The antennae are adjusted for separation and direction to give maximum power transfer, which occurs when separation is a multiple of the wavelength. With this system, however, tuning is not critical, and once adjusted the system is stable over a long time period. The system has good axial resolution in detecting small opaque projectiles (30 mm long by 6 mm diameter). Projectile shape is not critical. The system is less reliable with transparent (plastic) projectiles, at least at velocities less than 1.5 km/sec.

In the Aerophysics Range at General Motors Defense Research Laboratories[6.29], where transverse focused microwave probes are used for wake ionization studies, part of the transmitter energy for the probe is diverted through a pair of horn antennae a few centimeters uprange of the probe antennae to produce a trigger beam which is used to activate the probe recording instrument. The probes operate at frequencies of 35 GHz and 70 GHz.

6.8.2.3 Light-Increase Systems

When event luminosity is of sufficient intensity to hamper or defeat a light-decrease sensor, the sensor-trigger system can be made to respond to a light increase instead. If the luminous source is a moving projectile, the sensor must be masked to restrict its view angle to detect the projectile at the selected point in its trajectory. A device used in the AEDC 1000-Foot Hypervelocity Range[6.13], to prevent stray light from

prematurely triggering the system, is shown schematically in Figure 6.71. The field of view of the sensor is confined within the slotted opening of an optical cavity in the opposite range wall. The cavity is formed by two exponentially curved sheets of metal joined along a common seam and closed at the ends. The interior surfaces are coated with a non-reflecting black paint. The shape of the cavity prevents light rays entering it from returning to the exterior. Optical noise from stray light is thus reduced to near zero. The sensor responds when the luminous source (model) is within its fan-shaped field of view. If the structure walls opposite the sensor are effectively blackened and, if stray light is not intense, the system operates reliably without the cavity. Since dust is a good light scattering agent, maintenance can be reduced and system reliability improved if the components of the system are arranged such that both the window covering the sensor and the background surfaces viewed remain as dust free as possible. Gravity can be exploited here.

6.8.2.4 Dual-Mode Systems

Systems which can respond to either light increase or decrease are useful, since they are capable of operating over a wide range of ambient densities and velocities without fore knowledge of the luminous output of the model. Some light-decrease systems can be adapted to respond to a light increase as well. For example, in the arrangement of Figure 6.66 the sensor can view a luminous projectile as well as the reflected image of the light source and will respond in either mode. In all of the arrangements illustrated in Figures 6.62 through 6.65 a defocused image of the luminous projectile shock layer will be swept across the face of the sensor. Given an appropriate detector circuit, these systems can be operated as light-increase or dual-mode systems. There are usually problems associated with achieving sufficient sensitivity and directional selectivity of such systems to ensure reliable operation, however. One method of improving both of these factors is shown in Figure 6.64, where a second focusing mirror is placed to sweep a more sharply focused projectile image over the sensor. The sharpness of focus permissible will be tempered by the width of flightpath coverage required for reliability. This mirror is placed in such a way that the image which it forms will pass the sensor slightly ahead of that formed by the light-decrease mirror. In addition, the light-decrease mirror may be shielded to restrict its field of view to the collimating strip mirror.

If the system is to operate on either a light-decrease or a light-increase signal, the detector circuit must be designed to respond to either mode. One way to achieve this capability is demonstrated by a parallel light screen system recently installed in the NOL Hyperballistics Range[6.64] to supplement the lower sensitivity system of Figure 6.66. The output amplifier of the phototube sensor modifies the sensor output according to its polarity, as illustrated in Figure 6.72. If the projectile is nonluminous, the amplified phototube output is as shown in Figure 6.72(a). If the projectile is luminous, the phototube output is of opposite polarity in which case the amplifier distorts the signal to produce an over-shoot of the proper polarity from which the trigger pulse is taken, as shown in Figure 6.72(b). The trigger pulse then occurs at slightly different times in the two modes.

With a sensor-trigger system which will respond to either a light increase or a light decrease, the system may, under just the right circumstances, fail to respond if light reaching the sensor from a luminous projectile shock layer is just sufficient to replace that blocked from the photoscreen light source. A system which avoids this difficulty by responding to a light increase for both luminous and non-luminous projectiles is in use in the Hypersonic Range at the Royal Armament Research and Development Establishment[6.65] (Fig.6.73). The sensor, a 1P21 photomultiplier, views the flightpath diagonally across the photographic station. It is restricted by apertures to a field of view 9 cm high by 2.5 cm thick, in the flight direction. The region of the flightpath is imaged on the sensor cathode by a lens. Light from a small 48-watt coiled-filament lamp mounted near the sensor is directed, by two plane mirrors, along a path nearly coincident with that viewed by the sensor. The two paths intersect at the flightpath, where a magnified image of the lamp filament is focused by a lens placed near the lamp. The image size, being approximately 9 cm by 1 cm, coincides closely with the field of view of the sensor. When a projectile enters this field of view the sensor will respond either to light from the lamp reflected by the projectile or to light emitted from the projectile if it is luminous. The signals are of the same sign, but larger in the latter case.

6.8.2.5 Electromagnetic and Electrostatic Sensors

Sensing devices to detect projectiles, where extraneous light, vibration, or other noise sources are troublesome, have been developed at the Naval Research Laboratory[6.43, 6.44, 6.52]. These devices must be placed close to the trajectory.

One can be made to discriminate between two or more projectiles. It is electromagnetic in principle and consists of two coaxial and collateral solenoids which surround the trajectory. A direct current in the outer solenoid produces a strong magnetic field which has its axial gradient along the trajectory. A conducting but non-magnetic projectile moving through this field, experiences a continually changing field strength which induces an internal eddy current. This eddy current in turn produces a secondary magnetic field which counters slightly the strength of the primary field, thereby inducing an emf in the inner solenoid. A projectile of magnetic materials locally strengthens the primary field more than the eddy current weakens it, so that the emf induced in the inner solenoid is of opposite sign to that induced by a conducting non-magnetic projectile. As the projectile passes through the magnetic field, the induced emf in the inner solenoid varies as a sine wave, changing sign at the moment the projectile reaches the center of the field. This sign change is used as the detection signal. A nonconducting projectile or fragment induces no emf.

Another device operates on the same electrostatic principle as the Liebessart spark. It requires a projectile velocity high enough to ionize part of the gas in the shock layer. Two electrodes face each other across the

trajectory with the gap electrically stressed to 90% or more of its breakdown voltage by a pulse-forming network. As the projectile passes through the gap, its conducting shock layer triggers a spark in the gap, which discharges the pulse network and produces a detection signal. This technique has proven successful in detecting projectiles of 1.55-mm to 5-mm diameter moving at 4 km/sec, with an electrode spacing of approximately 2.5 cm, 1 kV across the gap, and range pressures up to 5.3 mb. Both coaxial blunt-ended rods and parallel rods or bars have been used successfully as electrodes.

6.8.2.6 Reliability Considerations

More often than not, sensor-trigger systems are subjected to noise fields or spurious signals of various kinds, and if multiple units are closely spaced or operated from a common power supply, there is the likelihood of mutual interference.

Radio-frequency noise from the discharge of sparks, from high-voltage generators, or from other sources, can enter the system through power lines and exposed conductors and components, including elements of the sensors themselves. Optical noise from adjacent light sources, or from the system's own light source due to supply current ripple, can cause spurious triggering. The reliability of the system depends on the degree of success with which it can be isolated from such disturbances. Methods of isolation include shielding from RF and visible radiations, electrical and optical filtering, use of short cabling, shock mounting and massive construction to attenuate vibration, and use of transistorized circuits to avoid microphonic sensitivity. With optical systems particularly, there is often an optimum viewing direction. Other measures have been discussed throughout this section.

Advantage can sometimes be taken of the shape of the sensor output pulse both to reduce timing uncertainty and to discriminate between true and false signals. A typical pulse is sketched in Figure 6.74. The rise time of the pulse (time separation between O and C) is a function of the projectile shape and velocity, the penumbra of the light screen or viewing aperture, and the sensor response characteristic. If the trigger responds to the magnitude of the sensor signal, it will be delayed by this variable rise time, or a large fraction of it. The timing uncertainty can be reduced by designing the trigger to respond to the maximum in the first derivative of the signal at B, or in the second derivative at A. False signals having the same rise time (i.e., the same frequency) but lower amplitude can be discriminated against by triggering on the larger-magnitude derivative of the true signal at B.

The best possible application of all of these techniques is sometimes insufficient to reduce false triggering from spurious signals to an acceptable level. Also, with counterflow facilities, luminous transients and bits of debris in the counterflow may pass the sensors causing premature triggering. In such cases, a blanking circuit may be employed so that a signal pulse from the sensor is accepted only within a short time increment when the projectile is in flight. At all other times, the blanking circuit prevents the trigger pulse from being formed. This technique may be applied in a number of different ways. For example, a blanking voltage applied to one or more triggers in the range may be removed by a signal taken from the launching gun, time-delayed to allow the projectile to approach the first sensor. If there is a series of trigger or photographic stations which mutually interfere, the blanking circuit may be arranged such that the signal from each station unblanks the next successive station[6.40]. An alternative approach is to control the entire blanking function with a sequencer. To prevent multiple triggering of a photographic station by sabot fragments or other debris passing the sensor, a single-shot thyratron trigger circuit, self-resetting after a suitable time delay, is sometimes used. Where the light source is energized by a capacitor, this may also be accomplished by preventing the capacitor from recharging.

6.9 INTERPRETATION OF THE PHOTOGRAPHIC RECORD – M.E.Wilkins

The optical systems and their components described thus far produce (usually) a shadow picture of the model and certain distance measuring references or fiducial marks. After the picture is developed, the picture is used to measure positions and angles of the model as they were at the instant of exposure. The picture may also be used to study the flow configuration about the model in flight, and that aspect is discussed in Chapter 8. In this section, we consider the accurate measurement of the positions and angles.

Many factors contribute to the accuracy of the final results – the type of film used, the size and shape of the reference points of both the model and fiducial system, the quality of the photographs, the instruments used for making measurements on the film, and the judgment of the person reading the film.

6.9.1 Film Selection

The emulsion selected must achieve adequate contrast with the light available and should have a minimum grain size for clarity of enlarged images. Of great importance is the dimensional stability of the film base during development and storage. Glass photographic plates offer the best dimensional stability since glass is affected by only thermal changes (0.0009 % per ^{o}C). Polyester-base films are affected by both thermal and humidity changes; in thermal expansion about three times that of glass, and from about 0.0015 to 0.0035 % per 1% change in relative humidity over a range of film base thickness of 7 to 2½ mil (0.178 to 0.064 mm) respectively. Polyester-base films, however, are usually sufficiently stable for precise work. Acetate-base film is approximately 50% less stable than the polyester in both thermal and humidity changes[6.66, 6.67, 6.68].

6.9.2 Model Reference Points

The design of the model should provide at least one reference point and line which will define its position and attitude on the film. Many models have natural references, e.g., pointed noses. All axially symmetrical bodies have a well-defined axis of symmetry. Cruciform wings provide excellent roll position references. In some cases, however, references are best added to the model. For example, a ballasted sphere might require a small pin protruding at the base to indicate the axis location, and an axially symmetric body might also, in certain cases, benefit from such a pin. Two or more pins placed off the axis of symmetry may be needed to determine the roll position. An example of a particularly difficult configuration on which to make position and attitude measurements is given in Figure 6.75. The model has an ogive-cylinder body with three highly swept wings spaced 120^{0} apart. Since the wings extend from the tip to the base of the body, a projection of the model will not disclose the body except for the nose tip. Consequently, a base plug (in this case a screw which also served to hold the model to the sabot during launch) was attached to the base of the body to identify the model axis. The nose tip was used as a reference for x, y, and z measurements from fiducial references which do not appear in the figure. The tip and the base plug were used to define the angles of pitch and yaw, and thus to compute the position of the model center of gravity from the measured position of the tip. The roll angle was obtained from the projected positions of the model wing tips and the base plug. In this case the base plug is necessary to obtain the roll angle accurately. (One wing tip was clipped for positive identification). Assuming that distortions due to the diffraction and the refraction of light are the same along both wing edges, measurements are made from the axis (base plug) to each wing tip. Subtracting these two measurements cancels the optical distortion, and the two possible roll angles can be determined. (An orthogonal view is necessary to select the correct angle). This example will make clear both the need for and types of approaches to measuring aids designed as part of the model.

When more than one possible reference point exists on a model, the best choice may not always be immediately evident. The choice usually depends upon how well one point is visible in all the shadowgraphs of that test. For example, for the model shown in Figure 6.75, the x, y, and z measurements would have been made to the base plug instead of to the nose tip but the base plug image was occasionally partially obscured by flow coming off a wing. When a series of photographs is taken of a model at different stations, the same reference point or points on the model should be used in each. This compensates for systematic distortions in the location of the point due to refraction and diffraction. Similarly, readings of the film from several stations of the same test should be done by one person, so that subjective differences in selecting the reading point will not be introduced.

6.9.3 Fiducial System Reference

At each shadowgraph station it is necessary to relate the position of the model to that of the measuring reference system, so that the overall motion from station to station can be defined. This is most easily accomplished by allowing part of the reference system to be photographed with the model (cf. Figs.6.4, 6.7(b), 6.11(c)). The fiducial reference photographed should define the direction along which measurements are made. Plumb lines and taut wires are frequently used for this purpose. Symmetry of the part photographed is valuable, since it obviates the need to estimate the position of an edge. (Edges are indefinite in shadowgraph pictures because of diffraction, finite light-source size, etc.) Thus, measurements to the end of the image of a rod or column are not reliable unless a correction can be applied for the error due to diffraction or unless the error is compensated by being repeated in all stations. Wires, notches, spherical beads, and pinholes can be used to advantage. Where a direction reference (for angular measurements) is required, taut wires, straight edges, or pairs of pinholes are desirable. The best reference systems also provide information from which changes in optical alignment, magnification, etc., can be corrected.

6.9.4 Film Measurement

Given the images of the model and measurement references on film, the problem is narrowed to accurate measurement of distances and angles between them. For negatives of moderate size film (say up to 25 cm) machines are available to make measurements to a scale reading accuracy of about 0.002 mm (2 microns). However, with larger film sizes sometimes used in conical light field shadowgraph systems, up to 0.5 meter, for example, accuracy and ease of measurement are more difficult to obtain.

The degree of accuracy obtainable is frequently limited by the quality of the photograph from which measurements are to be taken. It is obvious that with even the most precise measuring instruments relatively poor accuracy will be obtained from blurred or indistinct images. Since the photograph of a model in flight must always have a finite time of exposure, some motion of the model is always present in the picture. Additionally, sharpness of the image is reduced by various effects such as finite light source size, and diffraction. These effects should be minimized by design wherever possible, but it is clear that the sharpness of the photographic image will often be the limiting factor in the accuracy obtained.

A simple technique for reading film is illustrated in Figure 6.76. It consists of laying a transparent grid over the film negative to be read. (In this case the grid is a glass photographic replica of an accurate master grid - the numbers have no significance here being actually spaced one inch (2.54 cm) apart.) The fiducial reference consists of a straight edge appearing at the top of the picture with vee notches every 0.6-inch (1.524 cm). After aligning the grid marks with the reference images, the coordinates of all the necessary points are read from the grid, possibly with the aid of a magnifying glass. Angles may be measured with a protractor or deduced from the coordinates. This process can be quite rapid and is frequently accurate enough to produce excellent results (linear dimensions accurate within 0.2mm). However, it allows opportunities for human error and, for high precision, involves more labor than required if more mechanized equipment is used.

A mechanical film reader consists basically of a film holder and a reticuled viewer, with provision for accurate relative motion in one or more linear or angular coordinates. The measurements of distances and angles are given by accurately machined lead screws, micrometers, etc. The determination of which parts should move is a design consideration which will not be pursued here. The measurement of the displacement will be discussed briefly, followed by some observations about optical viewers.

The translational movement of either the viewer or the film is usually effected by means of the calibrated lead screw which is in effect the length standard of the measurement. Backlash in the gearing mechanism should be eliminated to the extent possible. If present it can be compensated for by making all measurements from the same direction.

An alternative method of measurement which is free of backlash problems makes use of the moiré fringe counting technique[6.69]. Moiré fringes are produced when light passes through two transparent gratings mounted face to face with the rulings inclined to one another at a small angle. The fringes are observed to be nearly perpendicular to the rulings. When one grating is moved in a direction perpendicular to the lines with the other remaining fixed, the fringes move across the field at right angles to the direction of grating movement. The spacing of the fringes represents a magnification of the spacing of the ruling. Hence, a visual or an optical scanning count of the fringes passing a particular point is a measure of the number of rulings passing that point. A pair of gratings is required for each direction in which measurements are to be made. (Angular measurements may also be made with radial gratings.)

Another design choice in film viewers is the choice between microscope viewing of the images and enlarged image projection onto a screen. The microscope type (Fig.6.77) is probably the simpler of the two. The microscope is carriage-mounted and focused on the film, backlighted with a diffuse light source. The microscope has a reticule (usually 90^{o} cross hairs) for alignment on the model and measurement references. The microscope may have a calibrated rotating reticule so that angles may be determined with the microscope alone or the film holder may rotate for angular measurements.

In the projection type (Fig.6.78) a high intensity point light source is used to project the film image onto the screen which contains the reticule. The reticule can be physically fixed on the screen and the screen rotated to obtain angular measurements, or an image of the reticule can be optically projected onto the screen and the image rotated. The latter method has more versatility. The image may be a shadow of cross hairs giving a dark line reference, or an image of an illuminated slit which provides a bright line reference. By use of filters the color of the illuminated slit can be chosen to give contrast with the film image.

It is possible to eliminate the human judgment factor, at least in part, by use of a scanning densitometer which is programmed to locate the model and reference profiles by measuring relative densities of the film and to output the desired coordinate information on punch cards or tabulation sheets. This approach is useful for certain applications and is being increasingly exploited where many frames of cine film must be read. But accuracy, using this approach, appears difficult to achieve in the ballistic range where photographic exposures often vary considerably from one station to another and where the photographs may also include extraneous markings, such as smears on windows, fingerprints, blemishes on the film, etc., which can cause such a reading instrument to misinterpret what it sees. At present, the reading of ballistic-range film usually requires human judgment to choose the coordinate positions of the various references.

6.9.5 Design Considerations for Comfort and Speed in Reading

Since numerous measurements to high precision are required on many negatives, film reading is a slow and laborious task. In the design of a manual film reader, consideration of comfort and ease of operation can lead to improved speed and accuracy of reading.

The moving parts of a film reader, whether manually or motor driven, should be geared so as to provide relatively fast motion as well as exceedingly slow motion in approaching a reference line or point. When the distance between references is quite large, it is desirable to cover the major part of the distance as quickly as possible.

The direction of motion should be related to its control in the sense expected by the operator. It adds to the difficulties and is time consuming if the image moves in the opposite of the expected or natural direction.

6.9.6 Summary

With well designed film readers, well exposed pictures, a good measurement reference system, and care, linear coordinates accurate to 0.05 mm can be routinely obtained. Angular accuracy depends on the base length of the model being measured, and can be estimated from the linear accuracy. For example, on models 10 cm long, the angular accuracy implied by cumulative positional errors of 0.05 mm at either end is only 0.001 radian or 0.06^{o}, while with a model with a reading length of 1 cm, the error would be 0.6^{o}. The most essential ingredient to the acquisition of quality data, after the precautions of system design have been taken, is the motivated, conscientious reader.

REFERENCES

6.1 May, Albert
Williams, T.J.
Free-Flight Ranges at the Naval Ordnance Laboratory. US Naval Ordnance Laboratory Rept NAVORD 4063, July 18, 1955.

6.2 Morgan, K.
Velocity Instrumentation in the CARDE Aeroballistic Range. Canadian Armament Research and Development Establishment Tech. Rept. 456/65, July, 1965.

6.3 Holder, D.W.
North, R.J.
Wood, G.P.
Optical Methods for Examining the Flow in High-Speed Wind Tunnel. AGARDograph 23, November, 1956.

6.4 Tanner, L.
The Design and Use of Interferometers in Aerodynamics. ARC R & M 3131, HMSO, London, 1959.

6.5 Keen, Stanley M.
Application of the "Slit-Aperture" Camera for Observation and Data Acquisition in Projectile Studies. Proc. Fifth International Congress on High-Speed Photography, Washington, DC, 1960, SMPTE 1962, pp.375-378..

6.6 Lecomte, C.
Utilization d'une Camera a Miroir Tournant pour la Photographie de Maquettes à Grand Vitesse. Proc. Sixth International Congress on High-Speed Photography, The Hague, September 17-22, 1962; Tjeenk Willink & Zoon NV-Haarlem, 1963, pp.434-442.

6.7 Meninger, R.C.
Butenbach, R.W.
Millimicrosecond Photography with an Image Converter Camera. IRE National Convention Record, Part V, May, 1957, p.88.

6.8 Brooks, Robert E.
New Dimension for Interferometry. Electronics (McGraw-Hill), May 15, 1967, pp.88-93.

6.9 Wuerker, Ralph E.
Research on Electrostatic Charged Droplet Streams. US Air Force Aerospace Research Laboratories Rept. ARL 67-0211, October, 1967.

6.10 Charters, A.C.
Thomas, R.N.
The Aerodynamic Performance of Small Spheres from Subsonic to High Supersonic Velocities. Jour. Aero. Sci., Vol.12, No.4, October, 1945, pp.468-476.

6.11 Braun, Walter F.
The Free-Flight Aerodynamics Range. US Army Ballistic Research Laboratories Rept. No.1048, July 1958.

6.12 Anon.
Aero and Hydro-Ballistics Research Facilities. US Naval Ordnance Laboratory Rept. NOL R 1264, July, 1967.

6.13 Lukasiewicz, J.
Stephenson, W.B.
Clemens, P.L.
Anderson, D.E.
Development of Hypervelocity Range Techniques at Arnold Engineering Development Center. Arnold Engineering Development Center TR-61-9, June, 1961.

6.14 Anderson, R.Wayne.
High-Speed Photography Using Ultraviolet Radiation to Eliminate Visible Light Masking in Self-Illuminating Events. Proc. Fifth International Congress on High-Speed Photography, Washington DC, October 16-22, 1960, SMPTE, 1962.

6.15 Dyke, W.P.
Grundhauser, F.J.
Collins, F.M.
Stunkard, N.W.
Recent Developments in Flash Radiography at Hypervelocities. Advances in Hypervelocity Techniques. Plenum Press, New York, 1962. Proc. Second Symposium on Hypervelocity Techniques, Univ. of Denver, March 20-21, 1962.

6.16 Léger, E.G.
Beaulieu, R.
Stereo Flash X-ray Photo Attitude Station for Use on Ballistic Ranges. Canadian Armament Research and Development Establishment Tech. Rept. 563/67, April, 1967.

6.17 Clay, W.G.
Slattery, R.E.
Ferdinand, A.P.
Kilcline, C.R.
Application of Nanosecond Light Pulses to Ballistic Range Measurements. AIAA Jour., Vol.5, No.2, February, 1967, pp.364-365.

6.18 Clemens, P.L.
Hendrix, R.E.
Development of Instrumentation for the VKF 1000-Ft Hypervelocity Range. Advances in Hypervelocity Techniques. Plenum Press, 1962, Proc. Second Symposium on Hypervelocity Techniques, Univ. of Denver, March 20-21, 1962.

6.19 Cords, Paul H. Jr
Thurston, Paul A.
Noyes, William R.
A Modern Reflective Shadowgraph System for Use in High-Velocity Aeroballistic Ranges. Proc. Fifth International Congress on High-Speed Photography, Washington DC, October 16-22, 1960. SMPTE, 1962. Lib. of Congress catalog card 57-9846.

6.20 Rogers, W.K.
The Transonic Free-Flight Range. US Army Ballistic Research Laboratories Rept No.R-1044, June, 1958.

6.21 Clemens, P.L.
Kingery, M.K.
Development of Instrumentation for a Hypervelocity Range. Arnold Engineering Development Center TN-60-230, December, 1960

6.22 Morrison, R.H. — Ames Research Center, Moffett Field, Calif: Private communication, March, 1968.

6.23 Nolan, Philip — *High Intensity, Fractional-Microsecond Light Sources.* Proc. Fifth International Cong. on High-Speed Photography, Washington DC, October 16-22.1960, SMPTE, 1962.

6.24 Moden, J.C. — *Short-Duration Spark Light Sources of Extreme Luminance.* Proc. Fifth International Cong. on High-Speed Photography, Washington DC, October 16-22, 1960, SMPTE, 1962.

6.25 Fischer, Heinz; Gallagher, C.C.; Tandy, Peter — *Improved Nanosecond Light Sources.* Proc. Sixth International Cong. on High-Speed Photography, The Hague, September 17-22, 1962, Tjeenk Willink and Zoon NV-Haarlem, 1963, pp. 152-157.

6.26 Charters, A.C. — *The Spark Photography Range.* Proc. Sixth International Cong. for Applied Mechanics, Paris, France, September, 1946.

6.27 Kovasznay, Leslie, S.G. — *High Power Short Duration Spark Discharge.* The Review of Scientific Instruments, Vol.20, No.9, September, 1949.

6.28 Lankford, John L. — *Feasibility Study of the Determination of Shock Detachment Distance and Ablation on Luminous Bodies Using a Laser Light Source.* US Naval Ordnance Laboratory TR 67-18, February 1, 1967.

6.29 Anon. — *Aerospace Research Capabilities.* General Motors Defense Research Laboratories, TR 63-223, April, 1964. (Revised).

6.30 Boissevain, Alfred G. — *Experimental Investigation of the Damping in Roll of Cruciform Triangular Wing-Body Combinations at Mach Numbers from 1.5 to 6.0.* NACA RM A54B15a, April, 1954.

6.31 Liddiard, T.P., Jr; Jacobs, S.J.; Kabik, I. — *An Explosive Light Source of Low Energy for 30-Nanosec Schlieren or Shadowgram Photography.* Jour. Soc. Motion Picture and Television Engineers, February, 1965.

6.32 Dike, R.S.; Kemp, E.L. — *Quick Closing Light Shutter.* Review of Sci. Instr., Vol.36, No.8, August, 1965, pp. 1256-7.

6.33 Pirroni, J.S.; Stevens, R.R. — *High-Speed Electromagnetic Shutter.* Review of Sci. Instr., Vol.38, No.3, March, 1967, pp. 382-3.

6.34 Kendall, P.A. — *High-Speed Electromechanical Shutter for Time-Resolved Spectroscopy.* Applied Spectroscopy, Vol.18, No.2, 1964.

6.35 Denardo, B.P.; McGee, J.E. — *Simplified Rapid Opening Mechanical Gate Valve.* Review of Scientific Inst., Vol.37, No.10, October, 1966.

6.36 Schmitz, F.A.; Nims, D.J. — *Explosive High-Speed Shutter.* Review of Sci. Inst. Vol.37, No.4, April, 1968.

6.37 Chace, W.G.; Fish, C.V. — *Exploding Wire Blast Shutter.* Applied Optics, Vol.2, No.4, April, 1963.

6.38 Jenkins, Francis A.; White, Harvey E. — *Fundamentals of Physical Optics.* McGraw-Hill, 1957, Lib. of Congress catalog card 56-12535.

6.39 Musal, H.M. Jr; Primich, R.I.; Blore, W.E.; Robillard, P.E. — *Millimeter Radar Instrumentation for Studying Plasma Effects Associated with Hypersonic Flight.* Proc. of the IEEE First International Congress on Instrumentation in Aerospace Simulation Facilities, Paris, September 28-29, 1964, PL Clemens, ed. (cf.GM-DRL Rept.TR 64-02J, August, 1964).

6.40 Palkin, S.N.; Reznikov, B.I.; Studenkov, A.M.; Bykov, V.N. — *Issledovaniye unosa massy legkoplavkikh modeley na ballisticheskoy ustanovke.* In Aerofizicheskiye Issledovaniya Sverkhzvukovykh-Techenii. Izdatel'stvo "Nauka", Moscow, 1967, pp. 274-283. (available also as NASA Technical Translation TTF-11, 309, November, 1967)

6.41 Hruby, Ronald, J.; Sander, Ronald, C.; Berggren, Robert E. — *Microwave Technique for Measuring Projectile Time History in Light-Gas Guns.* Proc. IEEE Second International Congress on Instrumentation in Aerospace Simulation Facilities, Stanford Univ., August 29-31, 1966. P.L. Clemens, ed.

6.42 Hall, Donald A.; Atkins, W.W. — *New Technique for Measurement of Velocity of High-Speed Objects.* Proc. Fifth International Congress on High-Speed Photography, Washington DC, October 16-22, 1960, SMPTE, 1962, pp. 372-374.

6.43 Swift, H.F.; Baker, J.R. — *Hypervelocity Capability and Impact Research - Electroballistic Program.* US Naval Research Laboratory Memo Rept. 1623, July, 1965.

6.44 Swift, H.F. — *The Air Force Materials Laboratory Hypervelocity Ballistic Range.* US Air Force Materials Laboratory TR 67-2, January, 1967.

6.45 Seiff, Alvin — *A Free-Flight Wind Tunnel for Aerodynamic Testing at Hypersonic Speeds.* NACA Rept. 1222, May, 1955.

6.46 Struth, Wolfgang — *Kurzzeitaufnamen von Schussen mit Hyperschallgeschwindigkeit in Reagierende Gase.* Proc. Sixth International Congress on High-Speed Photography, The Hague, September 17-22, 1962, Tjeenk Willink and Zoon NV-Haarlem, 1963, pp.443-449.

6.47 Pennelegion, L. — *Microwave Interferometry Studies in Free-Piston Gun Tunnels. Advances in Hypervelocity Techniques.* Plenum Press, 1962, Proc. of Second Symposium on Hypervelocity Tech. University of Denver, March 20-21, 1962.

6.48 Kerwin, William J — *Chronograph Times Supersonic Models.* Electronics, April, 1957, pp.152-155.

6.49 Koch, Bernhard — *Mesure Radioélectrique de la Vitesse des Projectiles.* L'Onde Electrique Vol.32, 1952, pp.357-371.

6.50 Koch, B
Simon, G. — *Synchronizierung Ballistischer Reihenaufnahmen Mittels Radioelektrischer Geschwindigkietmessung.* Proc. Sixth International Congress on High-Speed Photography, The Hague, September 17-22, 1962, Tjeenk Willink and Zoon NV-Haarlem, 1963, pp.409-412. (See also: Giraud, M.; Koch, B.; and Simon, G.: "En Vol Libre par Photographies Successives Déclenchées et Synchronisées par Radar". Proc. Seventh International Congress on High-Speed Photography, Zurich, September 12-18, 1965, Verlag Dr. Othmar Helwich, Darmstadt, 1967, pp.225-229).

6.51 Clemens, P.L. — Arnold Engineering Development Center: Private communication, August, 1968.

6.52 Bailey, S.O.
Clark, A.B.J.
Hall, D.A.
Swift, H.F. — *Facilities and Instrumentation of the NRL Hypervelocity Laboratory.* US Naval Research Laboratory Rept.5271, February 18, 1959.

6.53 Knapp, R.E.
Hendrix, R.E. — *Experimental Projectile Kinematic Studies in a Two-Stage Light-Gas Gun.* Arnold Engineering Development Center TR 65-60, March, 1965.

6.54 Anderson, G.F.
Kelly, J.G. Jr — *An Experimental Method for Measuring Continuously the Velocities of the Shock and Contact Discontinuities in a Shock Tube.* Proc. IEEE Second International Congress on Instrumentation in Aerospace Simulation Facilities, Stanford Univ. August 29-31, 1966. P.L. Clemens, ed.

6.55 Gates, D.F.
Haislmaier, R.J.
Hill, L.L. — *A Doppler Radar System to Obtain Water Impact Drag Coefficients.* Proc. of the IEEE Second International Congress on Instrumentation in Aerospace Simulation Facilities, Stanford Univ., August 29-31, 1966. P.L. Clemens, ed.

6.56 Shĩnbrot, Marvin — *A Least-Squares Curve Fitting Method with Applications to the Calculation of Stability Coefficients from Transient Response Data.* NACA TN-2341, 1951.

6.57 Graves, Kenneth E.
Silberberg, George C. — *Versatile Sequence Timer and Timing Generator for High-Speed Cameras.* Proc. Sixth International Congress on High-Speed Photography, The Hague, September 17-22, 1962, Tjeenk Willink and Zoon NV-Haarlem, 1963, pp.413-422.

6.58 Wenig, Jacob — *A Time Delayed Generator for High-Speed Phenomena.* Proc. Sixth International Congress on High-Speed Photography, The Hague, September 17-22, 1962, Tjeenk Willink and Zoon NV-Haarlem, 1963, pp.423-426.

6.59 Hall, D.A.
Bailey, S.O. — *Synchronization of a High-Speed Prism Camera by Frame-Counting Technique.* Jour. SMPTE, Vol.68, March, 1959, pp.151-152.

6.60 Christman, D.R.
McMillan, A.R.
Gehring, J.W. — *Development and Application of High Velocity Impact Range Instrumentation.* Proc. IEEE Second International Congress on Instrumentation in Aerospace Simulation Facilities, Stanford Univ., August 29-31, 1966. P.L.Clemens, ed.

6.61 Berton, J. — *Etude de Barrière Hyperfréquence pour le Déclenchement de Photographies dans le Tunnel de Tir.* Laboratoire de Recherches Balistiques et Aérodynamiques Note 1023 EAS - PV 1.

6.62 Loyen, R. — *L'Equipment de Déclenchement des Prises de Vues Photographiques de Tunnel Hyperbalistique de Vernon.* Technique et Science Aéronautiques et Spatiales, January - February, 1966, pp.31-35.

6.63 Fuller, P.W.W. Royal Armament Research and Development Establishment: Private communication, July, 1968.

6.64 White, E.L. Fedenia, J.N. *Projectile Detection of Luminous and Nonluminous Bodies.* IEEE Transactions on Aerospace and Electronic Systems, Vol.AES-2, No.1, January, 1966, pp.13-20.

6.65 Wall, C.R. *Photography of Projectiles of Near Orbital Velocities.* Proc. Sixth International Congress on High-Speed Photography, The Hague, September 17-22, 1962. Tjeenk Willink and Zoon NV-Haarlem, 1963, pp.566-572.

6.66 Anon. Kodak Tech Bits, 1964, No.3. A Kodak Publication for Scientists and Engineers. Sales Service Division, Eastman Kodak Company, Rochester, NY 14650.

6.67 Anon. The Kodak Compass, A Bulletin on Industrial Reproduction Processes and Materials, No.2, 1963. Sales Service Division, Eastman Kodak Company, Rochester, NY 14650.

6.68 Anon. Kodak Professional Color Lab Letter, Summer 1968, Vol.5, No.3. Professional, Commercial, and Industrial Markets Division, Eastman Kodak Company, Rochester, NY 14650.

6.69 Guild, J. *Diffraction Gratings as Measuring Scales.* Oxford Univ. Press (London), 1960.

Fig.6.1 Yaw-card puncture made by a finned projectile (courtesy of US Naval Ordnance Laboratory)

Fig.6.2 Yaw-card station in the CARDE Aeroballistic Range. In the foreground is a shadowgraph velocity station with an infra-red light screen (courtesy of Canadian Armament Research and Development Establishment)

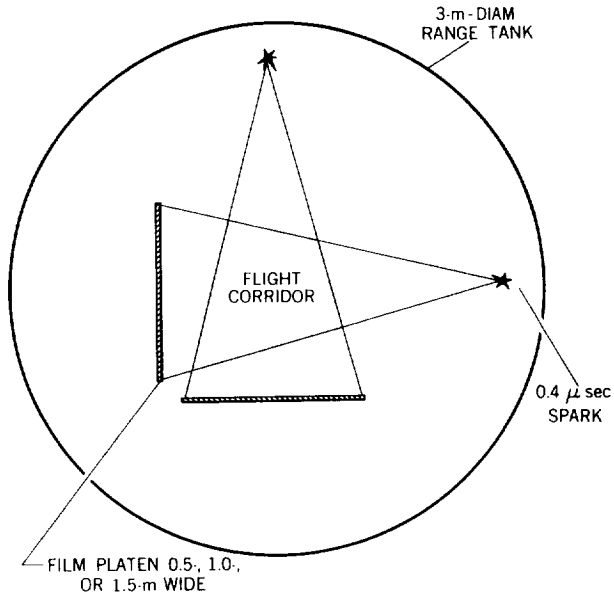

Fig.6.3 Schematic of shadowgraph configuration in the Ames Pressurized Ballistic Range.

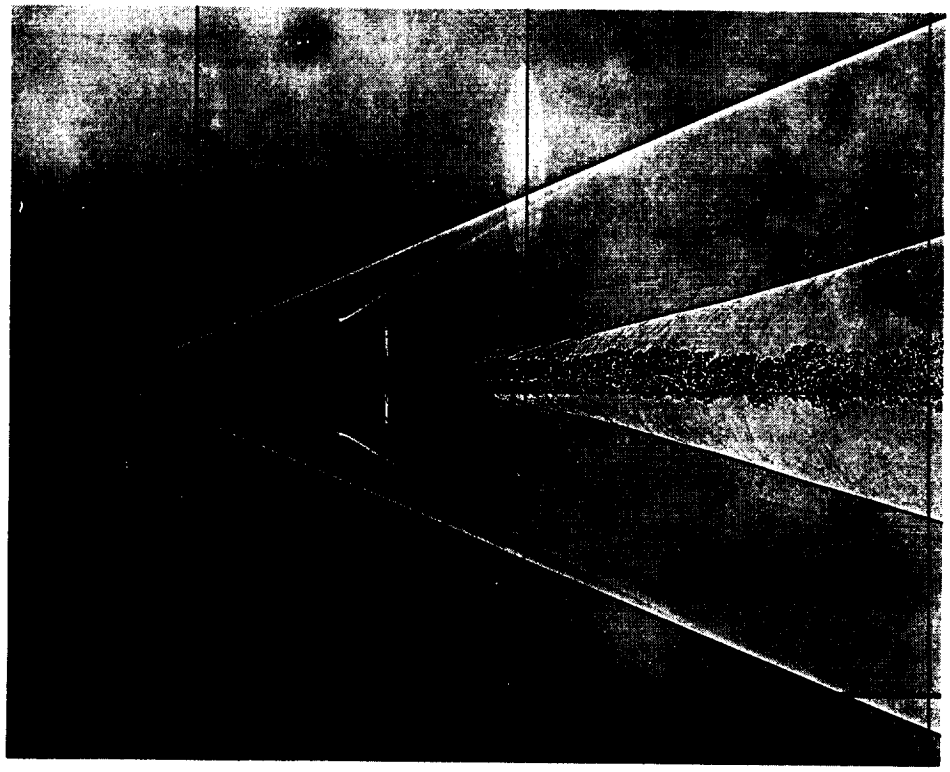

Fig.6.4 Shadowgram of slender cone obtained in the Ames Pressurized Ballistic Range. Mach No. = 3.

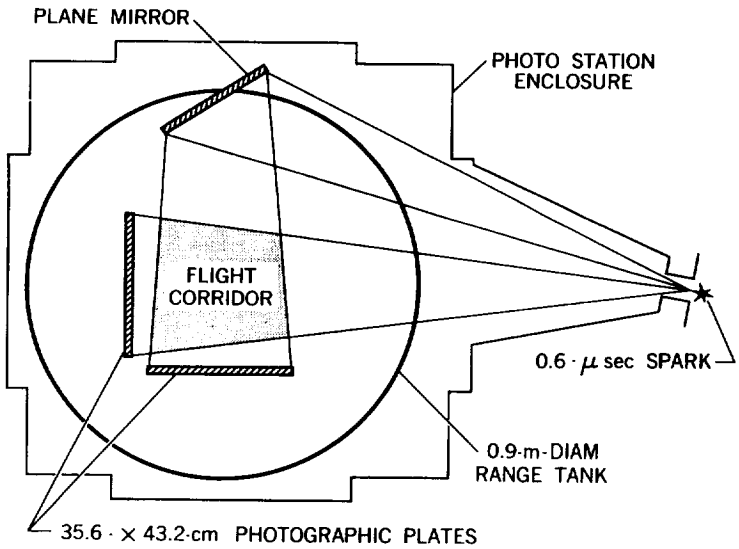

Fig.6.5 Schematic of shadowgraph configuration in the NOL Pressurized Ballistics Range.

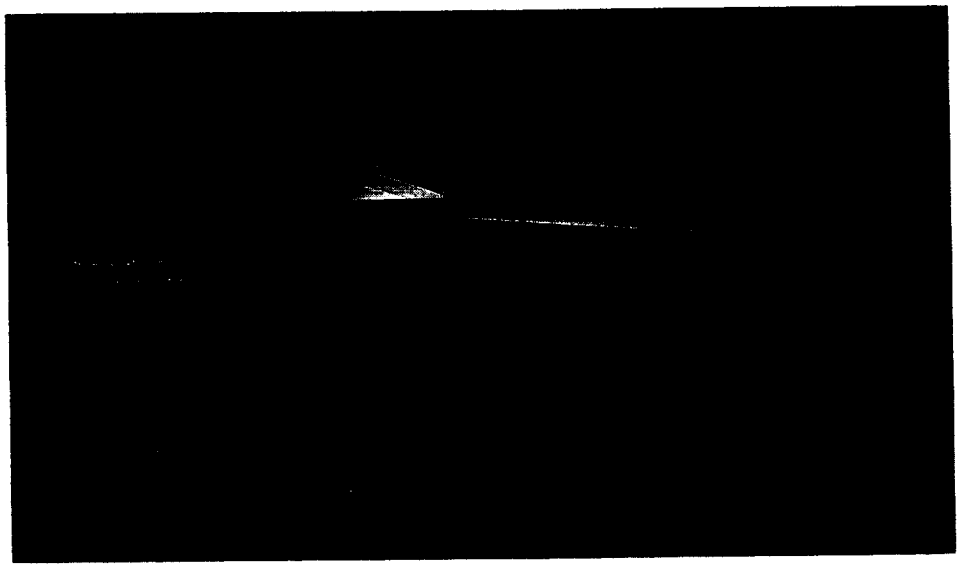

(a) horizontal light beam.

(b) vertical light beam.

Fig.6.6 Orthogonal shadowgram of a finned 10-deg. cone in the NOL Pressurized Ballistics Range. Mach number: 5; range pressure: 436 mm Hg. (courtesy of US Naval Ordnance Laboratory)

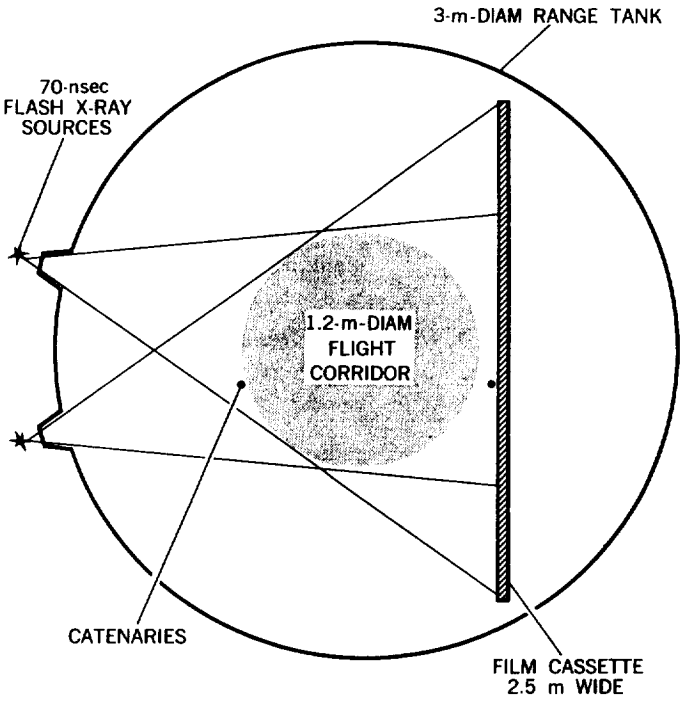

Fig.6.7(a) Schematic of nonorthogonal shadowgraph configuration in CARDE Range 5 (courtesy of Canadian Armament Research and Development Establishment)

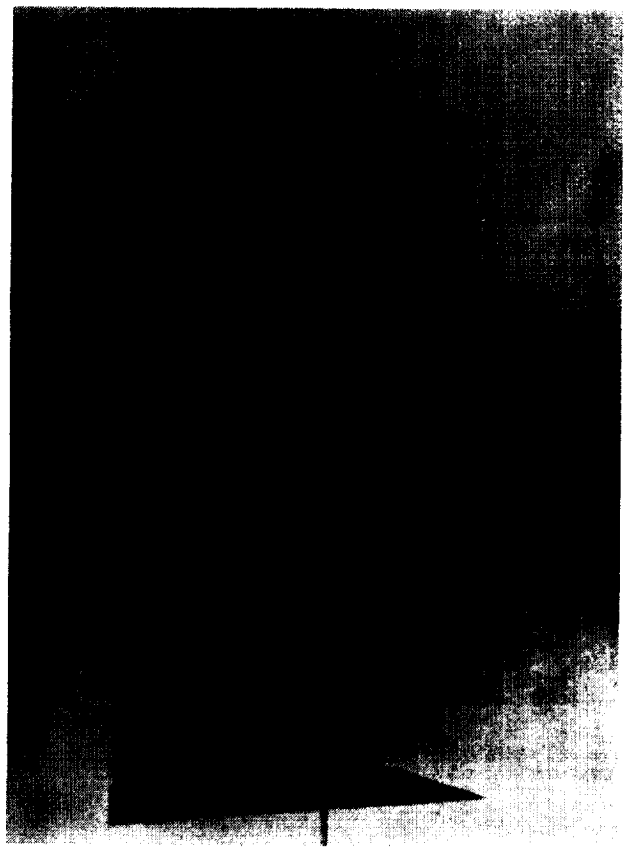

Fig.6.7(b) X-ray shadowgram of a cone in flight; taken in CARDE Range 5. Velocity, 4.5 km/sec; Film exposure, 50 nsec (courtesy of Canadian Armament Research and Development Establishment)

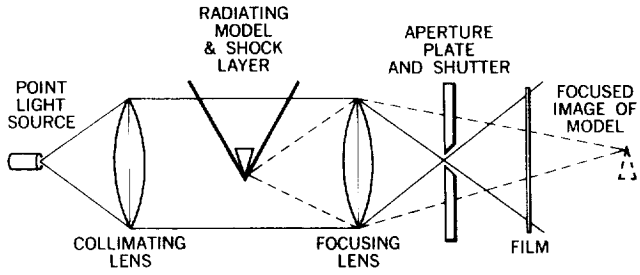

Fig.6.8 Schematic of a focused shadowgraph using lens optics

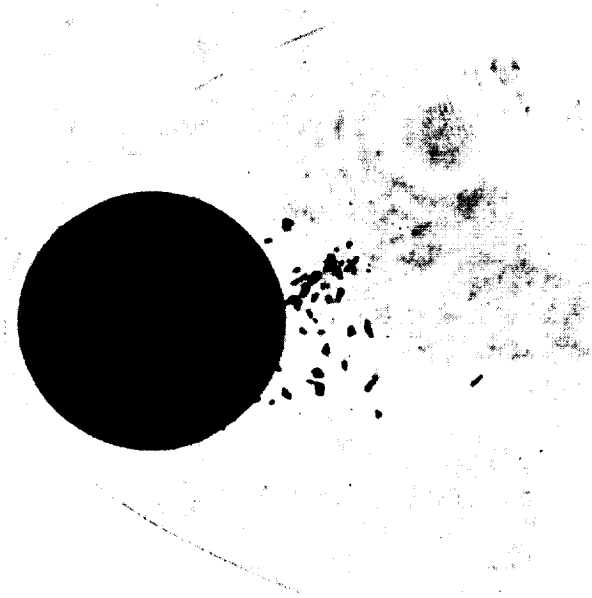

Fig.6.9 Shadowgram of a 4.8-mm-diameter phenolic sphere, exposed with a 20 nsec pulse of a ruby laser. Sphere is moving at 5.9 km/sec in air at 40 torr. Spalled surface fragments are visible in the wake (courtesy of Massachusetts Institute of Technology - Lincoln Laboratory)

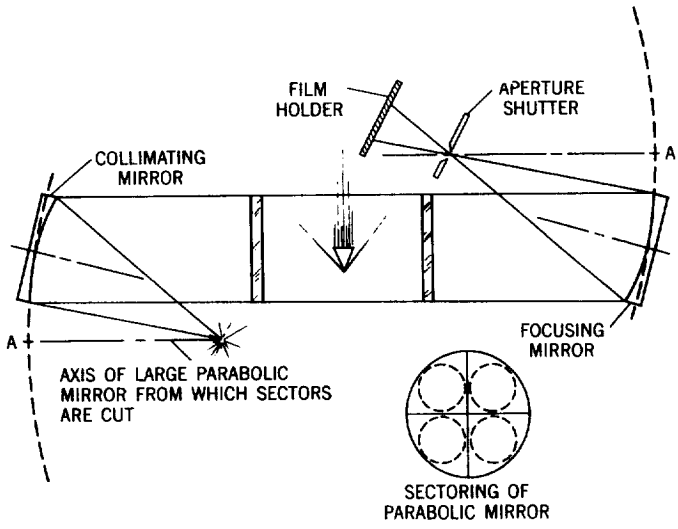

Fig.6.10 Schematic of a focused shadowgraph using mirror optics

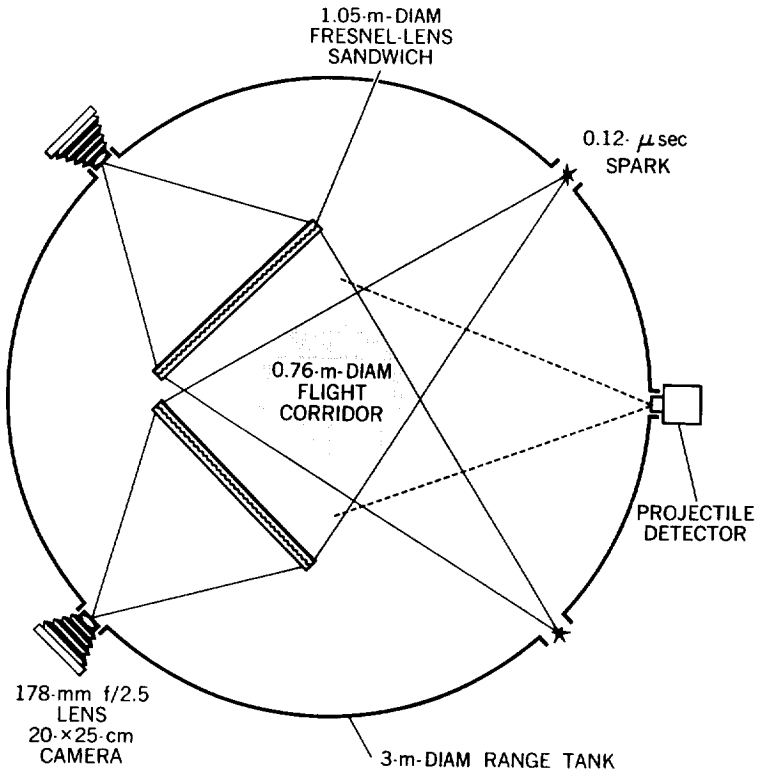

Fig.6.11(a) Schematic of shadowgraph configuration in the von Kármán Gas Dynamics Facility 1000-ft Hypervelocity Range

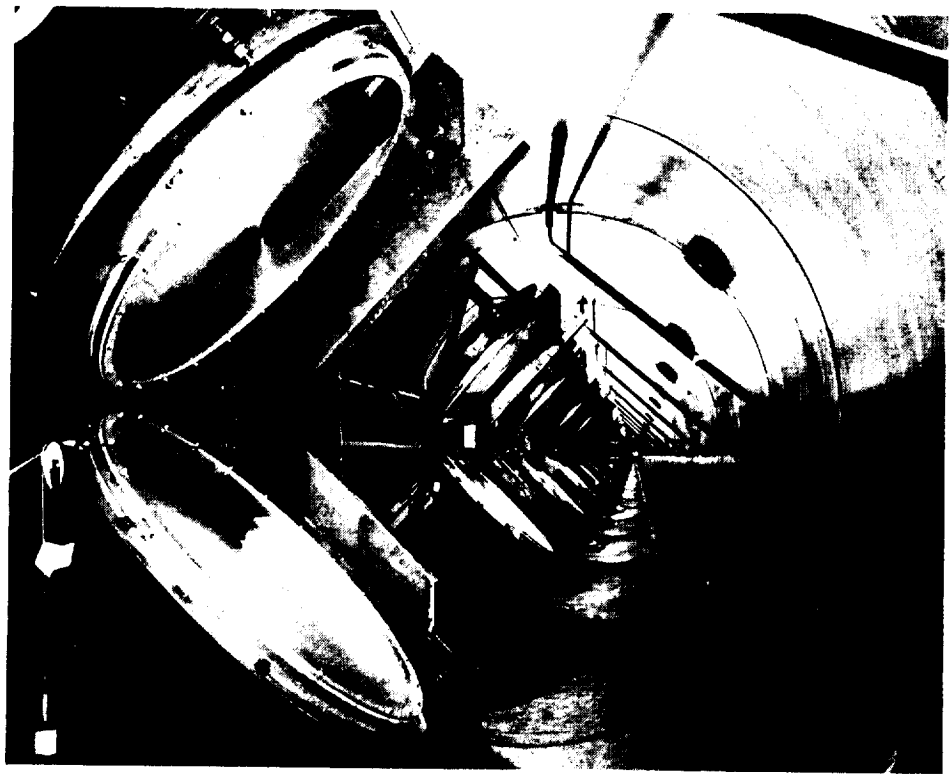

Fig.6.11(b) Uprange view of Fresnel-lens shadowgraph stations in the VKF 1000-ft Hypervelocity Range (courtesy of von Karman Gas Dynamics Facility, Arnold Engineering Development Center)

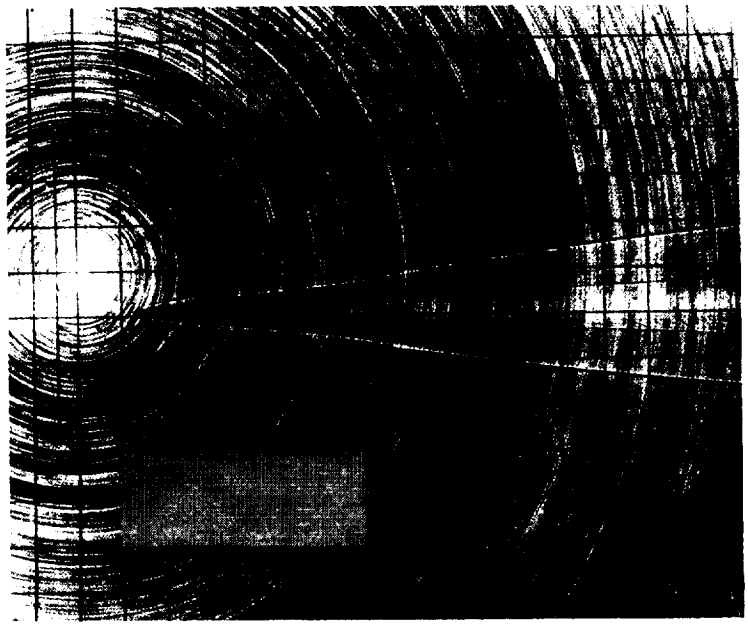

Fig. 6.11(c) Fresnel-lens shadowgram of a 6-deg-semi-angle cone in the VKF 1000-ft Hypervelocity Range. Model base diameter: 20 mm; velocity: 5.1 km/sec; range pressure: 0.2 atm. (courtesy of von Kármán Gas Dynamics Facility, Arnold Engineering Development Center)

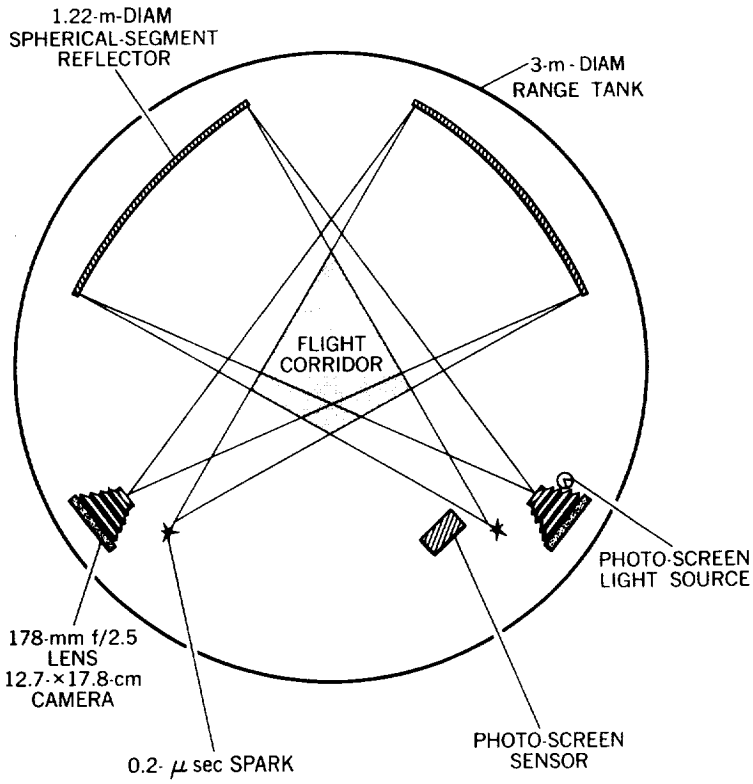

Fig. 6.12(a) Schematic of shadowgraph configuration in the NOL 1000-ft Hyperballistics Range

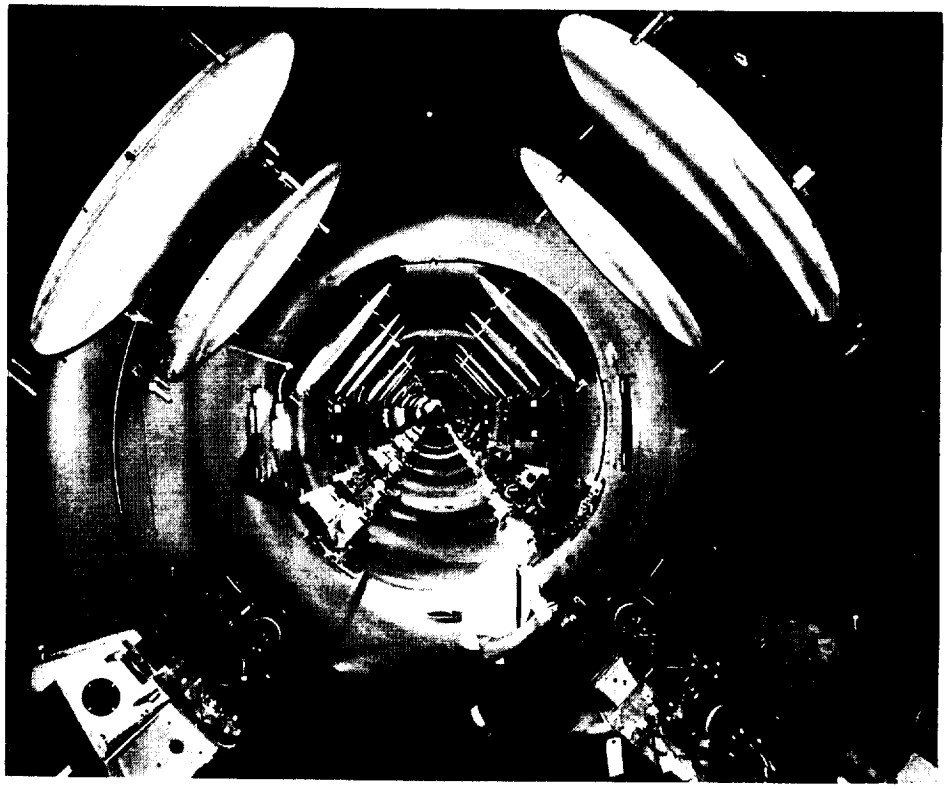

Fig.6.12(b) Uprange view of reflector shadowgraph stations in the NOL 1000-ft Hyperballistics Range (courtesy of US Naval Ordnance Laboratory)

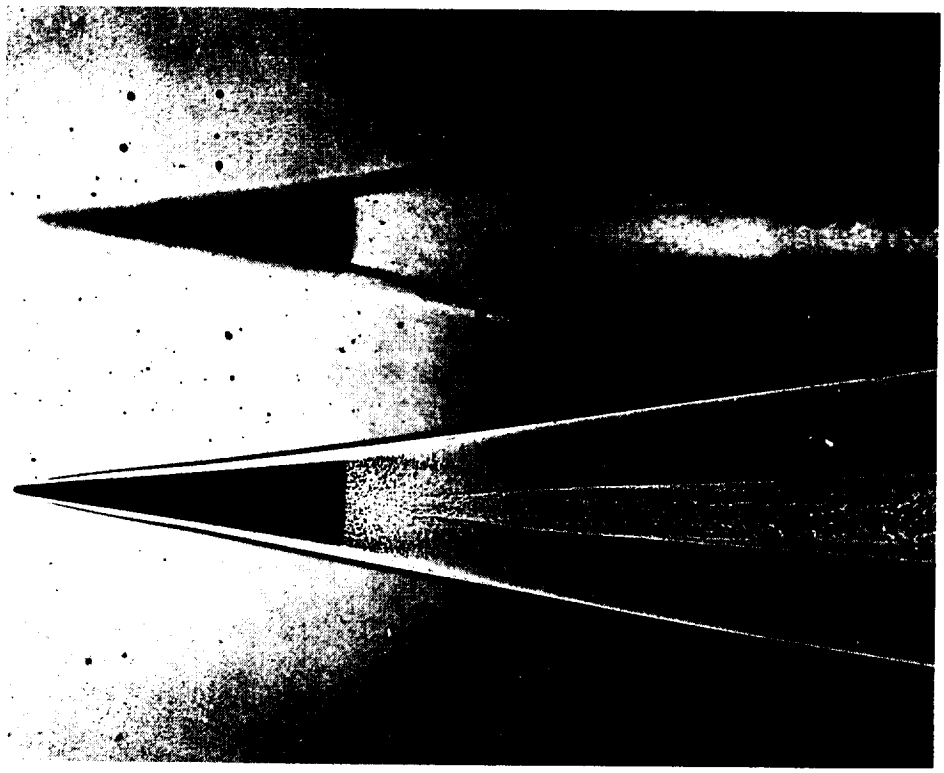

Fig.6.12(c) Reflector shadowgram of slender cone in the NOL 1000-ft Hyperballistics Range. Model base diameter: 32 mm; velocity: 3.4 km/sec; range pressure: 1 atm. See also Figure 6.25 (courtesy of US Naval Ordnance Laboratory)

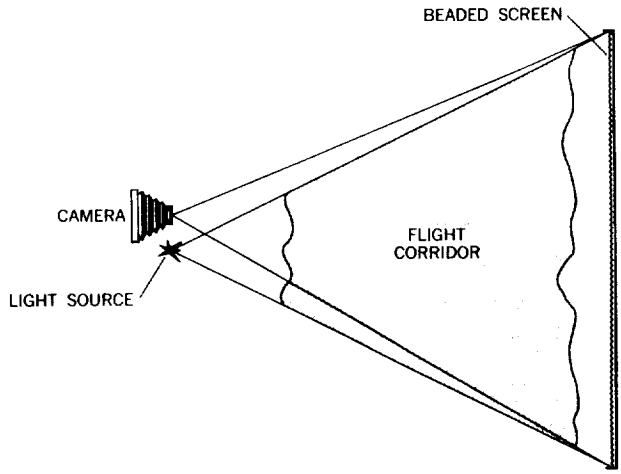

Fig. 6. 13 Schematic of a reflective-screen shadowgraph

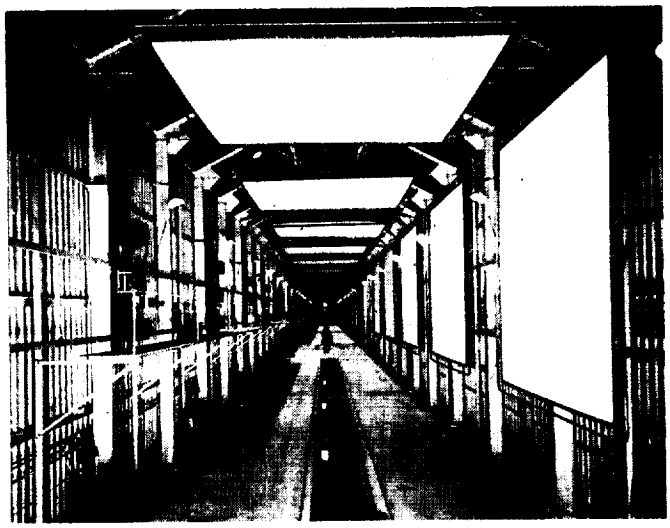

Fig. 6. 14(a) Downrange view of the BRL Transonic Range (courtesy of US Army Ballistic Research Laboratories)

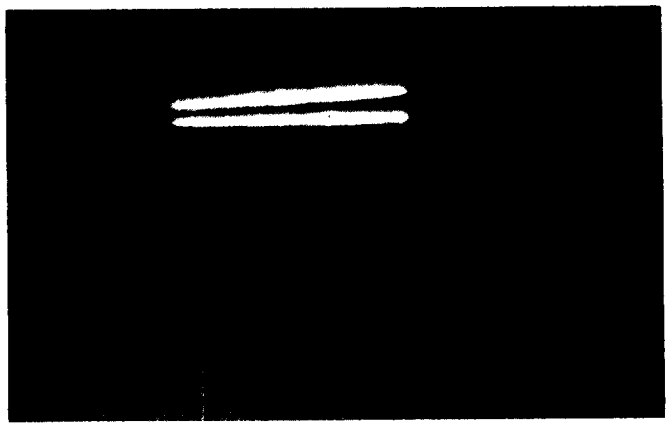

Fig. 6. 14(b) Shadowgram of a double-cone model taken in the BRL Transonic Range. Model diameter: 157 mm; velocity: 616 m/sec (courtesy of US Army Ballistic Research Laboratories)

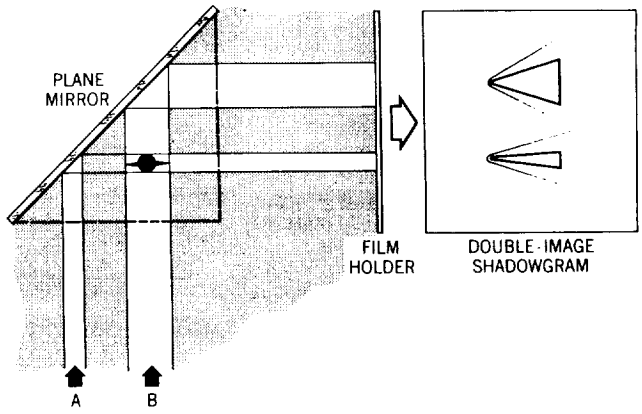

Fig.6.15(a) A simple orthogonal-view shadowgraph

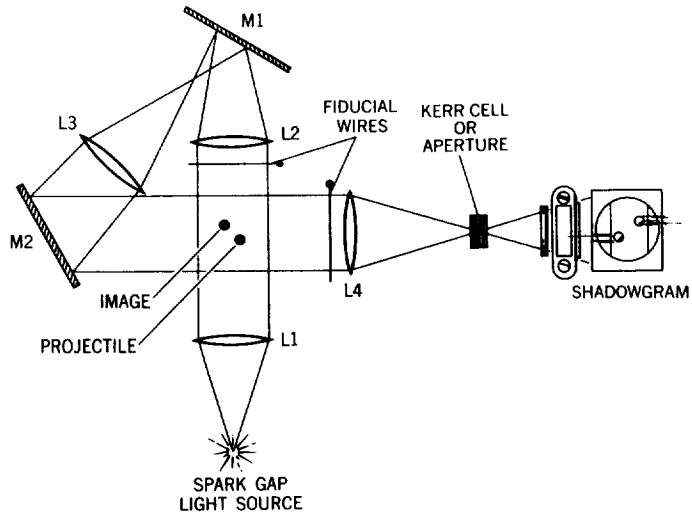

Fig.6.15(b) Schematic of a focused orthogonal-view shadowgraph using a folded light path

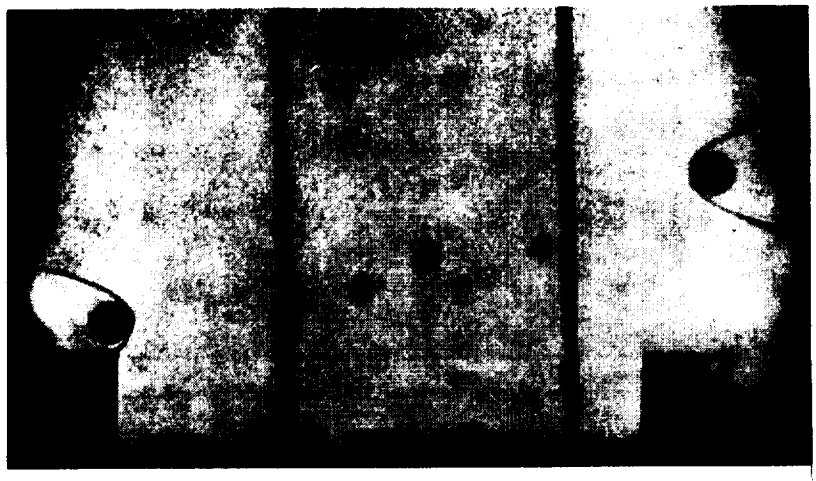

Fig.6.16 Shadowgram obtained in a small range using the configuration of Figure 6.15(b)

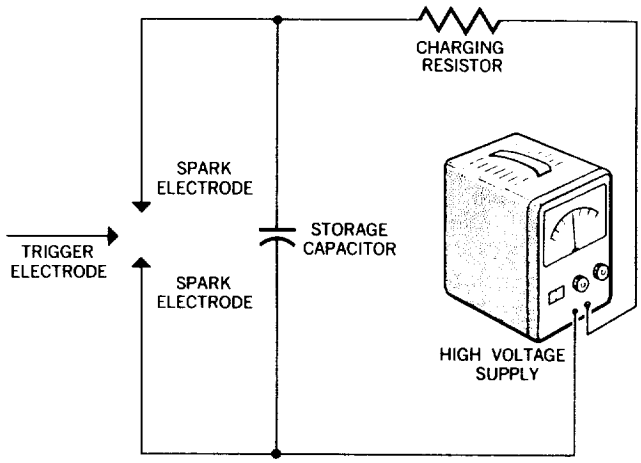

Fig.6.17 Schematic circuit diagram of capacitor-discharge-spark-gap light source

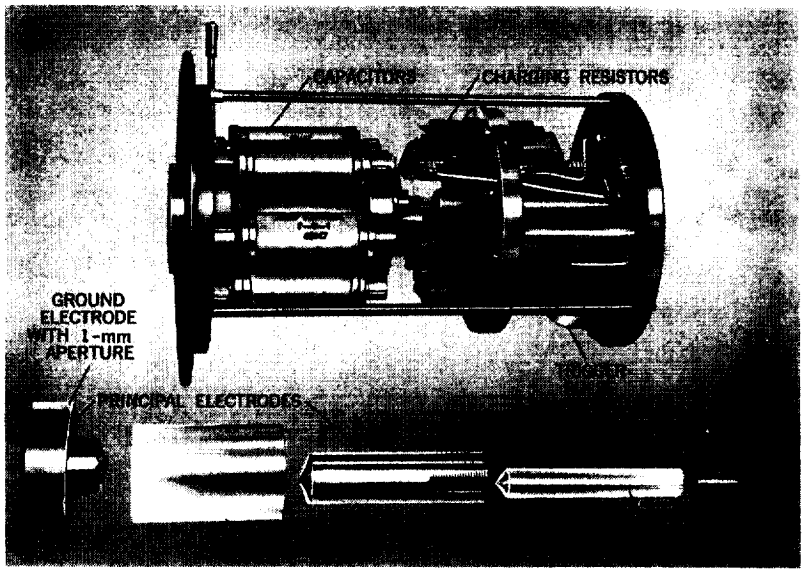

Fig.6.18 Capacitor-discharge-spark-gap light source

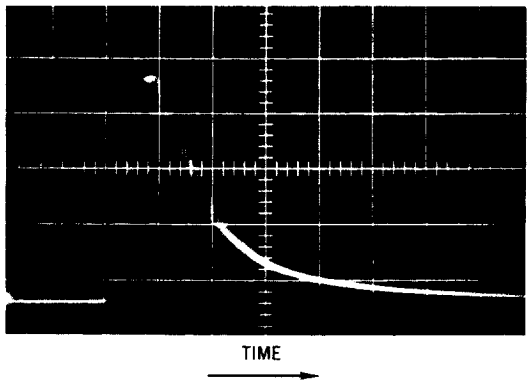

Fig.6.19 Light flux as a function of time of a capacitor-discharge-spark-gap light source; time scale: 0.2 microseconds per division

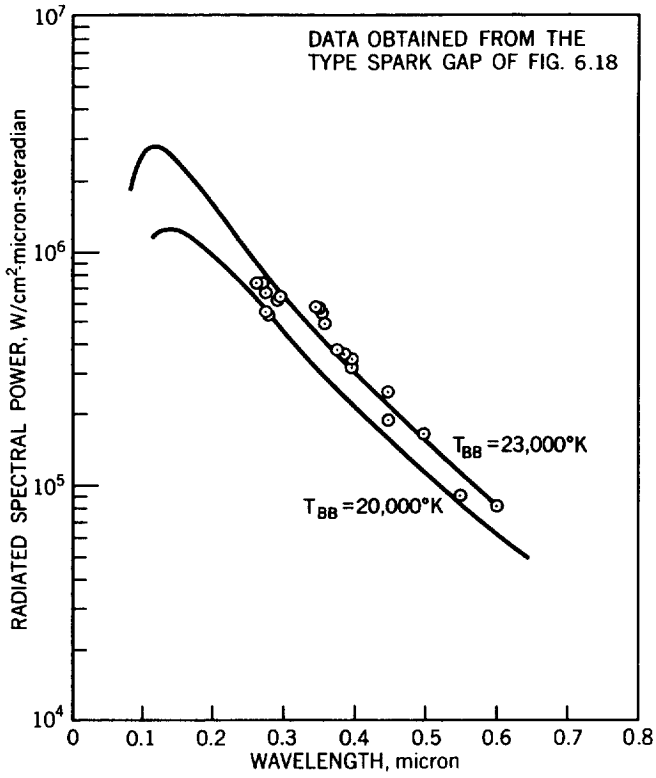

Fig.6.20 Radiated power as a function of wavelength for the type of spark gap of Figure 6.18

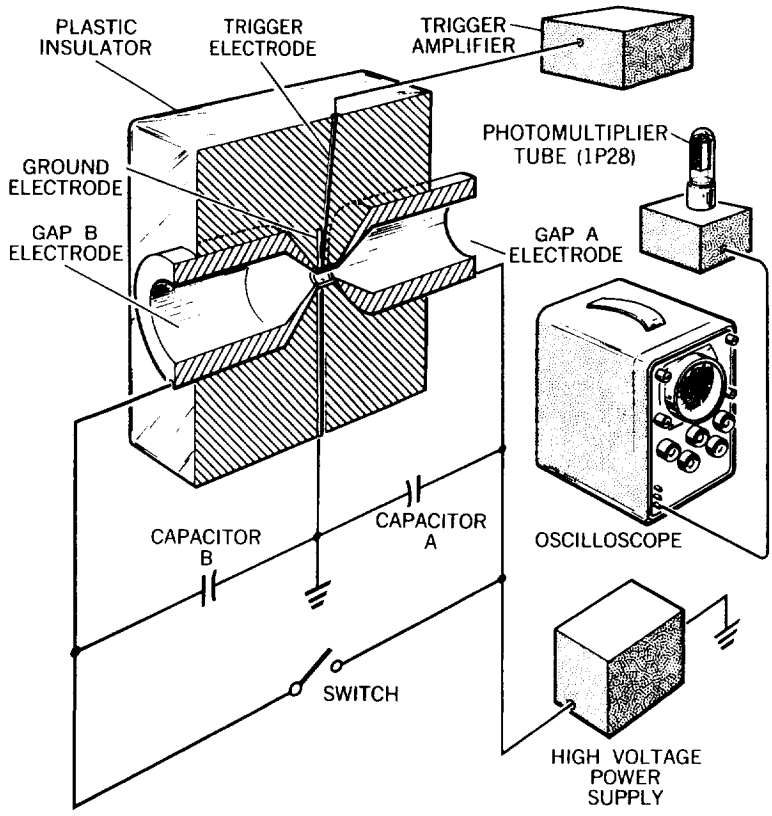

Fig.6.21 Schematic diagram of apparatus for spark-gap absorptivity test

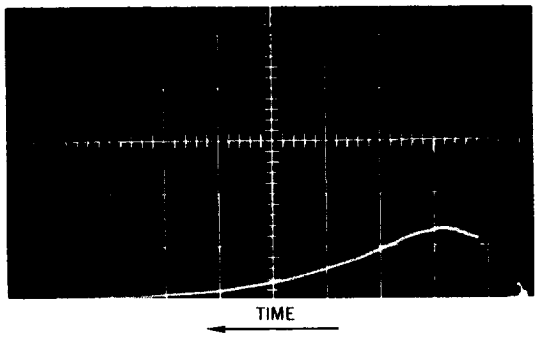

(a) Light output with capacitor A charged

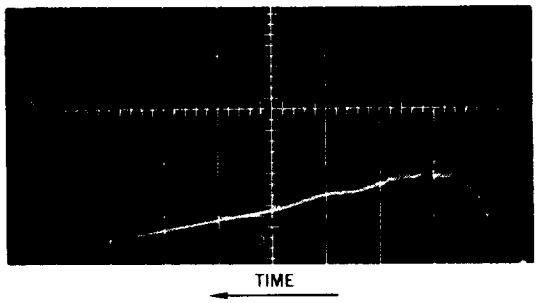

(b) Light output with capacitor A and B charged

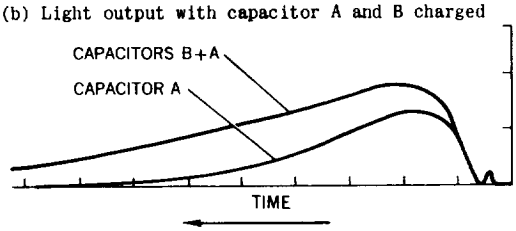

(c) Tracing of curves (a) and (b) from above

Fig. 6.22 Light-output records from spark-gap absorptivity tests

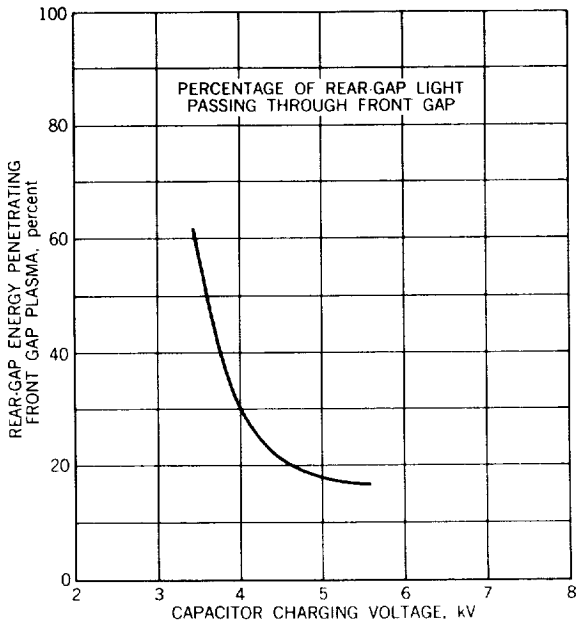

Fig. 6.23 Percentage of light from gap B being transmitted through gap A as a function of capacitor charging voltage

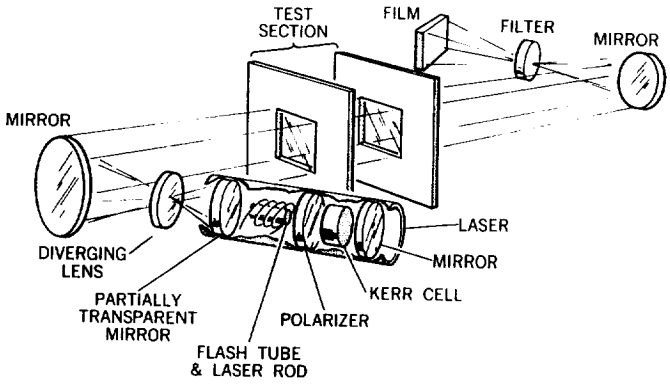

Fig.6.24 Schematic diagram of laser - shadowgraph system

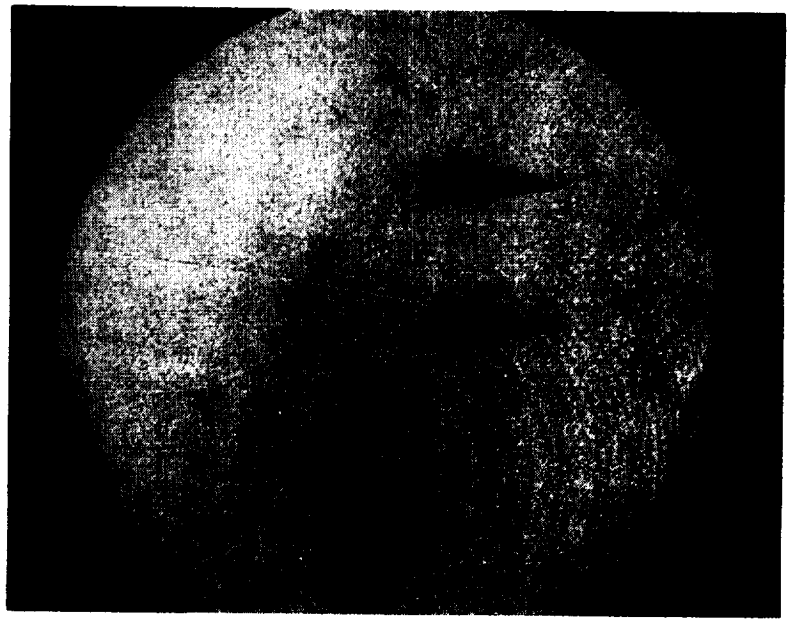

Fig.6.25 Laser shadowgram from the NOL 1000-ft Hyperballistics Range; velocity of 5.2 kilometers per second, and pressure of 33 millimeters of mercury (courtesy of the US Naval Ordnance Laboratory, White Oak, Maryland)

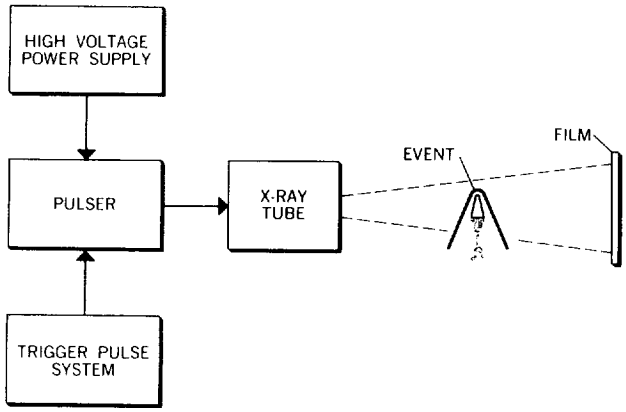

Fig.6.26 Schematic diagram of X-ray photographic system

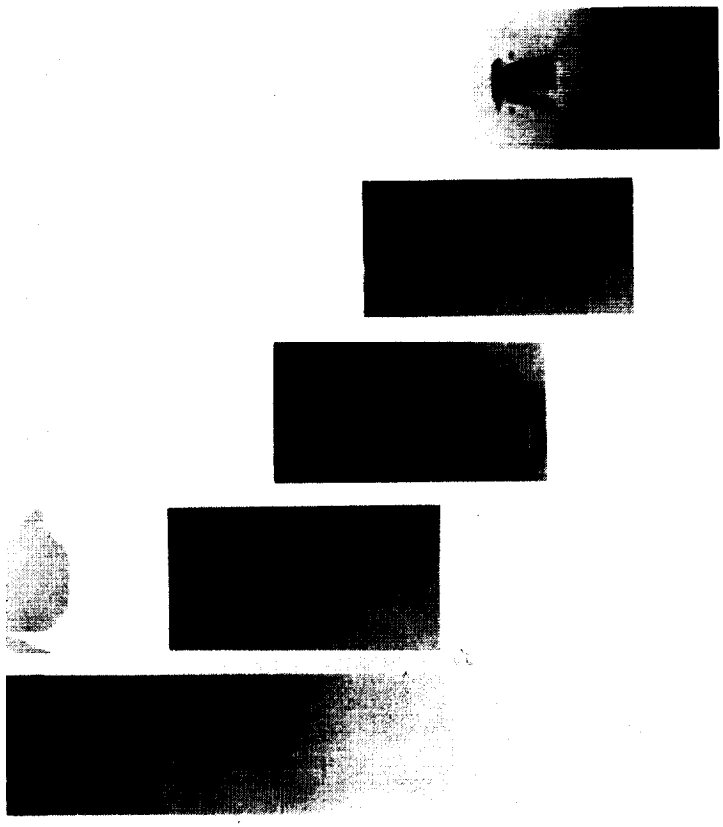

Fig.6.27 X-ray photographs of a model and sabot taken near the muzzle of the launch gun in the Ames Pressurized Ballistic Range

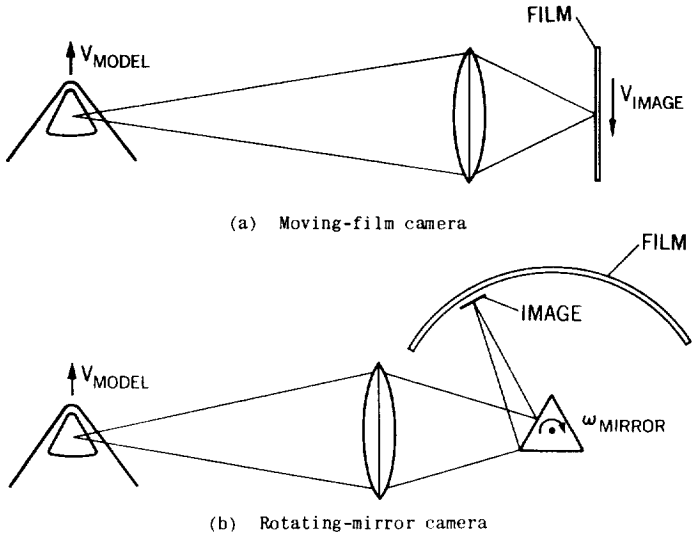

Fig.6.28 Image-movement compensation

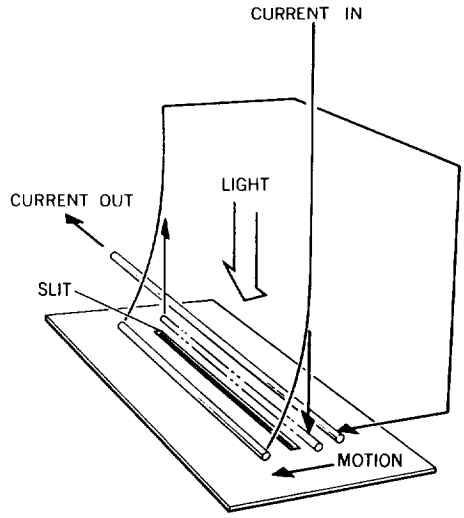

Fig.6.29 Galvanometer impulse shutter

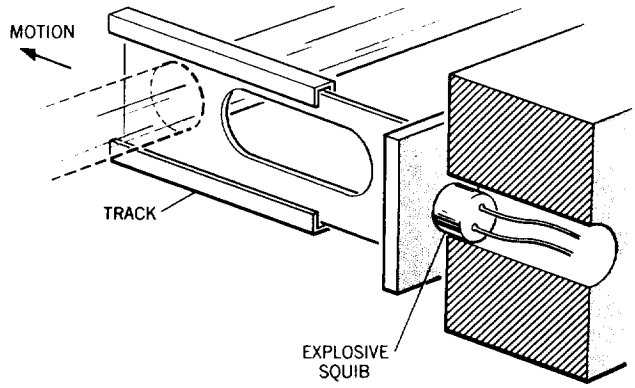

Fig.6.30 Explosively-driven blade shutter

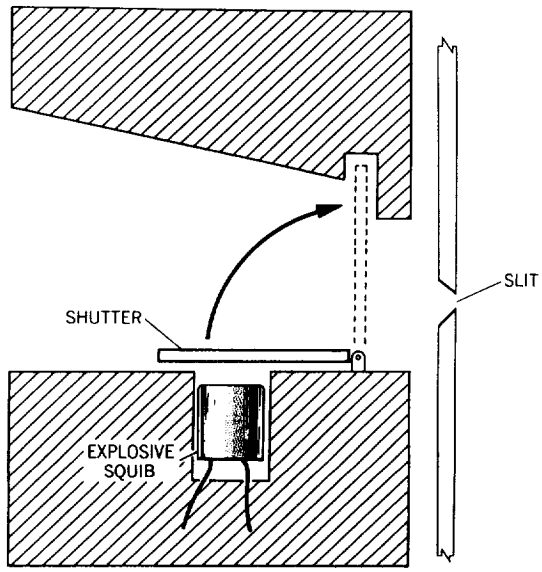

Fig.6.31 Explosively-driven pivoting shutter

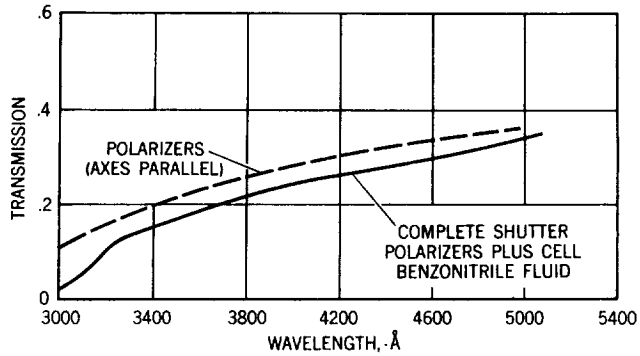

Fig.6.32 Spectral transmissivity of polarizers and complete Kerr-cell shutter

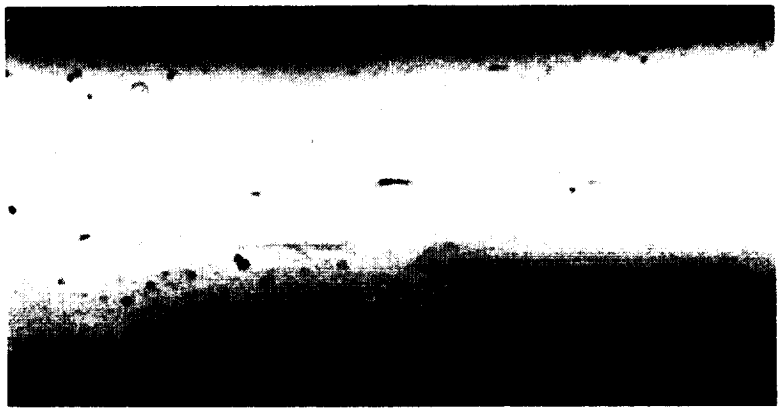

(a) 3-mm aperture at secondary image of source

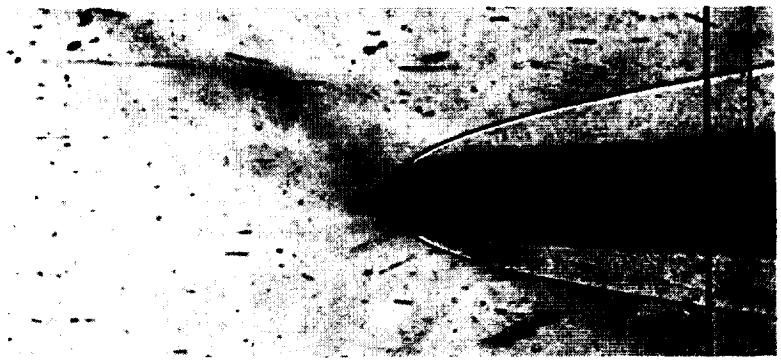

(b) 20-nsec Kerr-Cell shutter at secondary image of source

Fig. 6.33 Focused shadowgram of burning aluminum model. Velocity 6.0 km/sec; range density 0.25 atmosphere

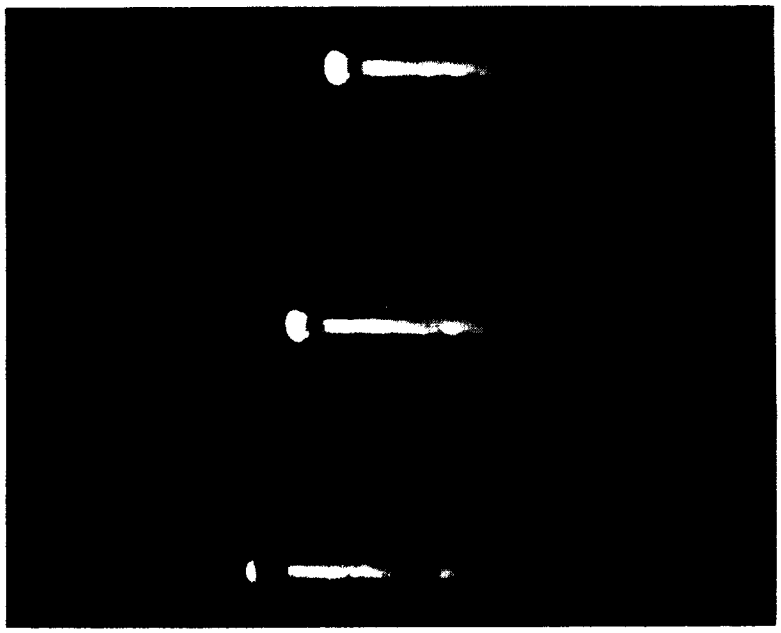

Fig. 6.34 Sequential image-converter photographs of 13-mm-diameter polyethylene slug. Velocity: 7.1 km/sec; range density: 0.1 atmosphere

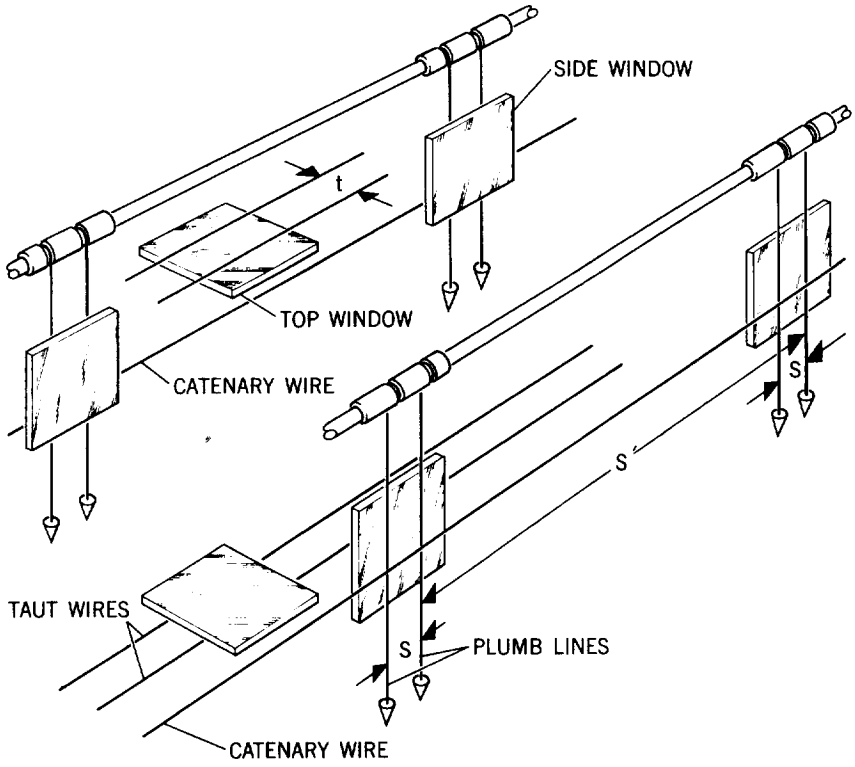

Fig.6.35 Schematic drawing of fiducial system used with collimated light

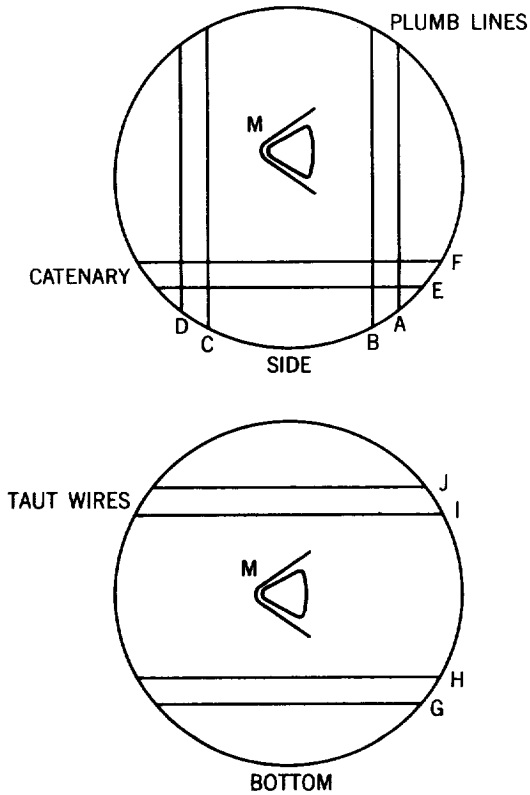

Fig.6.36 Images of fiducial wires in the side and bottom shadowgrams (circular window apertures)

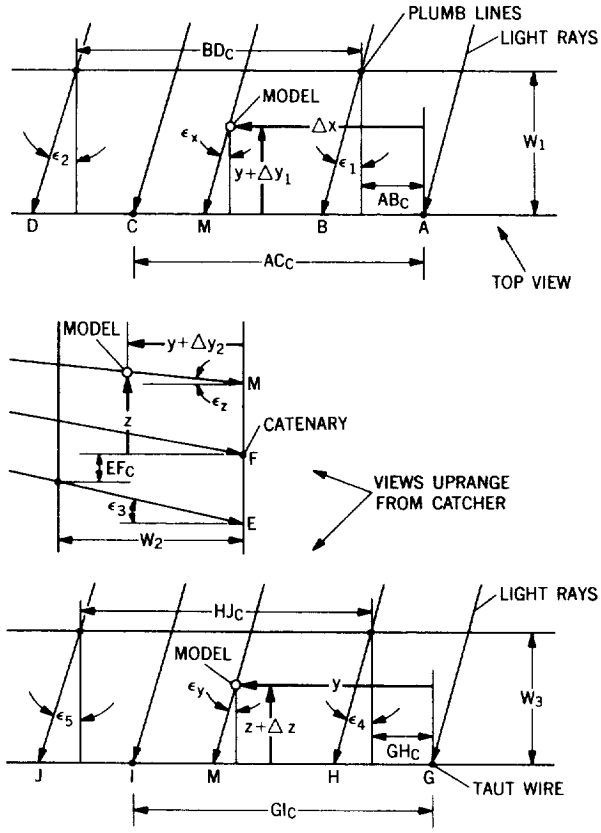

Fig. 6.37 Relationships between light rays, measurement references, and model-image location in one near-parallel-light shadowgraph station

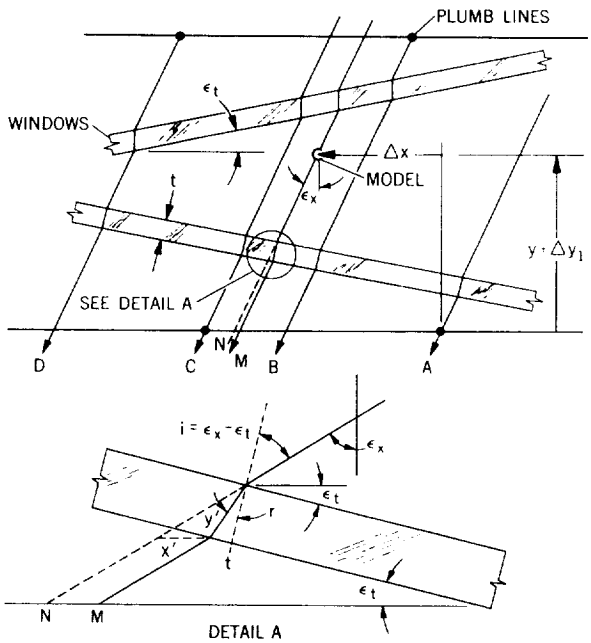

Fig. 6.38 Ray diagram illustrating the lateral displacement of a beam of light through two nonparallel glass windows

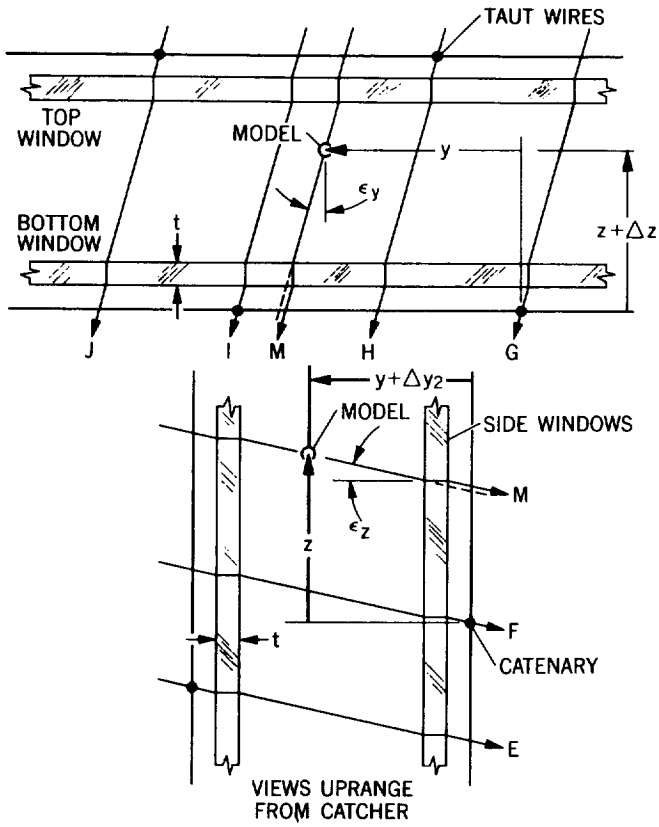

Fig.6.39 Ray diagram illustrating the displacement of light beams through two parallel glass windows

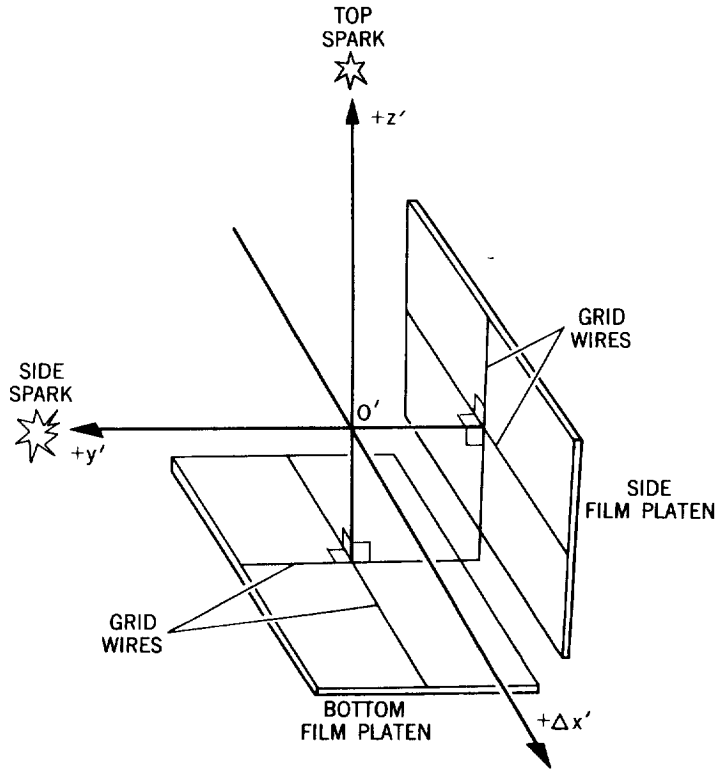

Fig.6.40 Schematic drawing of the station-coordinate system for a conical-projection direct shadowgraph

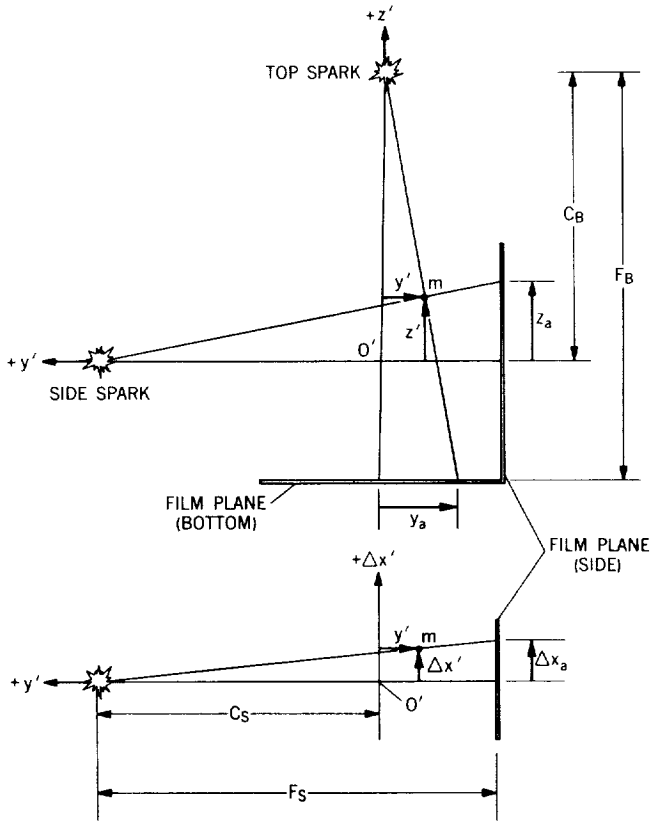

Fig.6.41 Ray diagram illustrating the magnification of the model image due to conical projection

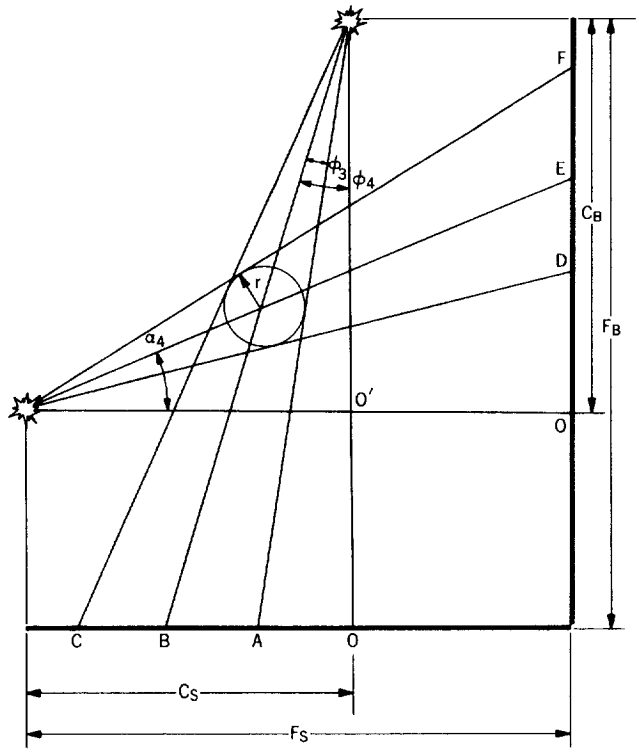

Fig.6.42 Illustration of the paths of the light rays about a sphere in a conical projection

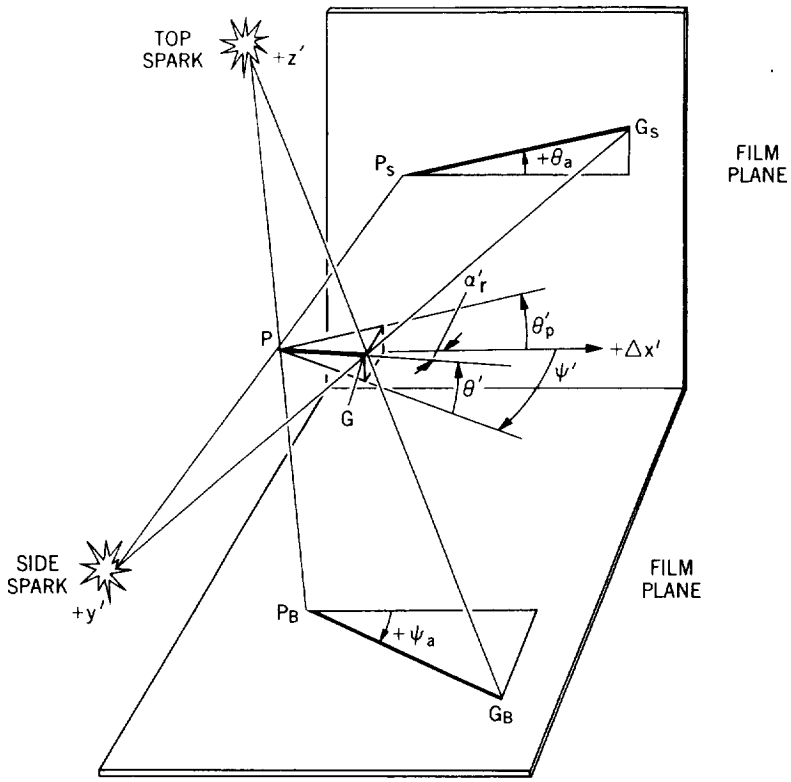

Fig.6.43 Ray diagram illustrating the distortions of the model attitude due to conical projection

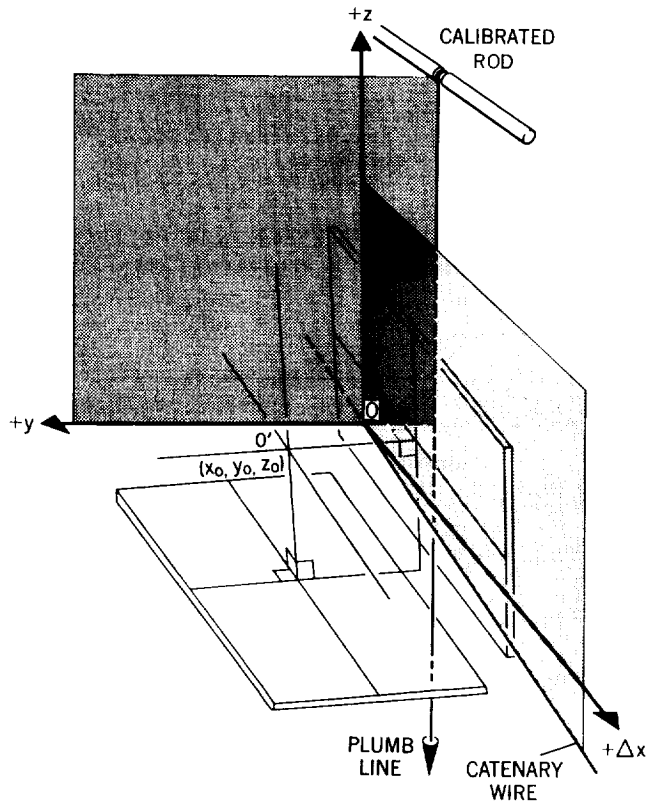

Fig.6.44 Relationship of the range- and station-coordinate system for a conical-projection direct shadowgraph

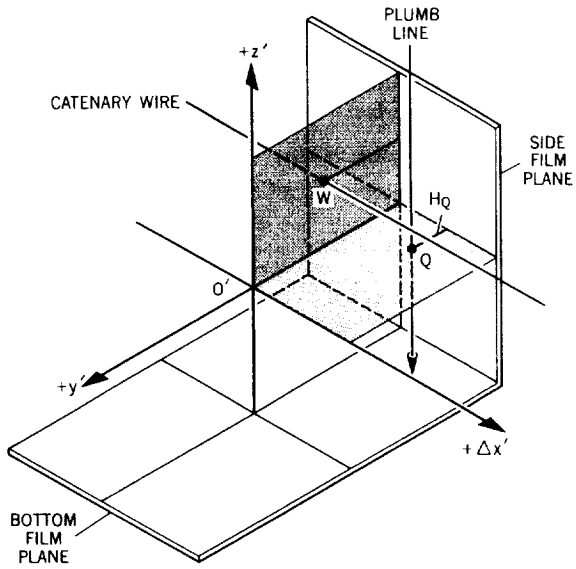

Fig.6.45 Location of the W and Q points in the station-coordinate system

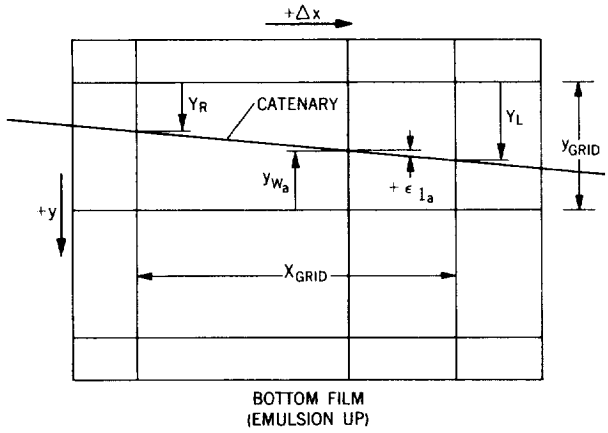

Fig.6.46 Wire images in the bottom film used to determine the apparent angle of yaw of the station-coordinate system with respect to the range-coordinate system

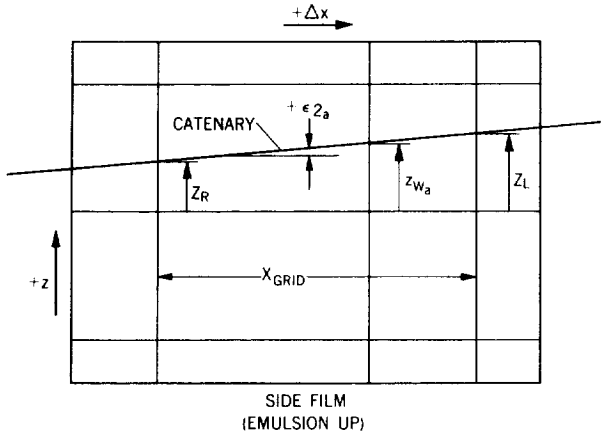

Fig.6.47 Wire images in the side film used to determine the apparent angle of pitch of the station-coordinate system with respect to the range-coordinate system

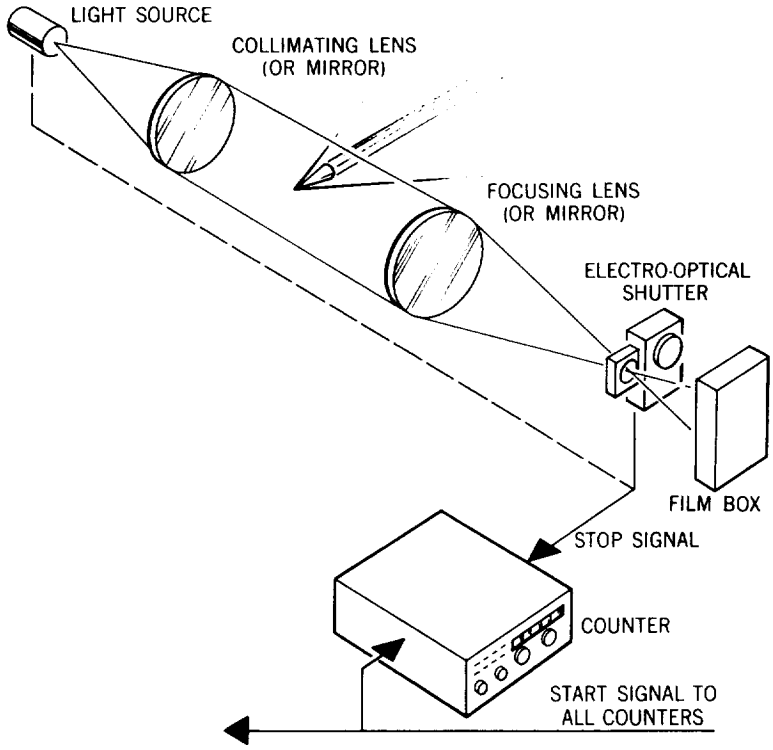

Fig.6.48 Hook-up of a one-channel electronic counter

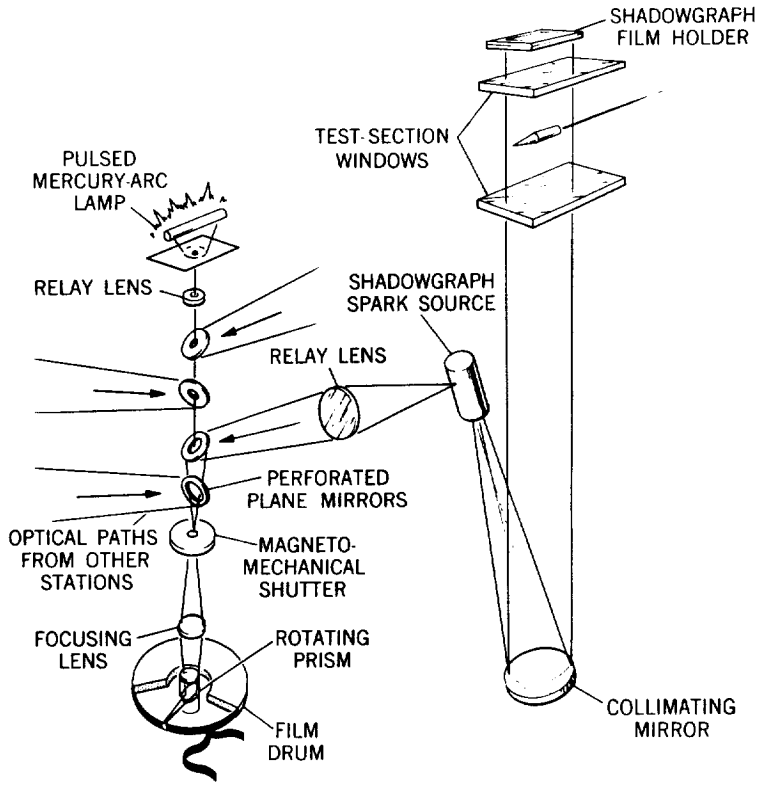

Fig.6.49 Sketch of a rotating-prism optical chronograph

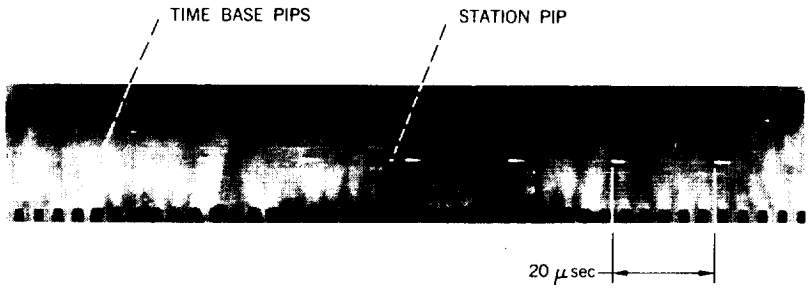

Fig.6.50 Segment of chronograph film record

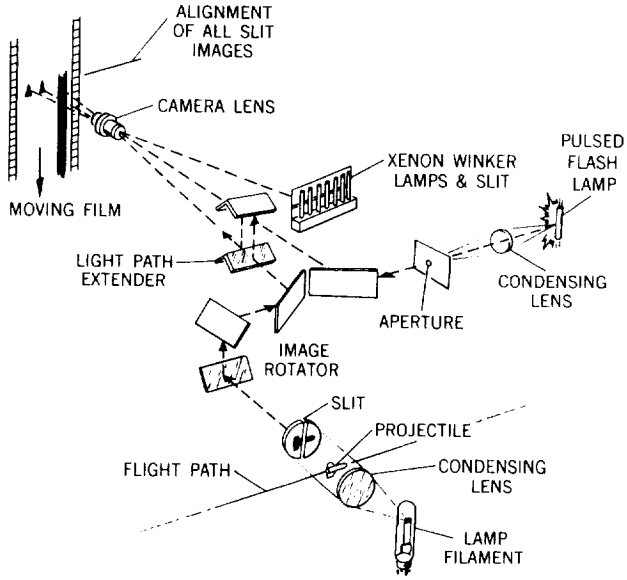

Fig.6.51 Sketch of a streak-camera optical chronograph

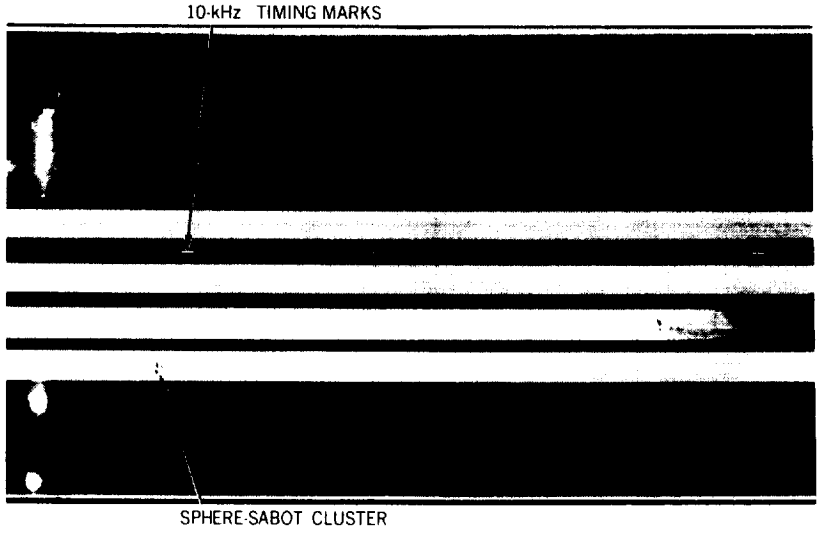

Fig.6.52 Portion of the film record from a streak-camera chronograph showing shadow images of a 4.8-mm-diameter aluminum sphere and segments of its sabot. The velocity of 5.76 km/sec was determined from this record (courtesy of US Naval Research Laboratory)

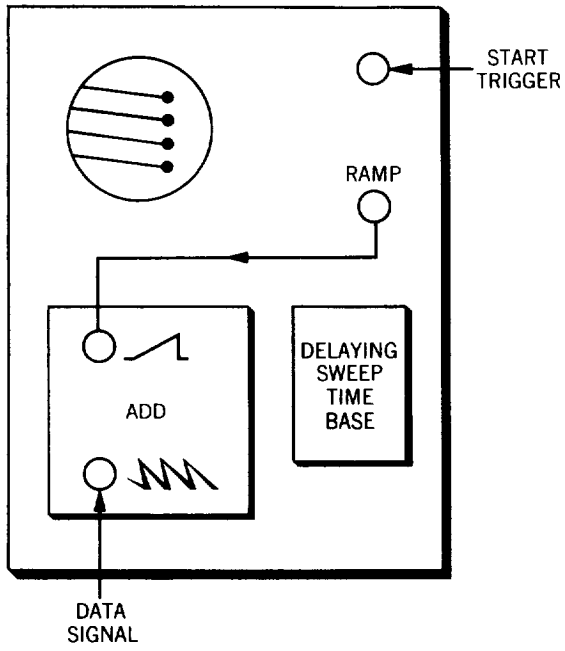

Fig.6.53 Oscilloscope hook-up for raster display (after Pennelegion, National Physical Laboratory, England)

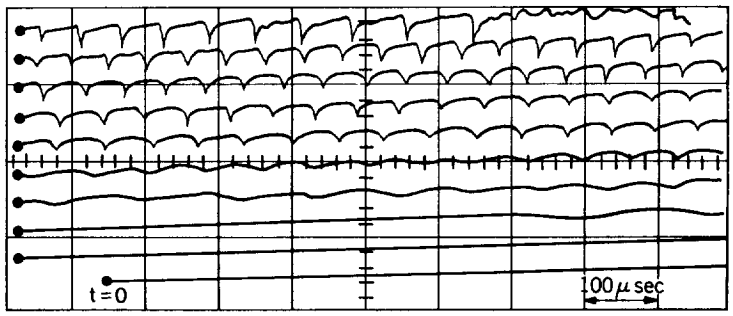

Fig.6.54 Raster-display oscilloscope record (after Pennelegion, National Physical Laboratory, England)

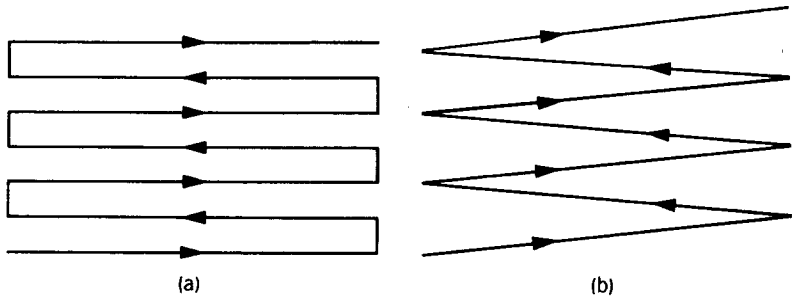

Fig.6.55 Alternative raster patterns

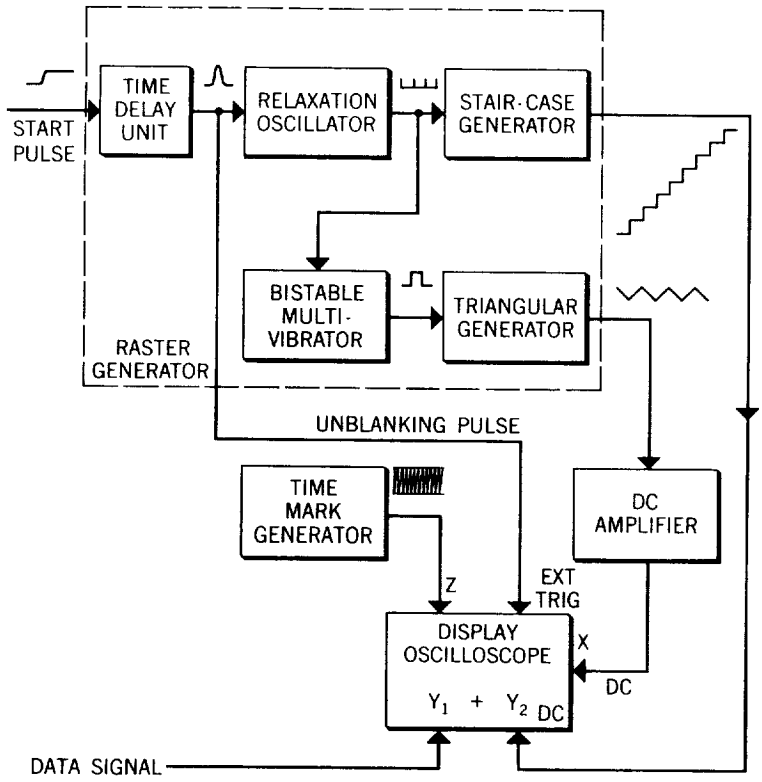

Fig.6.56 Block diagram of oscilloscope hook-up with external raster generator

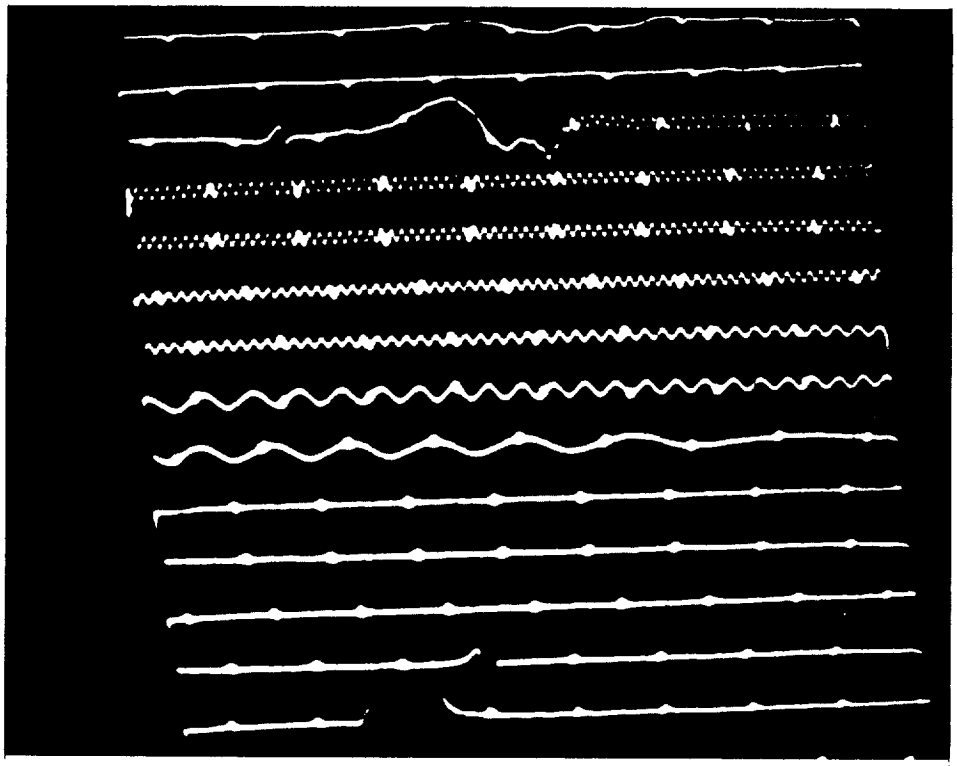

Fig.6.57 Oscilloscope record obtained with hook-up of Figure 6.56

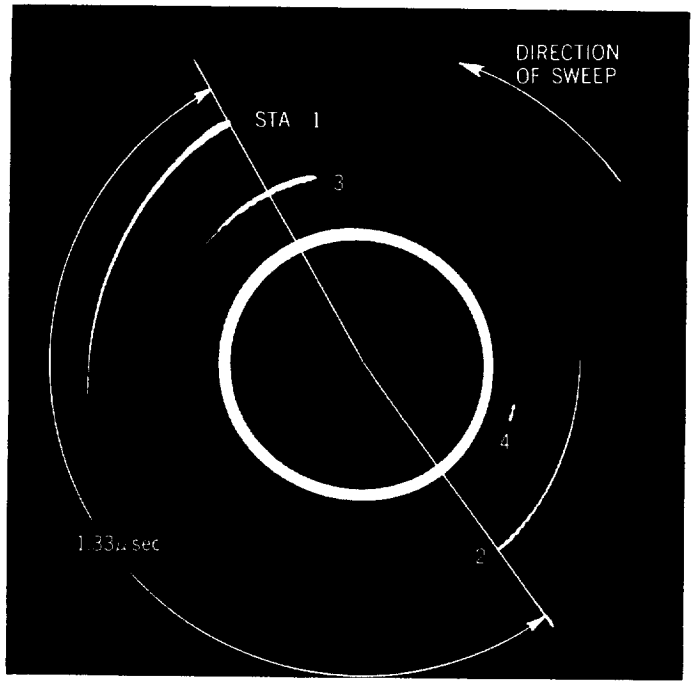

Fig.6.58 Circular-sweep oscilloscope record

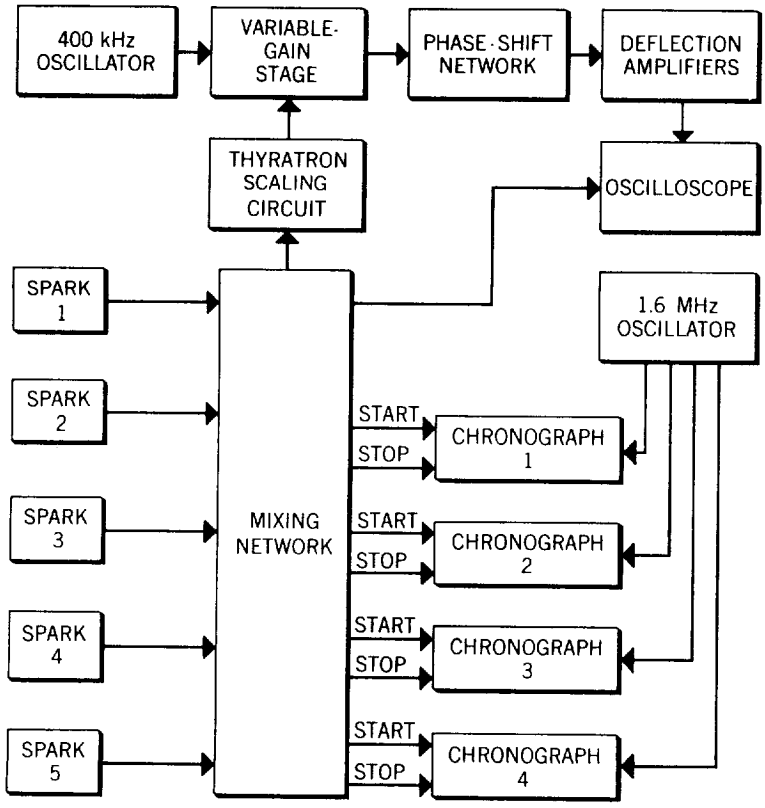

Fig.6.59 Block diagram of circular-sweep chronograph system

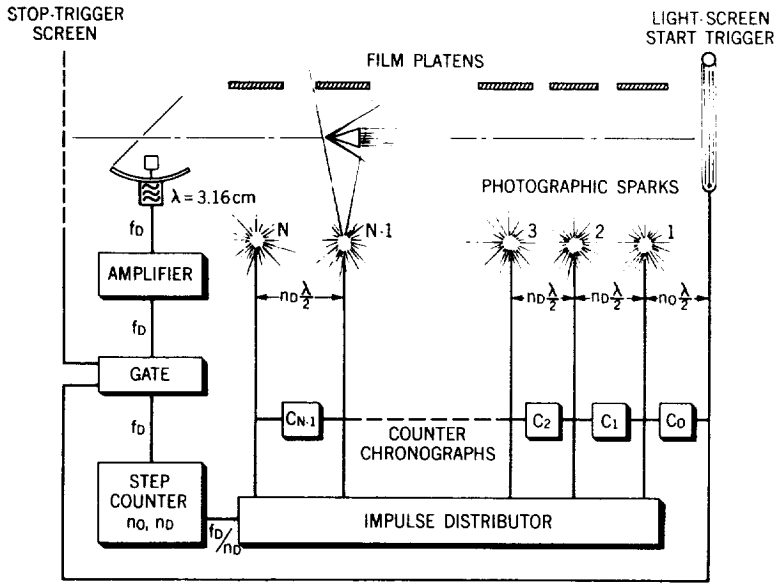

Fig. 6.60 Schematic of microwave-Doppler range instrumentation at ISL (courtesy of Deutsch-Französisches Forschungsinstitut, Saint-Louis)

Fig. 6.61 Multi-strand breakwire used to trigger microflash photograph of projectile. (Courtesy of US Naval Ordnance Laboratory)

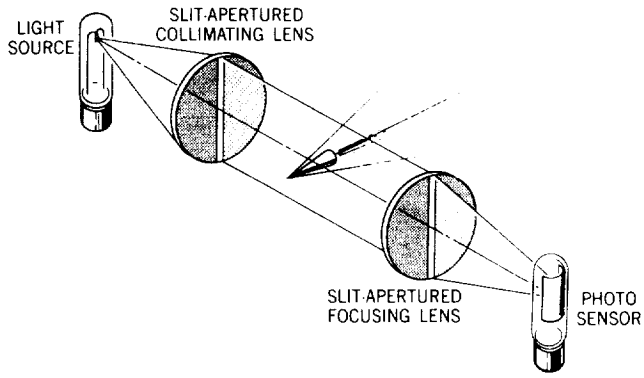

Fig. 6.62 Arrangement of a typical light-screen projectile detector

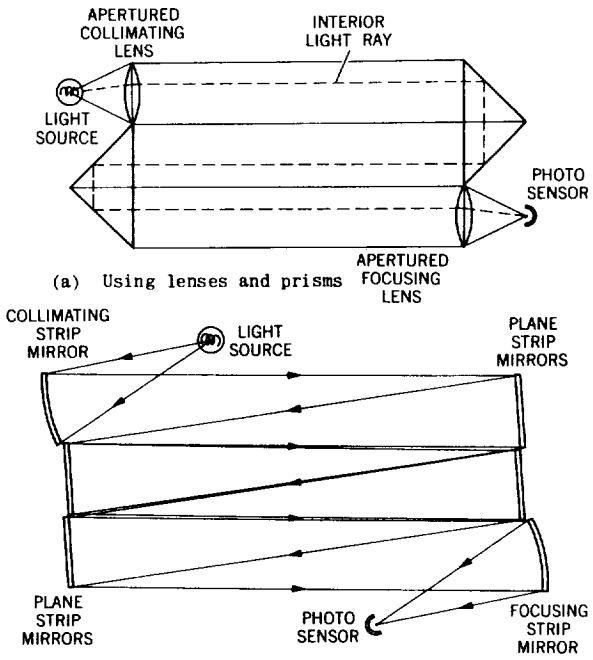

(a) Using lenses and prisms

(b) Using spherical and plane strip mirrors

Fig.6.63 Alternative arrangements of a folded multi-pass light screen

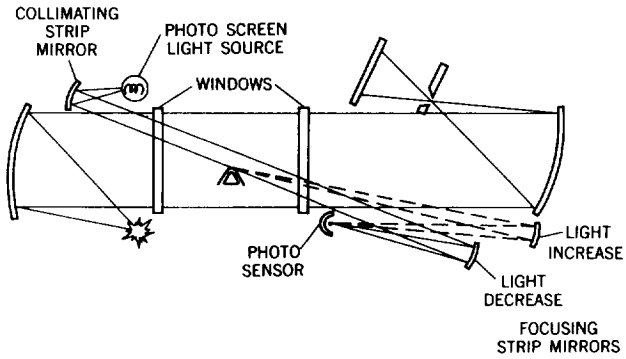

Fig.6.64 Schematic of a shadowgraph station with diagonal zero-time-delay light screen

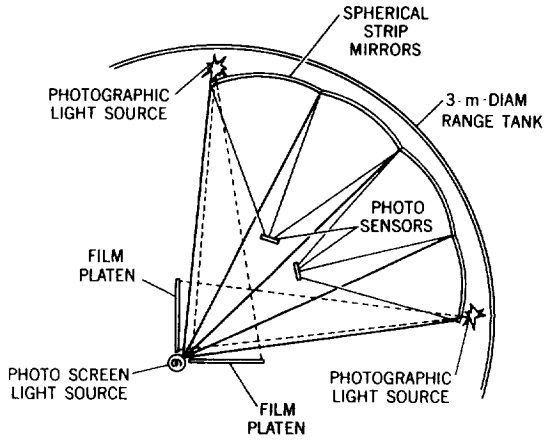

Fig.6.65 Sketch of multi-path zero-time-delay light screen used in the Ames pressurized ballistic range.

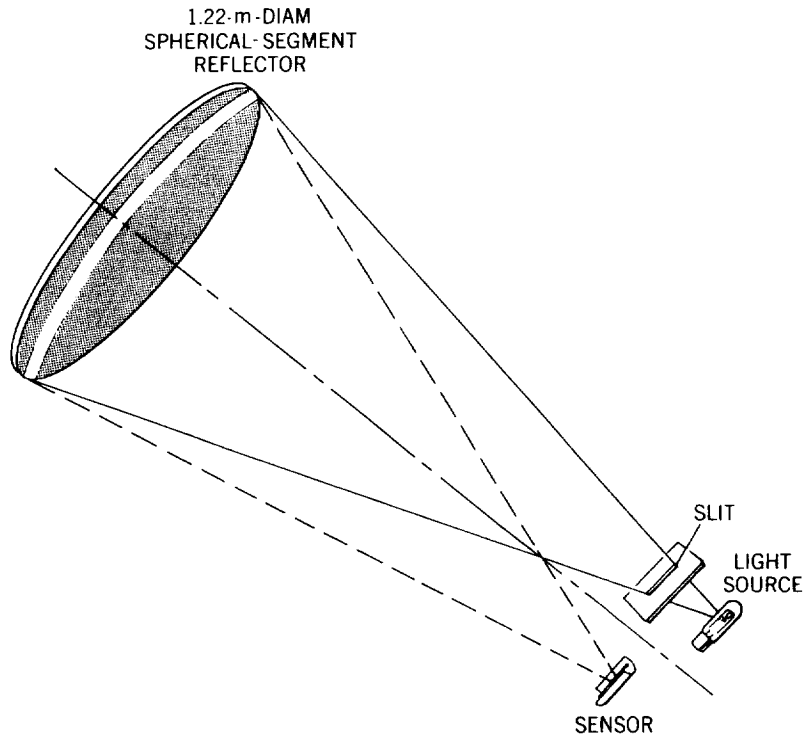

Fig.6.66 Zero-time-delay light screen used in the NOL 1000-ft hyperballistics range. (Courtesy of US Naval Ordnance Laboratory)

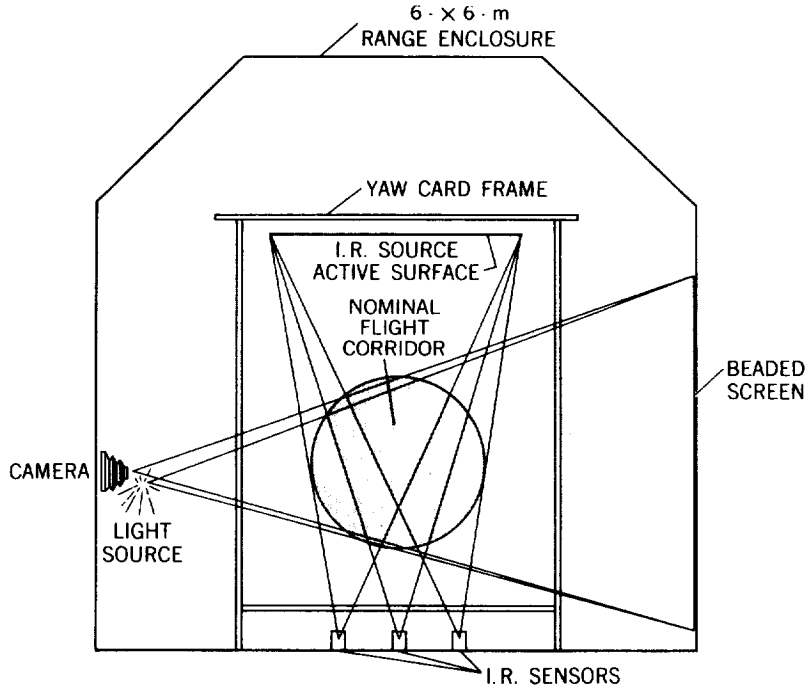

Fig.6.67 Schematic of CARDE Aeroballistic Range Station. (Courtesy of Canadian Armament Research and Development Establishment)

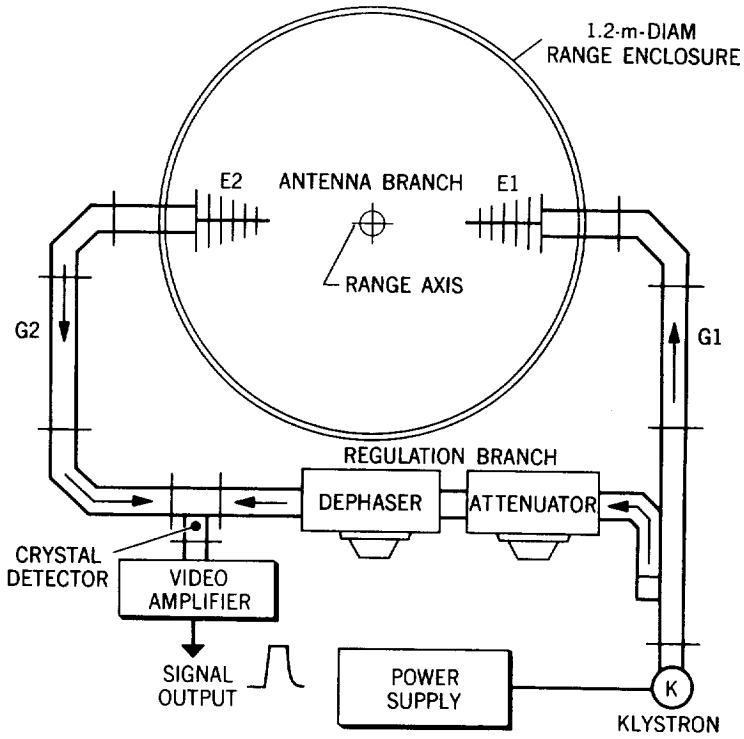

(a) Sketch of the apparatus

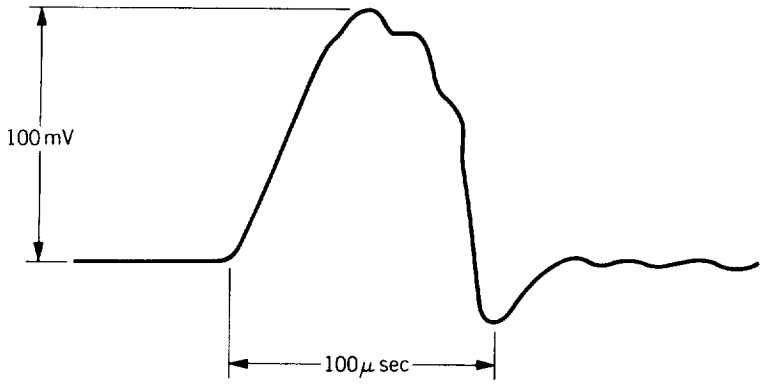

(b) Oscillogram of a typical output signal

Fig.6.68 Microwave-interferometer trigger developed at LRBA. (Courtesy of Laboratoire de Recherches Ballistiques et Aérodynamiques de Vernon)

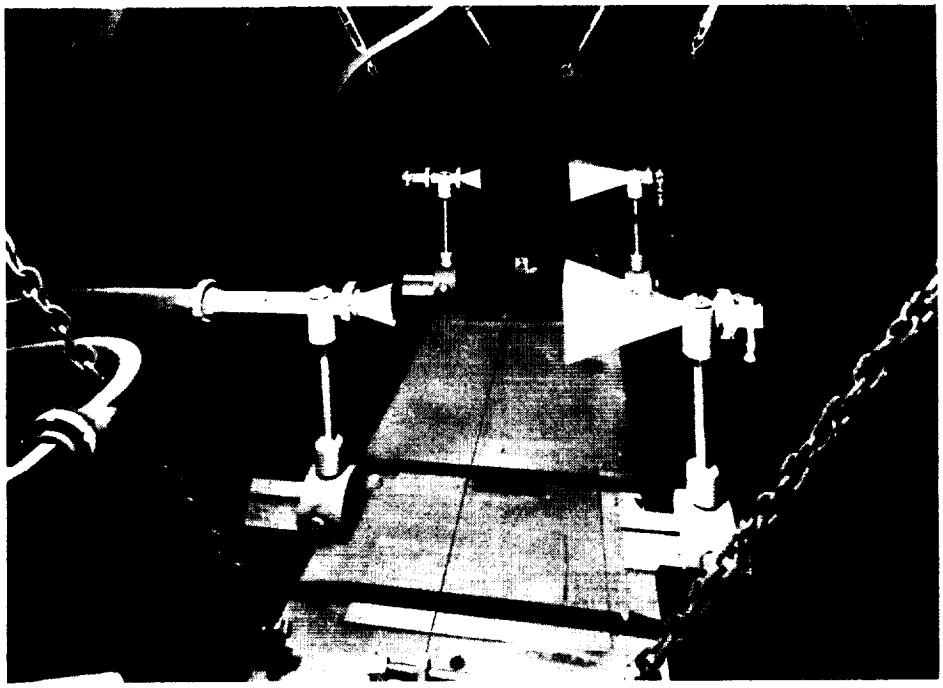

Fig. 6.69 Microwave-attenuation-trigger antenna horns on swinging support in range tank. (Courtesy of Royal Armament Research and Development Establishment. "British Crown copyright reserved. Reproduced with the permission of The Controller, Her Brittanic Majesty's Stationery Office")

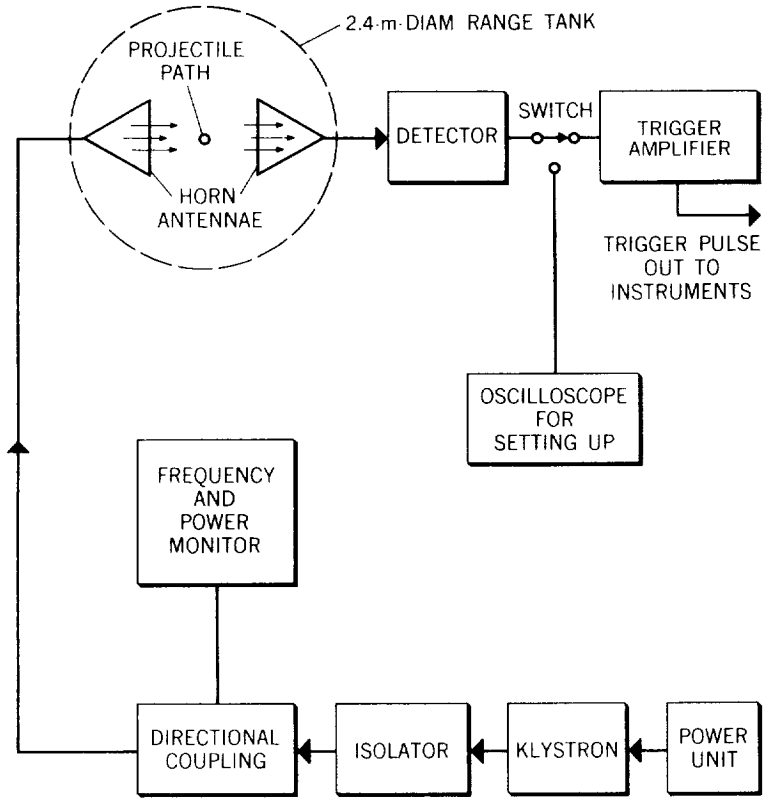

Fig. 6.70 Block diagram of microwave-attenuation-trigger circuit. (Courtesy of Royal Armament Research and Development Establishment)

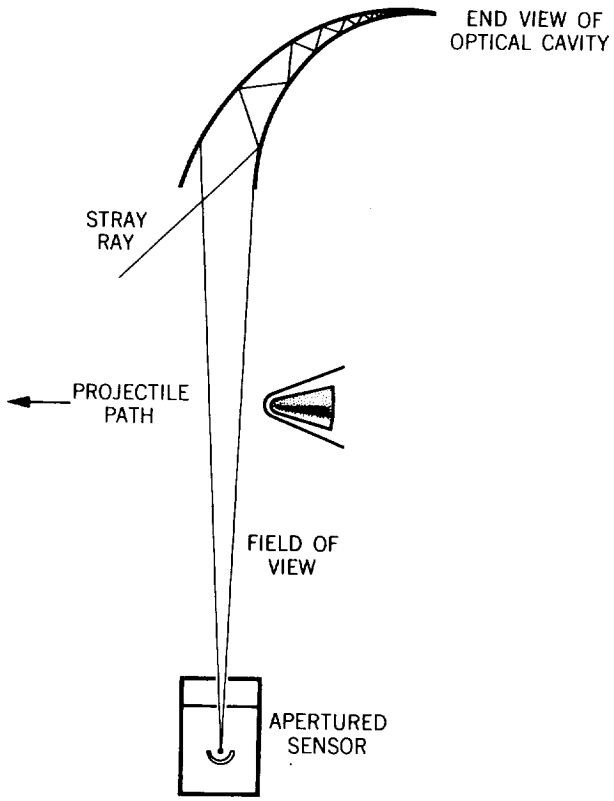

Fig.6.71 Schematic of an optical-radiation projectile detector

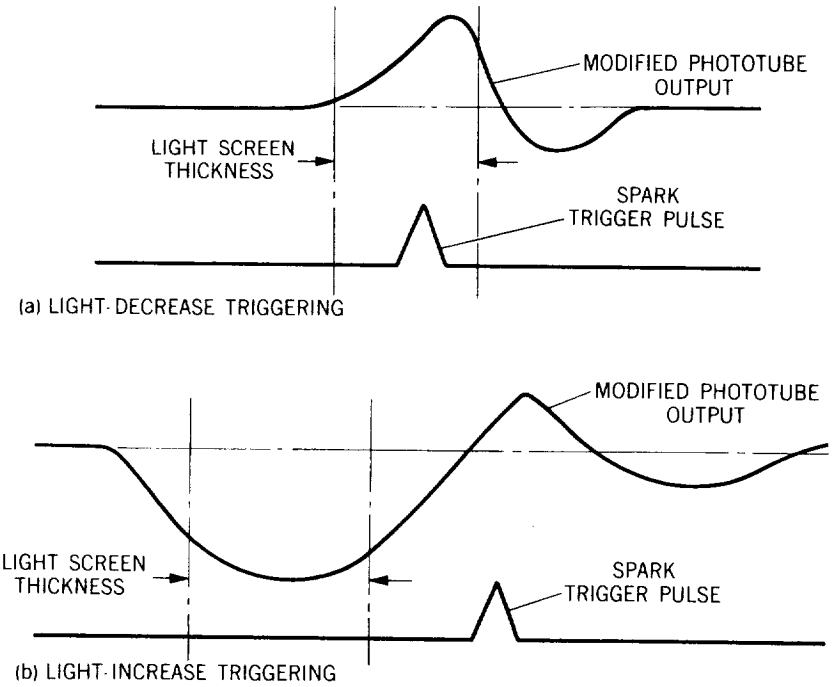

Fig.6.72 Dual-mode triggering. (Courtesy of US Naval Ordnance Laboratory)

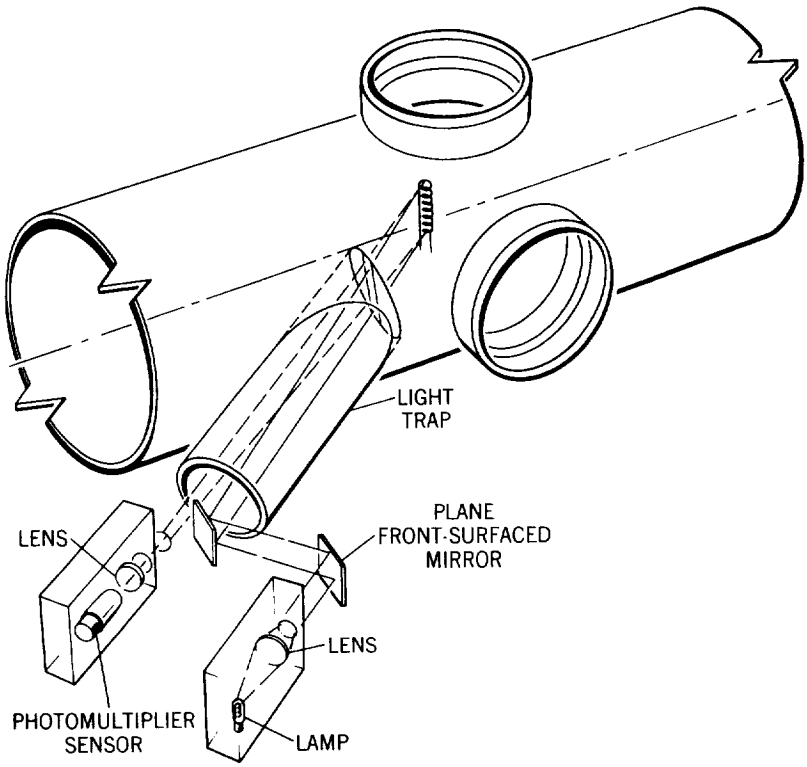

Fig.6.73 Light-increase sensor which responds to luminous or nonluminous projectiles (after Wall, Royal Armament Research and Development Establishment)

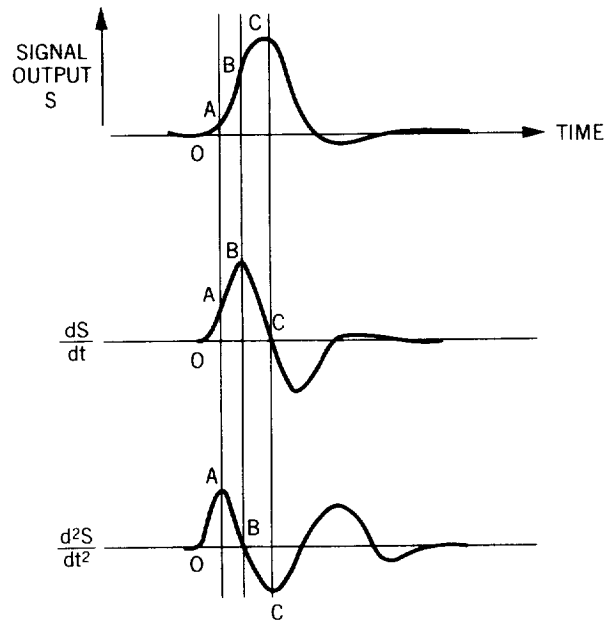

Fig.6.74 Triggering points on a typical sensor-output-signal trace

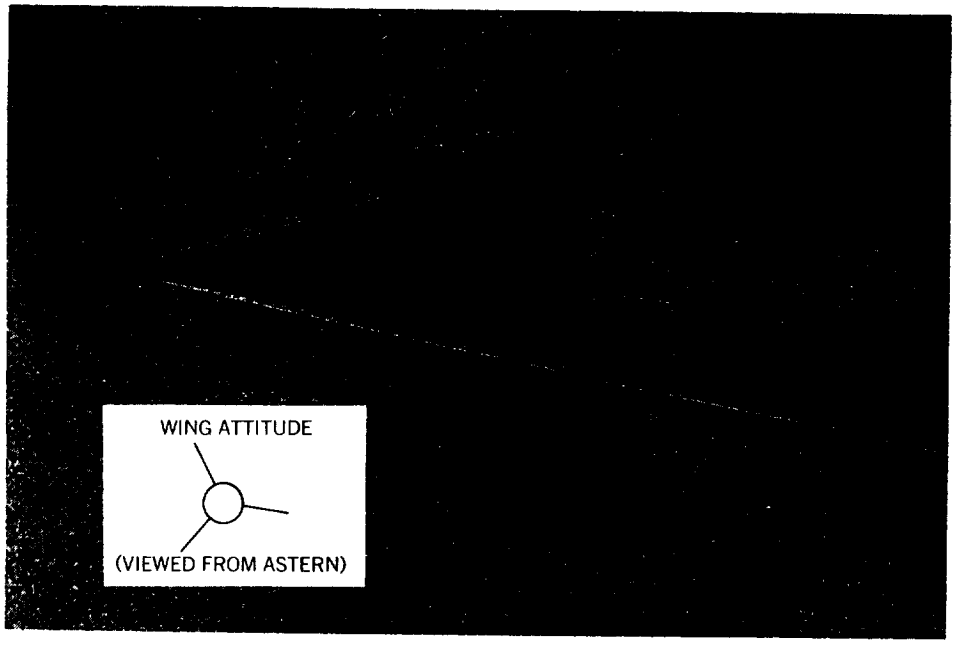

Fig.6.75 Shadowgram of three-wing model

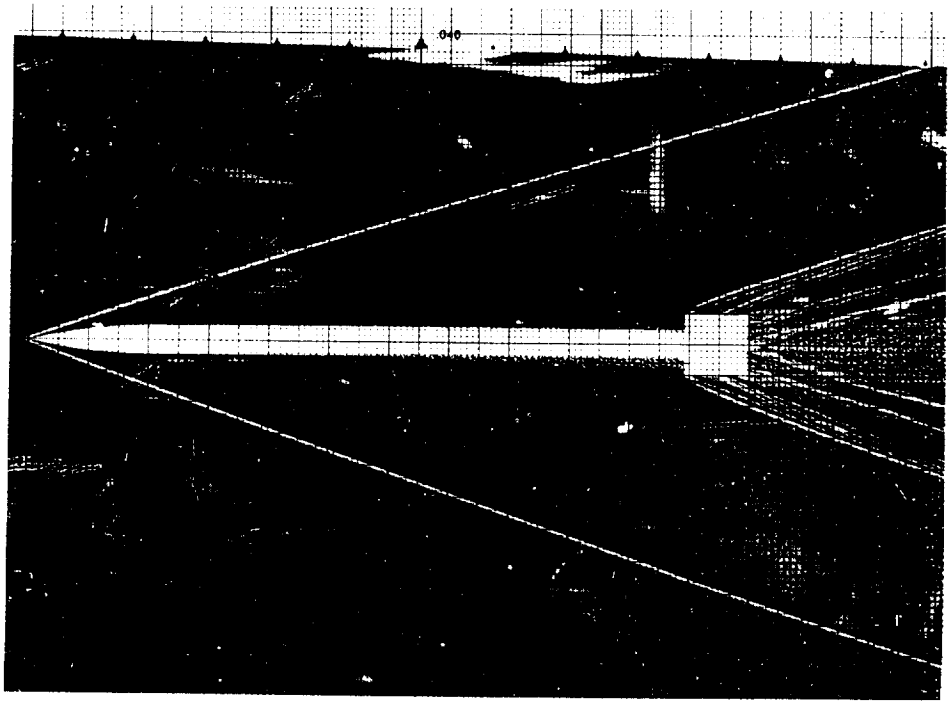

Fig.6.76 Photograph of glass grid superimposed on shadowgram negative

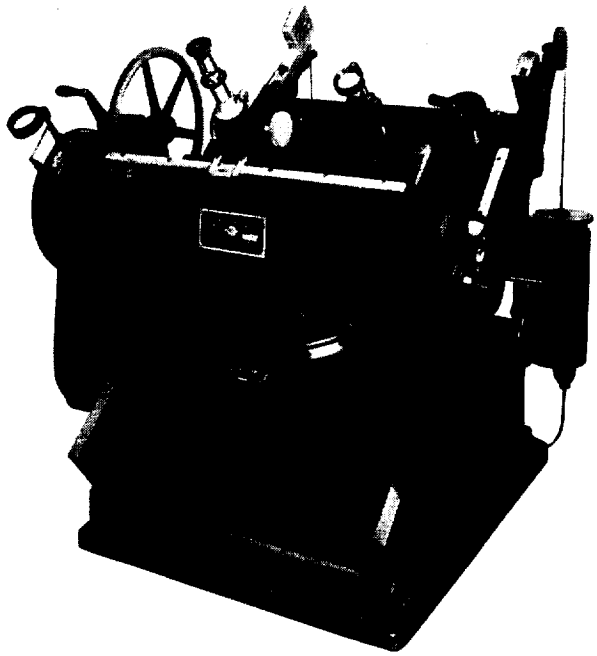

Fig.6.77 20.3- by 25.4-cm film reader with microscope

Fig.6.78 50.8- by 50.8-cm film reader with viewing screen